Influence of feedline configuration and its thermal mass distribution on cryogenic chilldown performance

A thesis submitted

in partial fulfillment for the award of the degree of

Doctor of Philosophy

by

Venkatesh N.

Department of Aerospace Engineering

Indian Institute of Space Science and Technology

Thiruvananthapuram, India

December 2024

Certificate

This is to certify that the thesis titled ***Influence of feedline configuration and its thermal mass distribution on cryogenic chilldown performance*** submitted by **Venkatesh N.**, to the Indian Institute of Space Science and Technology, Thiruvananthapuram, in partial fulfillment for the award of the degree of **Doctor of Philosophy** is a bona fide record of the original work carried out by him under my supervision. The contents of this thesis, in full or in parts, have not been submitted to any other Institute or University for the award of any degree or diploma.

Prof. A. Salih (Guide)
Professor
Department of Aerospace Engineering IIST,
Thiruvananthapuram

Dr. S. Sunil Kumar (Co-guide)
Deputy Director (Former),
Propulsion Research and Studies Entity,
LPSC, Valiamala, Thiruvananthapuram

डॉ. दीपु एम. / Dr. DEEPU M.
आचार्य एवं अध्यक्ष/Professor and Head
वांतरिक्ष इंजीनियरी विभाग
Department of Aerospace Engineering
भारतीय अंतरिक्ष विज्ञान एवं प्रौद्योगिकी संस्थान
Indian Institute of Space Science and Technology
अंतरिक्ष विभाग, भारत सरकार
Department of Space, Government of India
तिरुवनंतपुरम/Thiruvananthapuram - 695 547

Prof. M. Deepu
Professor and Head,
Department of Aerospace Engineering,
Indian Institute of Space Science and Technology,
Thiruvananthapuram

Place: Thiruvananthapuram
Date: December 2024

Declaration

I declare that this thesis titled ***Influence of feedline configuration and its thermal mass distribution on cryogenic chilldown performance*** submitted in partial fulfillment for the award of the degree of **Doctor of Philosophy** is a record of the original work carried out by me under the supervision of **Prof. A. Salih** and **Dr. S. Sunil Kumar**, and has not formed the basis for the award of any degree, diploma, associateship, fellowship, or other titles in this or any other Institution or University of higher learning. In keeping with the ethical practice in reporting scientific information, due acknowledgments have been made wherever the findings of others have been cited.

Place: Thiruvananthapuram
Date: December 2024

Venkatesh N.
(SC11D009)

This thesis is dedicated to my loving parents and family

Acknowledgements

First and foremost, I would like to express my deepest gratitude, from the bottom of my heart, to my research supervisors Prof. A. Salih, Department of Aerospace Engineering, Indian Institute of Space Science and Technology (IIST), Valiamala, Thiruvananthapuram and Dr. S. Sunil Kumar, former Deputy Director, Propulsion Research and Studies Entity of Liquid Propulsion System Centre (LPSC), Indian Space Research Organisation (ISRO), Valiamala, Thiruvananthapuram who gave me the opportunity to work on this highly interesting and challenging topic, which is of great relevance to launch vehicle application. I am deeply indebted to them for their able and continuous guidance and support that enabled me to progress and draw meaningful conclusions through this work.

I am deeply indebted to my Doctoral Committee (DC) Chairmen, Prof. V. Aravind and Prof. M. Deepu, Department of Aerospace Engineering, IIST, Valiamala, Thiruvananthapuram for their valuable suggestions made during the Doctoral Committee reviews. I am also extremely thankful to the members of Doctoral Committee; Dr. V. Narayanan, Director, LPSC/ISRO, Valiamala, Thiruvananthapuram and Prof. G. Venkatarathnam, Department of Mechanical Engineering, Indian Institute of Technology, Chennai for their valuable suggestions and guidance.

I am indebted to Prof. Raju. K. George, Dean R&D and Dr. V. Sennaraj, Deputy Registrar, IIST, Thiruvananthapuram for their constant encouragement during the course of study. I am indebted to Shri. M.S. Suresh, Project Director, Semicryogenic Propulsion Systems Project, LPSC/ISRO, Valiamala, Thiruvananthapuram and the management of LPSC/ISRO for granting me permission to take up this study and also for the tacit support extended throughout. I am also thankful to entire semicryo team, especially Shri. P.R. Ajayalal and Shri. R. Babu, for sharing my official workload that helped me put in concerted and continuous efforts for completion of my research work.

I am extremely thankful to Dr. Deepak Kumar Agarwal, Mr. Anant Singhal, Mr. Jophy Peter, Mr. Sivaprasad, and Mr. Ajesh of Propulsion Research and Studies Entity, LPSC/ISRO, Valiamala, Thiruvananthapuram for extending their wholehearted support in the conduct of experiments and Shri. Arun Kumar of CSC Entity, LPSC for ensuring a continuous supply of liquid Nitrogen for seamless conduct of experiments. I also thank the staff of Proto Fabrication Facility, LPSC/ISRO for the extensive support given to me for the fabrication of various parts required for realising the experimental set-up.

I am extremely indebted to my loving parents, wife and entire family for the moral and emotional support extended to me in abundance throughout the program. Above all, I thank the almighty for his blessings and imperceptible support, enabling me to satisfactorily complete the research work.

Venkatesh N.

Abstract

Feedlines carrying cryogenic fluids need to be pre-chilled 'apriori' to avoid two phase flow at the start of actual operation. This is very critical, especially in applications where only limited time and fluid quantity are available for chilling, as in the case of cryogenic rocket engines. The system and parameters need to be tuned to optimise the chilldown performance without any compromise on the mission requirements. This makes the chilldown process optimisation a very important component at the engine design phase itself. The chilldown process is highly sensitive to parameters like mass flux of cryogen, type of feedline insulation and heat in-leak, orientation of the feedline and its thermal mass distribution, thermophysical property of feedline material and its surface parameters like presence of coating, surface finish etc.. In the present work, influence of these parameters is experimentally studied employing stainless steel test sections insulated with poly-isocynurate foam with liquid Nitrogen as the simulant fluid. Experiments are performed using test sections of two different diameters. Measurements are made with the test section held horizontal and at different upward and downward orientations. Wall heat flux at different stations along the length of the test section is estimated by inverse heat transfer technique using the measured temperature data and its pattern of variation studied. Visualisation studies are performed to understand the flow structure prevailing in the test section during experiments with varying orientations and the trend in wall temperature profile is correlated with flow structure observed. Influence of thermal mass distribution of the feedline is investigated with additional thermal mass located near to the inlet as well as exit of the test section. Effect of thermophysical property, presence of metallic and nonmetallic coatings, and surface finish on chilldown performance are also evaluated experimentally. The experiments are followed up with numerical studies for varying orientations of test section to predict the wall temperature profile and results are compared with the experimental data.

The present study shows that chilldown performance is significantly improved with upward orientation as compared to horizontal or downward orientation and the reason for the same is corroborated with the observations from visualisation studies. Studies done to understand the effect of feedline thermal mass distribution show that additional thermal mass placed near to inlet gives better performance as compared to its placement near the exit. Studies on influence of thermal conductivity and coatings have given valuable inputs on measures to be adopted to optimise the chilldown performance. Findings of the present study would certainly help to explain the physics, improve the understanding on the effect of sensitive parameters on the chilldown performance of cryogenic feedlines and would certainly enable the designers to configure feed systems with improved chilldown performance.

Contents

List of Figures

List of Tables

Abbreviations

LN_2	Liquid Nitrogen
LAr	Liquid Argon
LOX	Liquid Oxygen
LH_2	Liquid Hydrogen
GN_2	Gaseous Nitrogen
CO_2	Carbon dioxide
FEP	Flourinated Ethylene Propylene
PDF	Probability Density Function
Cu	Copper
Nu	Nusselt number
Re	Reynolds number
VOF	Volume Of Fluid
PFA	Perfluoroalkoxy Alkane
CPI	Chilldown Performance Index

Nomenclature

Cp_{ts}	Specific heat of test section material (J/kgK)
Cp_{ins}	Specific heat of insulation material (J/kgK)
Cp_{l}	Specific heat of liquid cryogen (J/kgK)
T_{ins}	Temperature of insulation (K)
T_{ss}	Temperature of test section wall (K)
T_{f}	Temperature of Cryogen (K)
T_{w}	Wall temperature of test section exposed to cryogen (K)
T_{∞}	Ambient temperature (K)
T_{m}	Measured test section outside wall temperature (K)
T_{c}	Test section outer wall temperature computed (K)
T_{sat}	Saturation temperature of cryogen (K)
k_{ss}	Thermal conductivity of test section material (W/mK)
k_{ins}	Thermal conductivity of insulation material (W/mK)
k_{l}	Thermal conductivity of liquid cryogen (W/mK)
μ_{l}	Viscosity of liquid cryogen (Ns/m^2)
h_{fg}	Latent heat of cryogen (J/kg)
t	Chilldown time (s)
h_{in}	Heat transfer coefficient at test section inner wall (W/m^{2}K)
h_{out}	Heat transfer coefficient at test section outer wall (W/m^{2}K)
ρ_{ins}	Density of insulation material (kg/m^3)
ρ_{ss}	Density of test section material (kg/m^3)
ρ_{l}	Density of liquid cryogen (kg/m^3)
σ_{l}	Surface tension of liquid cryogen (N/m)
Δr_{ins}	Node to node distance within the insulation, (m)
Δr_{t}	Node to node distance within the test section, (m)
P_{sat,T_w}	Saturation pressure corresponding to wall temperature T_w (Pa)
$P_{sat,T_{sat}}$	Saturation pressure corresponding to T_{sat} (Pa)
F	Augmentation factor for forced convective heat transfer

M_{sp}, M_{nb}	Heat flux multipliers for single phase and nucleate boiling, respectively
S	Suppression factor for nucleate boiling heat transfer
q_{sp}	Single phase heat flux (W/m^2)
q_{nb}	Nucleate boiling heat flux (W/m^2)
T_{cell}	Boundary cell temperature (K)
X_{tt}	Martenelli parameter
S_{fc}	Suppression factor due to forced convection
S_{sub}	Suppression factor due to sub-cooling defined with respect to a reference temperature T_{ref}
ρ_m	Mixture density (kg/m^3)
v_m	Mass averaged velocity (m/s)
μ_m	Viscosity of mixture (Ns/m^2)
α	Void fraction
α_v	Void fraction of vapour
v_v	Velocity of vapour (m/s)
m_{l-v}	Mass transfer from liquid to vapour phase (kg/s)
m_{v-l}	Mass transfer from vapour to liquid phase (kg/s)
k_{eff}	Effective conductivity (W/mK)
E	Specific energy (J/kg)
m_{ts}	Mass of test section (kg)
m_c	Mass of cryogen consumed for chilldown (kg)
ΔT	Difference between ambient temperature and the value specified for chilldown completion (K)
σ_{HF}	Error in heat flux estimate, %
σ_T	Error in heat flux estimate due to error in measured wall temperature, %
σ_d	Error in heat flux estimate due to error in measured test section diameter, %
σ_t	Error in heat flux estimate due to error in measured test section wall thickness, %
σ_{cpss}	Error in heat flux estimate due to scatter in specific heat of test section wall material, %
σ_{kss}	Error in heat flux estimate due to scatter in thermal conductivity of test section wall material, %
σ_{cpins}	Error in heat flux estimate due to scatter in specific heat of insulation material, %
σ_{kins}	Error in heat flux estimate due to scatter in thermal conductivity of insulation material, %

Chapter 1

Introduction

Rocket engine feedlines as well as transfer lines in cryogenic storage systems are to be chilled from ambient condition to a certain specific desired temperature prior to admitting the cryogen at rated flow rates. This is essential to ensure a steady flow of cryogen and thereby achieve satisfactory performance of the system. It is also necessary from structural point of view, to chill the feedlines gradually, to avoid thermally induced stress and associated bowing effects. One way of achieving the desired temperature in the feedline is by chilling the line using the cryogen itself at a low flow rate. This process of bringing down the feedline wall temperature to an acceptable level is termed "chilldown" process and the time required to achieve a specified feedline temperature and fluid quality is called "chilldown time".

Chilldown process and chilldown time are very much influenced by parameters like mass flux of cryogen, orientation of feedline, its thermal mass distribution, type of insulation and heat in-leak etc. They are also influenced by the prevailing flow structure, which could be stratified, annular, inverted annular, bubbly, slug or plug etc..

Chilldown is also be affected by the prevailing heat transfer regime, which could be film boiling, transition or nucleate boiling, depending on the wall super heat and the fluid coming in contact with the wall. Typical pattern of heat flux variation and boiling regimes observed during the chilldown process of cryogenic feedline is shown in Figure 1.1. Initially, as the liquid cryogen enters into the warm feedline, feedline temperature is high and close to the ambient temperature. Liquid cryogen picks up heat from the feedline wall, resulting in the evaporation of liquid cryogen. This vapour generated forms a barrier between the liquid cryogen and the wall, thereby preventing the liquid cryogen from coming into direct contact with the feedline wall. This regime of heat transfer is described as film boiling regime and the heat flux experienced in this regime of heat transfer is expected to be low as compared to transition and nucleate boiling regimes. As chilldown progresses, the feedline temperature reduces gradually, heat flux decreases and the extent of vapour generation also decreases. As the wall cools to Leidenfrost temperature at which the heat flux is minimum, the liquid starts wetting the feedline wall. It then goes through an unsteady phase of intermittent liquid wetting and exposure. This regime is described as the transition boiling and the heat flux

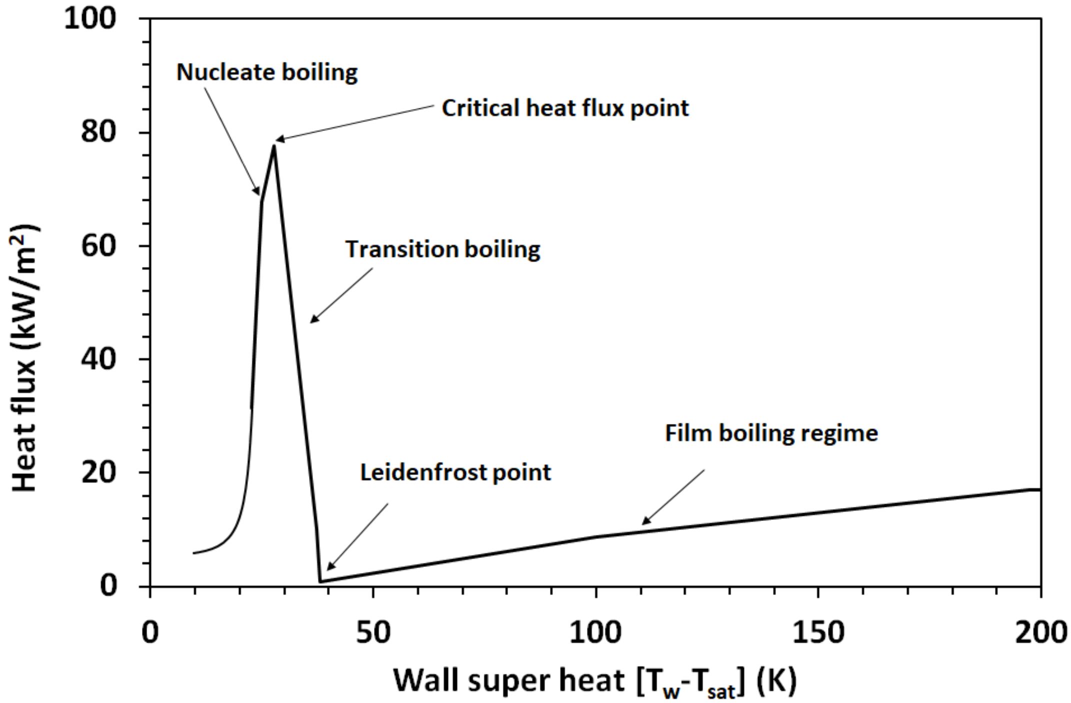

Figure 1.1: A typical plot showing the different boiling regimes encountered during chill-down, depending on the wall super heat

experienced is higher as compared to film boiling regime. As chilling proceeds further, it reaches the point of maximum heat flux defined as critical heat flux point and enters into the nucleate boiling regime, wherein liquid wetting of the wall and nucleate boiling results in enhanced heat transfer. With further progress in chilling, the heat flux decreases gradually, nucleate boiling stops and the process enters into single phase heat transfer with the liquid.

Apart from this, the heat transfer is also affected by the flow structure prevailing in the feedline, which could be stratified, bubbly, plug or slug, as shown in 1.2.

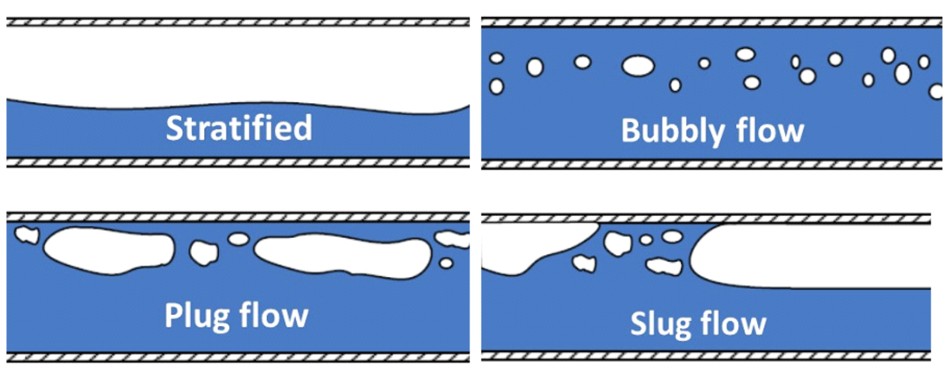

Figure 1.2: Different types of flow structure observed in feedlines during chilldown

Also, during the chilldown process, as the test section gets chilled, the thermodynamic process taking place in the test section changes with time and is depicted in Figure 1.3.

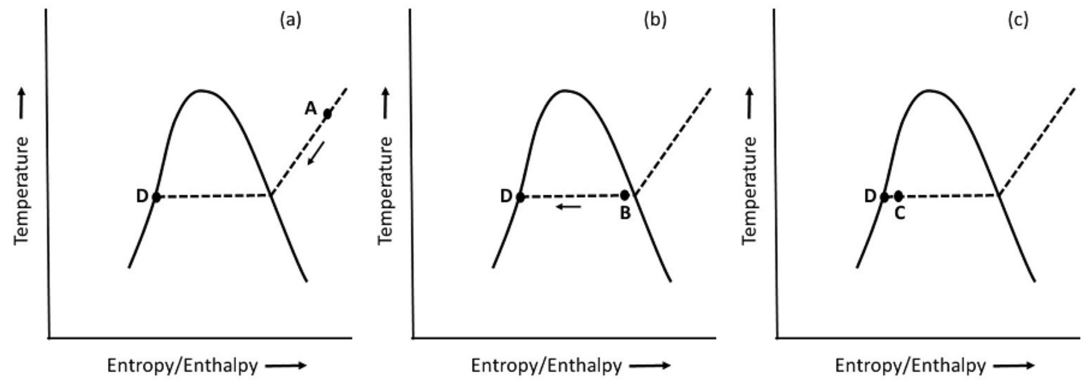

Figure 1.3: Thermodynamic process taking place in a cryogenic feedline during the chilldown process

The cryogen enters the test section at state D, in the liquid state, at a temperature close to its saturation temperature with negligible void fraction. As it moves along the feedline or test section, it picks up heat from the wall of the test section, resulting in increase of entropy as well as enthalpy. This heat absorption, results in phase change. During the initial phase of chilldown, heat addition is so large that almost complete phase change of the cryogen takes place and it leaves the test section in vapour form. The state of cryogen at the exit of the test section would then correspond to state A, as shown in Figure 1.3(a). As chilling proceeds, the wall gets gradually cooled and the temperature of the vapour leaving the test section reduces gradually. The quality of cryogen leaving the test section slowly changes to a two phase mixture. It then enters the vapour dome from the right amd reaches stage B as shown in Figure 1.3(b). With further chilldown, the quality is expected to improve and the state of the cryogen would shift to state C, as shown in Figure 1.3(c) and thereafter to a state very close to D with very low void fraction. This is the stage at which chilldown process is generally declared as completed and full flow of liquid cryogen is admitted into the feedline for the filling process.

Thus chilldown is a very complex process and its optimisation is of great significance, especially for cryogenic rocket engines for space application, as it can provide the advantage of reduction in chilldown time as well as optimised cryogen consumption, leading to payload advantage. A good understanding of the processes involved in chilldown is very much essential for its optimisation and to develop a good model for prediction of wall temperature profile, chilldown time and cryogen consumption.

Research on this topic started in the 1960s, almost in parallel with the development of rocket engines operating with cryogenic propellants. A detailed literature survey is done to get a good understanding of the work that has been carried out so far in this field and the outcome is brought out elaborately in Chapter 2. As can be seen from published literature, there are several studies carried out to understand the chilldown performance for horizontal and vertical orientations of test section and to estimate the wall heat flux using the measured wall temperature data. A number of correlations and methods have also been proposed to estimate the heat transfer coefficient and wall heat flux for the boiling regimes encountered during chilldown. However, studies to understand the influence of varying upward and downward orientations of test section are limited. Moreover, in the experiments performed, the inner diameter and length of the test section were limited to 11.68 mm and 572 mm respectively, whereas in rocket engines, the lines are expected to be of bigger size, both in terms of diameter and length. The visualisation studies performed so far are limited to horizontal and vertical flows only. Studies to capture the flow structure in experiments with varying angular configurations with upward and downward inclinations are absent. Studies are not attempted so far to understand the influence of thermal mass distribution of feedline on chilldown performance. Effect of metallic coating on chilldown performance is not addressed so far. Studies are also not done to evaluate the influence of nonmetallic coatings on the chilldown performance of test sections with varying thermal mass. It is in this context, that the present experimental studies are taken up. Apart from this, numerical simulations are also attempted for varying orientations of test section and results are compared with experimental data from the present study. Studies have brought out certain interesting findings that would help to understand better the physics associated with the chilldown process. It would also help to improve the design of cryogenic systems and thereby achieve better chilldown performance.

The objectives and scope of the present study are brought out in Chapter 3. The influence of sensitive parameters like feedline orientation, mass flux, thermal mass distribution, coatings, thermophysical property, surface finish etc. on chilldown performance of cryogenic feedlines are studied. Details of the experimental set-up used for these studies and test procedure employed are covered in Chapter 4. Detailed description of the experiments performed to understand the influence of test section orientations and mass flux, and the related test results including inferences are covered in Chapter 5. Apart from this, heat flux values for the bottom and top regions of the test section are estimated by inverse heat transfer technique, using the measured outside wall temperature and an assessment is made on the heat flux pattern for varying test section orientation. Experiments conducted using flow visualisation technique and their findings are brought out in Chapter 6. Numerical simulations carried out to capture the wall temperature profile and to bring in a better understanding on the physics associated with chilldown process with varying feedline orientations are covered in Chapter 7. Studies carried out to understand the influence of thermal mass distribution of feedline are brought out in Chapter 8. Experiments carried out to understand the influence of thermophysical property, surface coatings and surface finish on chilldown performance and their results are addressed in Chapter 9. Salient conclusions of the present study and outline for future work are discussed in Chapter 10.

Chapter 2

Literature survey

A detailed literature survey is carried out to understand the work that is done so far towards addressing the chilldown process associated with cryogenic feedlines and the salient details are covered in this chapter. Aspects addressed in published literature include experimental studies to understand chilldown performance, various correlations proposed for estimation of heat transfer coefficient and wall heat flux, flow visualisation studies, experimental studies with pulsed flow and role of non-metallic coatings for chilldown optimisation, numerical studies, etc. Based on the literature survey, gap areas that need to be addressed, to improve the understanding on the chilldown process are identified and the same is also brought out towards the end of this chapter.

2.1 Experimental studies on evaluation of chilldown performance

Initial studies performed were mainly to evaluate the chilldown time of short and long transfer lines. Cryogen consumption during chilldown, effect of sub-cooling and the influence of different types on insulation system on chilldown performance were also addressed by some of the researchers.

Burke et al. [1] were among the first to study experimentally the chilldown of long transfer lines of outer diameter 2 inches, thickness 0.065 inch and length varying from 60 to 175 feet using LN_2. Experiments were performed with un-insulated transfer line and line insulated with styrofoam. The evolution of wall temperature and pressure in the test section were studied using bourdon tube gauges, manometers and copper-constantan thermocouples. A sight glass was employed at the discharge side to visualise the flow structure and sighting of single phase liquid was defined as the end of chilldown. During the initial transient, a gush of cryogen flow followed by pressure surge and flow reversal were reported. The value of pressure surge observed was very close to the dewar pressure and thereafter the line pressure was seen to be gradually decreasing, as chilldown progressed. It was mentioned that the initial surge in pressure was due to sudden boil off and incapability of the system to handle large vent flow rates. Cryogen flow rate was reported to be gradually increasing thereafter as chilldown progressed and reached a steady value at the end of chilldown. An analytical model was proposed based on the energy balance approach to predict the chilldown time. Axial and radial temperature gradients in the test section were not considered in the model. Prediction made using the model was reported to be closely matching with the experimental result. The model also predicted a reduction in chilldown time with higher storage tank pressure, matching with the experimental observations. Experiments employing test sections of 3/16 inch inner diameter and three different outer diameters viz; 0.5 inch, 1 inch, and 2 inch, were performed by Chi [2] to study the chilldown characteristics of feedlines with LH_2. A lumped parameter based model was proposed for estimation of the wall temperature profile and prediction made using the proposed model was reported to be matching well with the experimental data. Cooldown time predicted was also reported to be matching well with the experimental results and the deviation reported was well within $\pm 21\%$. Heat transfer coefficient was reported to be varying with mass flow rate with an exponent of 0.8.

Brennan et al. [3] experimentally studied the chilldown of vacuum insulated copper transfer line of 19 mm outer diameter, 15.9 mm inner diameter and 61m length. Experiments were performed with subcooled and saturated LN_2 and LH_2. Based on the experimental data, it was concluded that temperature of liquid affected the cooldown time with LN_2, whereas no such effect was observed with LH_2. Very little pressure surge was observed in experiments in which the liquid was in saturated condition, both in the case of LN_2 and LH_2. The type of valve used to admit the liquid into the test section, line temperature near the valve, valve opening time, and condition of the liquid just upstream of the valve were reported to be having significant influence on the pressure surge observed during chilldown. It was also reported that the pressure surge could be controlled by introducing a restricting orifice to regulate the flow of cryogen into the test section. Heat transfer coefficient predicted using the pool boiling correlation was found to be in reasonable agreement with the experimental results for LN_2, whereas large mismatch was reported between the two for LH_2. It was mentioned that this could be due to large difference in surface tension and liquid to vapour density ratio for LH_2 as compared to LN_2.

Different methods that can be adopted for the chilldown of large diameter LOX and LH_2 feedlines were addressed by Schwartz and Commander [4]. Methods to estimate the thermal stress induced during chilldown were addressed. Estimates were made for the wall temperatures that could be achieved during chilldown of LOX and LH_2 feedlines and compared with experimental data.

Edeskuty [5] had addressed the various schemes that can be employed for chilldown of cryogenic systems. Methodologies that can adopted for estimation of cooldown time, various issues faced during chilldown of cryogenic systems like bowing, thermal stresses, pressure and flow surges, geysering etc. were also addressed.

Srinivasan et al. [6] conducted experiments with short transfer lines of inner diameter 12-19 mm, wall thickness 1.25-2 mm, and length 1000-1100 mm using LN_2 as simulant fluid. Both vacuum insulated and un-insulated lines were employed for the study. Test sections made of copper, aluminium, glass, and stainless steel were used. Superposition approach proposed by Giarrantano and Smith was used for estimation of heat transfer coefficient at the tube inner wall. Breen and Westwater correlation was used to estimate the contribution from pool boiling and contribution from forced convection was estimated using Dittus Boelter equation. It was reported that for the initial phase of chilldown, the measured wall temperature profile matched closely with the estimate made using zero mass flow rate. This was attributed to the presence of stagnant vapour barrier between the wall and the liquid, making the heat transfer closely resemble the situation in pool boiling. Whereas the difference between the two was apparent for lower wall temperature. Influence of gravity, buoyancy and pressure forces on inducing wall wetting etc. were discussed. It was also mentioned that for short transfer lines, the vapour formed would escape the test section and a film of uniform thickness would be maintained, irrespective of the flow rate employed for chilldown. Based on this, it was concluded that for short transfer lines, mass flow rate did not affect the chilldown time significantly.

Chilldown of foam insulated short transfer line was evaluated experimentally with LN_2 by Prasad et al. [7] using a test section of outer diameter 13 mm, inner diameter 10.6 mm, and length 1000 mm, made of copper material. Test section was insulated with polystyrene foam insulation of 120 mm thickness. Findings of the study were very similar to the ones reported by Srinivasan et al. [6]. It was also mentioned that theoretical estimate, which was based on pool boiling correlation, matched well with the experimental data. Based on this, it was concluded that the contribution from forced convection was very less for short transfer lines.

Steward et al. [8] conducted experiments with five different configurations of horizontal test sections to evaluate the wall temperature profile and chilldown time. Experiments were performed under subcooled and saturated conditions with LH_2 and LN_2. It was reported the pressure surge observed during the start of chilldown was higher with subcooled liquids and was attributed to sudden gushing of liquid exceeding the quantity that would produce a steady cooldown, its boiling and associated rapid expansion of vapour. Other methods like restricting the cryogen flow into the test section etc., to reduce the pressure surge during chilldown, were also discussed. A one dimensional analytical model was also proposed to estimate the wall temperature profile and cryogen consumption during chilldown. A good match was reported between the prediction made using the analytical model and the experimental data.

Experiments were conducted by Krishnamurthy et al. [9] using double jacketed horizontally held AISI321 stainless steel test sections of outer diameter 7.95 mm, wall thickness 0.56 mm, and length 2.57m, with an outer jacket of 25.4 mm outer diameter, to evaluate the influence of different types of insulation. Chilldown time was evaluated for two un-insulated conditions of jacket space filled up with air and CO_2, for conditions of vacuum insulation with varying jacket pressures and multi layer insulation. It was reported that influence was more pronounced in experiments with low flow rates employed for chilling. At low flow rate, chilldown time was much higher with air filled in the jacket space, as compared to vacuum insulation, whereas at high flow rates, the contribution from forced convection was predominant and hence the chilldown time was almost the same. In the case of jacket filled up with CO_2, at low flow rate, chilldown time was higher as compared to air filled case, probably due to solidification of CO_2 on the inner pipe. At higher flow rates, chilldown time was almost the same in both the cases. With vacuum insulation, cooldown time decreased with increase in vacuum level and increase in dewar supply pressure. No significant reduction in chilldown time was seen for dewar supply pressure more than 0.06MPa. With multi layer insulation, chilldown time was higher as compared to vacuum insulation due to additional time required to cool the insulation. An empirical correlation was proposed to predict the wall temperature profile as a function of the vacuum level maintained in the jacket. Prediction made using the model was compared with experimental data and good match was reported. Mass flow rates achieved with different types of insulation during steady state after chilldown were also compared. Liquid fraction was reported to be more during the initial phase of chilldown with coarse vacuum in jacket as compared to high vacuum and this was attributed to higher quantity of vapour formation and its radial expansion resulting in acceleration of liquid core. Whereas flow rate achieved after chilldown were higher for high vacuum case as compared to coarse vacuum. The observation was similar with multi layer insulation as well.

2.2 Correlations for estimation of heat transfer coefficient during chilldown

Parallely efforts were also taken by many to address other topics of interest in chilldown like predicting the heat transfer coefficients for different boiling regimes encountered during chilldown, using correlations derived from the experimental data. Kalinin et al. [10] proposed a new correlation for estimation of heat transfer coefficient in transition boiling regime based on the theory that nucleate and film boiling co-existed during transition boiling. Based on this, an approach of estimating the wall heat flux in transition boiling regime as a combination of nucleate boiling and contribution from heated surface to vapour was proposed. Heat flux contribution from nucleate boiling was estimated using Grigoryev's correlation and the contribution from the heated surface to vapour was estimated using the author's correlation itself, applicable for film boiling of saturated liquid. The proposed correlation considered wall superheat, and first and second crisis points to estimate the fraction of heated surface wetted by the liquid and arrive at the weightage factor to be considered for the nucleate and film boiling heat flux to estimate the total wall heat flux. Total heat flux was then estimated as a weighted average of the contributions from nucleate and film boiling. Correlations were also suggested for estimation of first and second crisis points based on experimental data available in published literature.

Steiner and Schlünder [11] performed experiments with LN_2 using a test section of inner diameter 14 mm and wall thickness 3 mm, made of copper material. On the flow pattern observed, it was reported that most of them related to wavy and slug flow regimes and plug flow was not observed in any of the runs. Based on the experimental data, it was reported that in the nucleate boiling regime, the heat transfer coefficient showed a strong dependence on heat flux. A new correlation, which was a modified form of Stefan's correlation with a factor introduced to account for mass flow rate and wettablity function, was proposed for Nu prediction for saturated flow boiling. Heat transfer coefficient predicted using the proposed correlation was reported to be matching with the experimental results well within $\pm 20\%$. It was mentioned that the proposed correlation could also capture the influence of mass flow rate on heat transfer coefficient. Critical heat flux values observed in the experiments were lower than values reported for pool boiling and difference was attributed to stratification of flow in a horizontal pipe, causing partial dry out. A correlation was also proposed for estimation of critical heat flux under forced flow boiling conditions.

Heat transfer under plug flow of film boiling regime was studied by Kurilenko and Dymenko [12] through experiments performed with LH_2 using a vacuum insulated steel test section. Based on the results, heat transfer process was reported to be similar to natural convection below a critical Re. Whereas for higher Re, ratio of Nu for natural convection to the one for forced convection was reported to be increasing with Re and proportional to $\mathrm{Re}^{0.8}$. A generalised correlation was proposed for predicting the Nu for upward and downward flows. It was reported that the prediction made using the proposed correlation matched well with the experimental data with scatter not exceeding $\pm 25\%$.

Experiments were performed by Katto and Ohno [13] with R-12 as test fluid, simulating vapour to liquid density ratio in the range of 0.109 to 0.306, to verify the validity of correlations proposed for estimation of critical heat flux. A stainless steel test section of outer diameter 12 mm, inner diameter 10 mm, and length 1000 mm was employed for the study. A new correlation with a revised applicability criteria based on vapour to liquid density ratio was postulated for estimation of critical heat flux. This newly proposed correlation along with the revised application criteria was reported to be showing a good match with experimental data, covering a wide range of operating conditions in terms of pressure and fluids.

Shah [14] compared the heat transfer coefficient values estimated by the correlations proposed by Klimenko, Shah and Rohsenow, using 12 sets of published experimental data for saturated boiling condition with cryogenic fluids. It was reported that Shah's correlation based on boiling number gave very good match for nine sets of data, whereas poor match was reported with Klimenko and Rohsenow correlations.

Using the published experimental data, Steiner [15] brought out the dependence of heat transfer coefficient in horizontal and vertical flows on parameters like reduced pressure, vapour quality, tube diameter, surface finish etc.. It was reported that in vertical flows, perimeter averaged heat transfer coefficient was not affected by vapour quality. In horizontal flows with low mass flux conditions, the observation was similar, whereas for high mass flux flows, heat transfer coefficient was reported to be decreasing with increase in vapour quality. Dependence of heat transfer coefficient on tube diameter was expressed as diameter to the power -0.4 for vertical flows and diameter to the power -0.5 for horizontal flows. Dependence on pressure on heat transfer coefficient was reported to be lesser in horizontal flows as compared to vertical flows. A new set of correlations were proposed for estimation of heat transfer coefficient for the nucleate boiling regime in vertical upward and horizontal flows. The correlations proposed considered parameters like tube diameter, surface finish etc. apart from reduced pressure, vapour quality etc.. Prediction made using the newly proposed correlation was compared with the experimental data of horizontal flows of cryogens and a close match was reported. New correlations were also proposed to estimate the heat transfer coefficient in film boiling regime in vertical and horizontal flows, by combining the heat transfer coefficients for gas and liquid phases. A new superposition correlation was also proposed for estimating the heat transfer coefficient in flow boiling.

A correlation to estimate the heat transfer coefficient for film boiling regime, both for saturated and subcooled boiling conditions, was proposed by Gungor and Winterton [16]. The correlation considered the heat flux contribution from forced convective heat transfer and nucleate boiling with suitable augmentation and suppression factors to account for enhancement in forced convection part and reduction in nucleate boiling effects. Augmentation factor for forced convection was expressed as a functional of Martinelli parameter and Boiling number, whereas the suppression factor for nucleate boiling was expressed as a function of two phase flow Re and augmentation factor for forced convection. Correlation proposed by Cooper was used to estimate the heat transfer coefficient under nucleate boiling condition and Dittus Boelter correlation was used for forced convective heat transfer prediction. It was reported that prediction by the newly proposed correlation matched well with experimental values and the deviation was well within $\pm 40\%$.

Kandlikar [17] proposed a new set of correlations for estimation of heat transfer coefficient in convective and nucleate boiling regimes, using published experimental data. This correlation was developed using 26 sets of experimental data generated for different fluids like water, R-11, R-12, Neon, Nitrogen etc. and used the superposition approach for prediction of heat transfer coefficient. Heat transfer coefficient values predicted by the proposed correlation were compared with the prediction made by other correlations available in published literature. Mean deviation was reported to be minimum with the newly proposed correlation. Also, it was mentioned that the dependence of heat transfer coefficient on vapour quality and heat flux was correctly captured by the newly proposed correlation.

A new generalised correlation for prediction of saturated and subcooled nucleate boiling, in tubes and annuli was proposed by Liu and Winterton [18]. The correlation was derived based on 29 sets of published data including cryogenic fluids. The correlation proposed for saturated boiling was similar to the one proposed by Kutateladze with forced convection and nucleate boiling terms raised to a power of 2. Forced convection augmentation factor was proposed as a function of vapour quality, Prandtl number and liquid to vapour density ratio, whereas the suppression factor for nucleate boiling was expressed as a function of augmentation factor for forced convection and flow Re. Correlation proposed for subcooled boiling was also similar to the saturated boiling correlation, except the fact that driving temperature difference considered for forced convective heat transfer was the bulk temperature. It was reported that prediction made using the proposed correlation gave a better match with experimental data as compared to other available correlations.

Van Dresar et al. [19] proposed a new correlation for estimation of Nu based on experiments carried out with a vacuum jacketed, vapour cooled test section of internal diameter 8.7 mm and length 26 cm, held at an upward inclination of 1.5° with respect to horizontal. Calibrated bellow, submerged in the supply dewar and driven by a stepper motor, was employed to achieve known steady state flow rates through the test section. Tests were carried out with LN_2 flow rates in the range of 0.2 to 20g/s and with LH_2 in the range of 0.02 to 0.2g/s. Plug, slug, annular and stratified flow regimes were reported. Based on the experimental data, new correlations were proposed for Martinelli parameter to estimate the friction factor and Nu to estimate the heat transfer coefficient, both for laminar-laminar and laminar-turbulent flows. With these proposed correlations, prediction was made for the experiments conducted and deviation for Nu from experimental values was reported to be <12% for laminar-laminar flows and <15% for laminar-turbulent flows.

A detailed survey of the experimental data and assessment of the existing correlations for predicting cryogenic two phase flow heat transfer was carried out by Hartwig et al. [20]. Six critical heat flux correlations and fifteen heat transfer coefficient correlations were selected for evaluation. Seven sets of quenching data were collected from literature to assess single and two phase flow heat transfer and critical heat flux. Based on the evaluation, it was reported that correlations by Zuber, Leinhard and Dhir under predicted the critical heat flux values, whereas correlations by Katto group, Mudawar and Maddox, Hall & Mudawar over predicted the values. It was also mentioned that none of the heat transfer coefficient correlations matched the experimental results. It was stated that the correlations developed based on heated tube tests may not be able to correctly predict the heat flux and heat transfer coefficients in chilldown, which are basically quenching studies with short transfer lines and very low thermal mass.

Based on literature survey and estimation of heat transfer coefficient for the different boiling regimes, Darr et al. [21] concluded that a new set of correlations were needed to predict the heat transfer coefficients for the different boiling regimes encountered during the chilldown process. Based on five sets of published data identified after detailed scrutiny, a set of improved correlations were proposed to estimate the heat transfer coefficient in film boiling, transition and nucleate boiling regimes. The correlation proposed for film boiling regime had two terms to account for the turbulent convection effects and the droplet to wall interaction. Turbulent convection term was a modified form of Dittus Boelter correlation, whereas the second term to account for droplet to wall interaction had Weber number and Jakob number to account for the effect of break-up of liquid core into droplets and contribution of latent heat to sensible heat in vapour. New correlations were also proposed for prediction of Leidenfrost temperature and critical heat flux. Nucleate boiling correlation proposed had a Weber number term included to account for large differences in surface tension between fluids. It was reported that the predictions made using the set of improved correlations matched very well with the experimental data available in published literature.

2.3 Initial studies to understand the flow structure

Very few studies were done in the 1980s and 1990s to capture the flow structure. Flow structure in vertical upward and downward flows was studied by Kalinin and Firsov [22], performing experiments with LN_2. Test sections employed were of diameter 12-70 mm and length 0.2 to 3.03m. Flow pattern and heat transfer characteristics were evaluated. Self-similar and nonsimilar rod flows, transition, dispersed annular and dispersed flow regimes were reported. The conditions under which these flow regimes were expected, both for upward and downward flows were also brought out. Correlation was proposed for predicting droplet size distribution and mean droplet diameter for dispersed annular and dispersed flow regimes. Correlations for heat transfer coefficient and frictional pressure drop for these flow regimes were also presented.

Das and Pattanayak [23] performed experiments with LN_2 and used a capacitance type sensor to identify the flow regime in vertical tubes. A vertical test section of 15 mm inner diameter was used and parallel plate capacitors placed at the end of the test section were used to measure the void fraction. The capacitor produced pulses of varying width in response to changes in void fraction and to capture the flow pattern, this was converted into a PDF with 25 intervals to cover the 0 to 100% void fraction range. The PDF pattern expected for different flow regimes like bubble flow, slug flow, annular flow etc. were reported.

2.4 Recent studies on heat flux pattern, flow visualisation and modelling for chilldown prediction

Though chilldown studies done earlier were mostly towards estimation of chilldown time and cryogen consumption, recent studies done in the last two decades were more focused towards experimentation to understand the heat flux pattern at different stations along the length of the feedline, influence of mass flux, generation of one dimensional models for chilldown prediction etc. Some of these studies also captured the flow structure observed during the chilldown process. Experiments were conducted by Jackson et al. [24] using a stainless steel 304 test section of 12.5 mm inner diameter and 1.27 mm wall thickness. Temperature measurements with E type thermocouples were employed at top, bottom and two sides along the length of the test section. A highly sensitive pressure sensor was used to measure the pressure drop across the test section. Experiments were performed with LN_2 and flow rate was measured using a venturi after gasification. Set-up also had a pyrex flow visualization section to capture the flow pattern using a high speed camera. It was reported that significant difference was observed between the surface temperature measurements at top and bottom. Inverse technique was used to estimate the heat transfer coefficient on the tube surface. Analytical estimation of the wall temperature and heat flux profile was also attempted using a one dimensional model. Flow structure related information obtained from the experiments were used to augment the convective gas phase heat transfer coefficient at the bottom wall in close vicinity of the liquid and a geometry influence factor, as proposed by Liao, was adopted for this. This modeling approach was first validated using an experiment involving gas phase heat transfer (estimation using Dittus Boelter equation) and then extended to experiments performed as part of the study.

Yuan et al. [25] conducted experiments using a horizontally held pyrex glass tube test section of internal diameter 11.1 mm, outer diameter 15.8 mm, and length 254 mm to address the influence of low mass flux on chilldown performance. The test section was placed in a vacuum chamber to minimise the parasitic heat in-leak. Mass flux of LN_2 achieved during gravity driven experiments was in the range of 18-23 kg/m^2s and 3.6-10.8 kg/m^2s in bellows driven experiments. Wall temperature profile, flow structure and heat flux pattern observed during the boiling regimes were reported. It was mentioned that in gravity driven experiments, chilldown started in the film boiling regime and the flow pattern observed was dispersed flow. Droplets changed to filaments as chilldown progressed. Intermittent liquid wall contact was reported in transition boiling followed by continuous contact and piling up at the bottom, resulting in stratified or wavy flow during nucleate boiling regime. Based on the experimental data, a phenomenological model was proposed for prediction of bottom wall heat flux. The heat flux at the bottom location in contact with the liquid was observed to be higher as compared to the top region, cooled by vapour phase. In the proposed model, vapour film thickness at the bottom was estimated using Chan's correlation. In the estimation of bottom wall heat flux, the fraction of the bottom wall in the vicinity of liquid filament was estimated through a factor similar to wettability function, derived from the experimental data and heat flux was estimated assuming conduction through the thin vapour layer. Whereas in the region experiencing single phase heat transfer by vapour, heat flux was estimated using the correlation proposed by Kao et al.. It was reported that the heat flux prediction made using the model matched well with the experimental results, except for the initial phase. Deviation in initial phase was attributed to highly transient back and forth bouncing of the liquid filaments from the wall, whereas the model had considered only stable liquid filaments at the wall.

Yuan et al. [26] proposed a one dimensional numerical model based on flow structure to estimate the chilldown time and wall temperature profile during chilldown of vertical sections. Model considered single phase convective heat transfer by vapour phase, dispersed flow, annular flow and single phase convective heat transfer by liquid, as conditions prevailing in the test section to estimate the heat transfer. Two phase transient conservation equations for mass, momentum and energy were solved along with suitable constitutive relations chosen to close the model. In the inverted annular flow regime, empirical correlations of Kawaji and Colburn were used to estimate wall to vapour heat transfer and shear stress was estimated using the correlation proposed by Kawaji and Banerjee. Whereas for the dispersed flow regime, different closure models were used to capture convective mode heat transfer to vapour from the wall (Hedayatpour et al.), heat transfer at vapour to liquid interface (Lee-Ryley model), direct heat transfer at the wall from droplets (Guo et al.), radiative heat transfer from the wall to vapour and liquid (Sun et al.), mass flux of liquid getting evaporated etc. Droplet drag was estimated using the correlation proposed by Rowe. The flow was modelled as single phase vapour when void fraction reached 0.99 and Dittus Boelter equation was used to estimate the heat transfer coefficient. Transition boiling regime was assumed, when the wall temperature reached rewetting temperature and Chen's correlation was proposed for both transition and nucleate boiling regimes. Using the model, predictions were made to estimate the wall temperature profile for the experiments conducted earlier on a vertical test section by Anton and Collier. The test cases considered covered both terrestrial and microgravity conditions. Good match was reported between the model results and experimental data. Based on the results, it was reported that the effect of gravity affected the wall temperature profile at locations downstream more significantly compared to locations upstream.

Hu et al. [27] conducted experiments with LN_2 using a pyrex test section of inner diameter 8 mm and outside diameter 10 mm, held inside an evacuated chamber to provide vacuum insulation and minimize the heat in-leak. Experiments were done for vertical upward and downward orientations of test section. Mass flux achieved was in the range of 20-80 $\mathrm{kg/m^2s}$. Wall temperature profiles for vertical upward and downward flows were addressed and it was reported that chilldown was faster in downward flows as compared to upward flows. Heat flux at inner wall and test section inner wall temperature were estimated by Burgraff method, using the measured outer wall temperature. Though magnitudes very different, heat flux profiles were almost similar for upward and downward flows. Two distinct peaks were seen in heat flux profile, one corresponding to the film boiling regime and the other during nucleate boiling phase. Heat flux profiles for nucleate boiling phase were almost similar for upward and downward flows and it was mentioned that this regime was not influenced by orientation. Based on the experimental data, it was mentioned that the effect of gravity was decreasing with increased mass flow rate and chilldown performance was similar for upward and downward flows with high mass flux. During chilling, flow structure was reported to be changing from dispersed flow to stretched bubble flow with bubbles of larger size, then to inverted annular flow followed by transition flow before entering finally into pure liquid flow. It was reported that with increase in mass flux, rewetting temperature also increased. The effect was reported to be more in downward orientation as compared to tests with upward orientation. Quenching front velocity was also reported to be higher for downward orientation as compared to upward flows.

Experiments with LN_2 at low Re and with LH_2 at high Re were performed by Hartwig et al. [28] to understand the chilldown performance under two different flow conditions. Re simulated was in the range of 1000 to 4000 in LN_2 experiments and in the range of $1.84\text{x}10^4$ to $4.33\text{x}10^5$ with LH_2. Test set up had a viewing section made of pyrex glass for flow visualisation. The flow structure observed in the experiments, during different stages of chilldown, were reported. Burgraff correlation was used to estimate the test section inner wall temperature and heat flux. It was reported that in the case of LN_2 experiments, film boiling followed by transition and nucleate boiling regimes were observed, whereas with LH_2, tests entered immediately into transition boiling and the maximum heat flux was achieved within seconds. This was attributed to the difference in properties of two fluids like low vapour to liquid density ratio, low surface tension and low kinematic viscosity for hydrogen as compared to nitrogen. Maximum heat flux observed in the sight glass section with low Re LN_2 was around 8000 W/m^2, whereas with LH_2, the value estimated was much higher at 40000 W/m^2. High chilldown efficiency was also reported for LH_2 and this was attributed to lower parasitic heat leak and higher flow rates causing turbulent mixing of the fluid. Critical heat flux values were estimated using the available correlations and compared with the experimental results. It was reported that the predicted values were not matching with any of the existing correlations, both for LN_2 and LH_2 experiments. In the case of Leidenfrost temperature, predictions by both Berenson's and Carey's correlation were reported to be close to the experimental values for LN_2. Whereas for LH_2, the temperature prediction by Berenson's correlation was 60.8K, not matching the experimental data, as they did not pass through the Leidenfrost point. Prediction by Carey's correlation was 287K and could not be validated, as LH_2 experiments started from an initial temperature of 250K.

A one dimensional model for the prediction of transient chilldown process, in a vertical downward flow with LN_2 as simulant fluid, was proposed by Darr et al. [29]. Test section considered for the simulation was a vacuum insulated SS tube of 1.27 cm outside diameter, 0.0508 cm thickness, and length 57.2 cm. Separate correlations were considered for the prediction of heat flux in film boiling, transition boiling, and nucleate boiling regimes. Experiments were also performed for different mass flux conditions for model validation. Results of simulation studies carried out for 55 test cases with mass flux varying from 61.2-1150 kg/m^2-s were compared with the experimental data and good match was reported.

Chilldown process of cryogenic flow line was studied by Jin et al. [30] conducting experiments using a vacuum insulated test section of 12.7 mm outer diameter, 1.25 mm wall thickness, and 7m length. Experiments were done with LN_2 for six different test conditions with mass flux simulated in the range of 19 kg/m^{2}s to 49 kg/m^{2}s. Wall and fluid temperature profiles observed at a station 5.5m from the inlet were presented. Burgraff correlation was used to estimate the tube inside wall temperature and heat flux, using the measured outside wall temperature. Critical heat flux values estimated from the experimental data were compared with the predictions made by various correlations available in published literature and it was reported that prediction by Darr's correlation matched well with the experimental results within 28%. It was also mentioned that Kutateladze correlation can be used with the constant B in the expression changed to 0.029 and with this modification, the values predicted were found to be falling well within $\pm 12\%$. With regard to minimum heat flux, it was reported that the values predicted by Zuber correlation were much higher at 3-5 times as compared to experimental data. Based on the experimental data, the heat transfer coefficient was reported to be proportional to (heat flux)$^{0.7}$, as in pool boiling.

Experimental studies were carried out by Jin et al. [31] using a horizontally held stainless steel 304 test section of 12.7 mm outer diameter, 10.2 mm inner diameter, and 7 m length provided with multi layer insulation. Experiments were conducted with LN_2 under saturated conditions and mass flux simulated was in the range of 26 to 73.6 kg/m^{2}s. Heat flux at the test section inner wall and inner wall temperature were estimated from the measured outer wall temperature by Inverse heat transfer method. It was reported that in the film boiling regime, heat flux at locations near to the inlet were seen to be decreasing with reducing wall superheat, whereas at far away locations, it was initially increasing and then decreasing. No significant difference was seen in the heat flux at these two locations in transition and nucleate boiling regimes. A one dimensional model based on mass, momentum and energy conservation equations was proposed for heat transfer coefficient prediction. Heat transfer coefficient in film boiling regime was estimated using the modified Dittus Boelter equation with two phase Re computed using Miropolski's correlation. Heat transfer coefficient in transition boiling and nucleate boiling regimes was predicted assuming a linear variation between Leidenfrost temperature and saturation temperature. Critical heat flux estimate was based on Katto and Kurata correlation. Leidenfrost temperature was estimated using Carbajo's correlation and critical heat flux temperature using revised Jens and Lottus correlation. Prediction made using the proposed correlation was compared with the experimental data and error in chilldown time estimate compared to the experimental value was reported to be less than 9%.

Jin et al. [32] conducted experiments with LAr using a stainless steel test section of outer diameter 12.7 mm, inner diameter 10.2 mm, and length 7 m provided with multi layer insulation to study the chilldown performance. Experiments were carried out for 18 test conditions with different mass flux in the range of 33.2 to 79.5 kg/m^{2}s. Inner wall temperature and heat flux were estimated by inverse heat transfer technique using the measured outer wall temperature and comparison was made with the heat flux values estimated for similar mass flow rate conditions with LN_2. It was reported that heat flux values reported with LN_2 were higher as compared to the values reported for argon and this was attributed to lower viscosity of LN_2 as compared to LAr and higher Re for LN_2 flows. Chilldown time and cryogen consumption were also reported to be higher with LAr as compared to LN_2 for the same reason of lower heat flux with the former. A new set of empirical relations were proposed for estimating the critical heat flux, temperature at critical heat flux point, minimum heat flux and temperature at minimum heat flux point. Predictions made with the proposed correlations were reported to be closely matching with the experimental results.

Jin et al. [33] performed experiments with LOX and LN_2, employing a horizontally held stainless steel 316 test section of outside diameter 12.7 mm, inner diameter 10.2 mm, and length 7m, insulated with 21 mm thick rubber foam. Chilldown was studied for fifteen different test conditions with LOX and ten different test conditions with LN_2. Mass flux of LOX simulated was in the range of 15.9 to 75.9 kg/m^2s. Wall heat flux was estimated by inverse heat transfer technique using the measured outer wall temperature data. Parasitic heat in-leak into the test section insulation by convective mode from ambient was estimated using the Churchill-Chu correlation and conductive heat in-leak into the test section inner pipe from the insulation were also considered. Based on the experimental data, it was reported that the wall heat flux in film boiling regime was higher for higher mass flux condition. Also heat transfer coefficient showed an increasing trend with reduction in wall superheat. An one dimensional model was proposed for estimating the wall heat transfer coefficient and chilldown time. New correlations were proposed for estimating the heat transfer coefficient for single vapour phase heat transfer and film boiling regime. In the expression for heat transfer coefficient in film boiling regime, effect of vapour quality was introduced using the Miropolski's correlation for estimation of two phase Re. New correlations were also proposed for estimation of critical heat flux and minimum heat flux points. The boiling regimes were decided based on the estimates for inner wall temperature and critical and minimum heat flux points. Heat flux in transition boiling regime was estimated assuming a linear fit between the minimum heat flux and critical heat flux points. Whereas in the nucleate boiling regime, heat flux was estimated considering a linear fit between the critical heat flux point and the wall temperature that defined the onset of nucleate boiling (assuming nucleate boiling heat flux to be zero at this point). Wall temperature predictions made using the proposed correlations were reported to be matching well with the experimental data. Chilldown time predicted were also showing a good match with experimental results and the deviation reported was well within $\pm 10\%$.

Chilldown performance of a cryogenic feedline was evaluated experimentally by Mohammed et al. [34] using a test section of outside diameter 7.94 mm, wall thickness 0.81 mm, 500 mm length, insulated with 56 mm thick polyurethane foam. During the experiments performed with the test section held horizontal, mass flux of LN_2 was varied from 66-102 kg/m^2s. Bottom wall temperature measured had clearly captured the three boiling regimes. It was mentioned that transition from film boiling to transition boiling occurred at a higher temperature with increase in mass flux, in agreement with published literature. Burgraff correlation was used to estimate the tube inner wall temperature and heat flux. It was mentioned that during the initial stages of chilldown, heat transfer coefficient was higher for higher mass flux condition and this was attributed to higher fluid velocity. Critical heat flux was also reported to be higher with higher mass flux. Experimental values of critical heat flux and minimum heat flux were compared with the estimates made using available correlations. Error in critical heat flux was reported to be within 30% for Mudawar correlation, whereas minimum heat flux estimates were largely differing from the experimental data. A new correlation was proposed for prediction of critical heat flux considering the thermal properties of quenched wall. It was reported that the proposed correlation matched the experimental results and the deviation was well within $\pm 30\%$.

Influence of higher wall thickness on chilldown performance was studied by Wang et al. [35]. In the experiments performed with LN_2, chilldown performance was evaluated on test sections of two different thicknesses of 2 mm and 5 mm, both having 14 mm inner diameter and 1000 mm length. They were made of stainless steel material and were provided with 70 mm thick pearlitic sand padding insulation. Inlet Re simulated was in the range of 4500 to 45,000. With increased Re, Leidenfrost temperature was reported to be increasing, bringing in a reduction in the film boiling regime. Increase in critical heat flux and a remarkable reduction in chilldown time were also reported. With regard to chilldown efficiency, it was reported that in experiments with low Re, chilldown efficiency decreased with increase in Re. Whereas in experiments with higher Re, it showed a stable value or a marginally increasing trend. Chilldown efficiency was reported to be lower with 5 mm thick tube.

2.5 Experimental studies to understand the influence of gravity on chilldown performance

Yuan et al. [36] studied experimentally the chilldown performance under terrestrial and microgravity conditions of 10^{-4} to 10^{-5}g. Difference in flow pattern prevailing under those two conditions were also captured through visualisation. Test section employed was a vacuum jacketed pyrex glass tube of outer diameter 15.8 mm, inner diameter 11.1 mm, and length 25.4 cm. The vacuum jacket had quartz windows to enable visualisation. Microgravity experiments were performed in a drop tower of 15.25 m height capable of simulating 1.7 s of free fall. Authors had brought out the wall temperature and heat flux profiles observed under terrestrial conditions and it was reported that the boiling regimes seen were very similar to pool boiling. Minimum heat flux values predicted using available correlations were very close to the experimentally observed values, whereas critical heat flux predicted by published correlations were very high as compared to experimental results. It was mentioned that this difference could be attributed to the fact that correlations were developed based on pool boiling studies. Flow structure observed under terrestrial and microgravity conditions were also described. Visualisation studies in terrestrial experiments had shown that during the film boiling regime, two phase flow in the form of vapour core with scattered small droplets or inverted annular flow prevailed in the test section. This was followed by quenching of the bottom wall with the heat transfer regime changing to transition and nucleate boiling, ending up with liquid phase convective heat transfer. Whereas under microgravity conditions, chilldown rate at the bottom of the test section was reduced by 0.66 to 0.90 times the values reported for terrestrial conditions. Liquid filaments were drawn into the core and replaced by low thermal conductivity vapour.

Results of experiments conducted by Yuan et al., both under terrestrial and microgravity conditions, were studied by Chung and Yuan [37], to address the effect of gravity on chilldown performance. In the experiments performed under terrestrial conditions with horizontal orientation of test section, heat transfer process at the bottom of the tube included film boiling, transition boiling and nucleate boiling, whereas it was mainly due to convection by superheated vapour at the top of the tube. The flow structure changed from dispersed flow to inverted annular flow and then to stratified or wavy flow as chilldown progressed. Dependence of heat flux on wall superheat was reported to be very similar to pool boiling. It was stated that effect of gravity was predominant for low mass flux conditions. Heat flux and rewetting temperature were reported to be lower under micro gravity conditions as compared to terrestrial condition. This was mainly attributed to liquid being drawn more into the core and thickening of vapour film at the tube bottom. Heat flux at the top of the tube was less affected, since it was cooled only by vapour phase.

2.6 Influence of test section orientation on chilldown performance

Though a large number of studies were carried out for horizontal and vertical flows, studies done to understand the influence of feedline orientation are not many. Effect of test section orientation and mass flux on chilldown performance was evaluated experimentally by Johnson and Shine [38] employing a stainless steel test section of 22 mm outer diameter, 1 mm wall thickness, and 2 m length insulated with poly-isocynurate foam, using LN_2 as simulant fluid. Mass flux employed during the experiments was in the range of 245-375 kg/m^2s. It was reported that the bottom wall temperature data showed signature of all the three boiling regimes viz; film boiling, transition and nucleate boiling, for all the mass flux conditions studied. The temperature drop in transition boiling was faster in experiments with higher mass flux as compared to lower mass flux conditions. Sensitivity of mass flux on chilldown performance was more predominant at lower mass flux conditions and chilldown time was reported to be lesser with higher mass flux. Effect of test section orientation on chilldown was studied by varying the inclination from horizontal to 15° upward in steps of 5°. It was reported that increase in test section upward orientation up to 10° resulted in chilldown improvement, whereas with 15° inclination, slight increase in chilldown time was seen, implying that there could be an optimum inclination to minimize the chilldown time. Heat flux values were estimated by inverse heat transfer technique using the measured wall temperature data and it was reported that peak heat transfer coefficient compared well with the values reported by Jackson et al.. It was mentioned that during the initial stages of chilldown, heat flux was higher for higher mass flux conditions. Heat flux was higher at upstream locations along the length of the test section, as compared to downstream ones and peak heat flux values observed were higher for higher mass flux conditions tested. Minimum heat flux predicted by Zuber correlation was reported to be matching with the experimental data, whereas critical heat flux estimated by Katto's correlation was reported to be very high as compared to experimental data. It was mentioned that the mismatch could be due to the fact that Katto's correlation was derived based on electrically assisted heat flux controlled experiments whereas the experiments performed and used for comparison were temperature controlled ones.

Darr et al. [39] experimented with a stainless steel SS304 test section of outer diameter 1.27 cm, inner diameter 1.168 cm, and length 57.2 cm, simulating vertical flows with LN_2 as test fluid. 54 chilldown experiments were conducted for different inlet conditions in terms of pressure, flow rate, subcooling etc. It was also mentioned that pressure fluctuations were observed with low to medium flow rate conditions and were almost eliminated at higher flow rates. Chilldown time was reported to be inversely proportional to the mass flow rate and mass flow rate increase of around 470% had resulted in a chilldown time reduction of around 58%. Burgraff technique was used to estimate the heat flux and inner wall temperature, using the measured outside wall temperature. Heat flux values estimated for film boiling regime were much lower as compared to those computed for transition and nucleate boiling regimes. Upstream stations were reporting higher heat transfer rate as compared to locations downstream. Mass flow rate was reported to be having the largest impact on heat transfer, higher the mass flux, higher was the heat transfer coefficient. Under high mass flux condition, heat transfer coefficient was seen to be increasing with pressure. Re-wetting temperature was reported to be strongly influenced by mass flux and inlet subcooling. It was found to be higher with higher mass flux and higher level of subcooling.

Darr et al. [39] conducted experiments employing a stainless steel test section of outside diameter 1.27 cm, inner diameter 1.168 cm, and length 57.2 cm, held inside a vacuum chamber to study the influence of inclination, mass flux and subcooling on chilldown performance. Tests were done for horizontal and upward and downward inclination of 30°, 45°, 60° and 90° with respect to horizontal. Experiments were performed with LN_2 as the simulant fluid and mass flux simulated was in the range of 5 to 1700 kg/m^2s. Equilibrium quality and subcooling were varied in the range of -0.13 to 0.4 and 0 to 14K respectively. Based on the experimental data, it was reported that for off vertical flows, the difference between surface temperature measurements at the bottom, top and sides was quite large for low mass flux conditions, whereas the measurements were much closer in high mass flux flows. At low to moderate flows, average temperature at a cross section reduced at a faster rate in upward flows, at slightly lesser rate in horizontal and still lesser rate in downward flows. Chilldown was observed to be independent of flow direction in experiments with highest flow rate tested. Burgraff correlation was used to estimate the inner wall temperature and heat flux. Heat transfer coefficient for horizontal, inclined and declined flows were bounded by the values observed in upward and downward flows. Though for upward flows, the heat transfer coefficient was observed to be increasing with mass flux as expected, the trend was different for downward flows with low mass flux. This was attributed to buoyancy effect, driving the vapour flow in the reverse direction. With lower mass flux, heat transfer coefficient was reported to be almost constant and not varying with increase in mass flux. As the mass flux increased, the heat transfer coefficient in vertical upward flows was observed to be increasing steadily, whereas in vertical downward flows, large swings were seen and the oscillations vanished in test cases with highest mass flux. Large variation observed in heat transfer coefficient was attributed to larger velocity difference between the two phases. Based on the experimental data, a new set of correlations were proposed for film boiling, transition and nucleate boiling regimes. The correlations proposed to estimate the heat transfer coefficient in film boiling regime considered the buoyancy effect at low flow rates, forced convective mode heat transfer under moderate flow rate conditions and heat transfer due to droplet to wall interaction at high flow rates. Whereas in the nucleate boiling regime, with wall superheat in the range of 8-10K to around 30K, the heat transfer coefficients values observed were much higher than liquid phase heat transfer coefficient. The newly proposed correlation for nucleate boiling considered Jakob number and Re to augment the liquid phase heat transfer. It was also reported that the prediction made using the proposed correlations matched reasonably well with the experimental values.

Experimental studies were carried out by Shukla et al. [40] on two stainless steel 304 test sections, S1 having 13.5 mm inside diameter and 1.2 mm wall thickness and S2 with 21 mm inside diameter and 2 mm wall thickness. Both the test sections had 1440 mm length and were insulated with polyurethane foam. Experiments were carried out for two different mass flow rate conditions of 10g/s and 66g/s, with LN_2. Flow rate was measured using a weighing balance. Surface temperature measurements were made at five different stations along the length of the test section, both at the top and bottom. Effect of test section inclination was studied by orienting the test sections at 5°, 10°, 20° and 30° with respect to horizontal. It was reported that in experiments with S1 test section, chilldown time reduced with increase in inclination, reached a minimum between 10° and 20° and started increasing thereafter. Whereas in experiments with 21 mm inside diameter, chilldown time continued to decrease up to 30° inclination and hence it was mentioned that the optimum inclination could be beyond 30°. Thus the optimum inclination for minimum chilldown time was reported to be a function of line diameter as well. It was also mentioned that in experiments performed with S2 test section with mass flow rate of 10g/s, chilldown was achieved at downstream station first ahead of upstream and this was attributed to unstable liquid to vapour interface and premature rewetting of the tube wall. This was not observed during experiments performed with higher mass flow rate of 66g/s. The authors proposed a model, similar to the one proposed by Darr et al., for prediction of wall temperature profile during chilldown. Results of experimental data were compared with the prediction made using the one dimensional model. Though the results showed a good match for the experiments with lower flow rate with S1 test section, large mismatch was reported for experiments with higher flow rate with S1 test section and for tests performed with S2 test section. It was mentioned that this was due to the fact that Bromley's correlation was predicting similar heat transfer coefficient values, both for low and high mass flux conditions.

2.7 Experiments with coatings, pulsed flow etc. to achieve improved chilldown performance

Attempts have been made by several authors to imporve the chilldown performance by employing low conductivity nonmetallic coatings or pulsed flows. Cowley et al. [41] studied experimentally the influence of different types of low conductivity coatings on heat transfer. Experiments were performed with cylindrical specimens of 9.5 mm diameter and 25 mm length, made of different materials like aluminium, brass, copper, steel etc. with coatings like clear varnish, asbestos, vaseline etc. of varying thickness in the range of 0.10 to 0.82 mm. Results were compared with bare specimens to capture the influence. It was reported that in the presence of low conductivity vaseline coating of 0.1 mm thickness, cooling time reduced to almost one fourth as compared to uncoated specimens and with further increase in coating thickness, the cooling time showed a slowly increasing trend.

The phenomenon responsible for higher heat transfer rate and improved chilldown in the presence of nonmetallic coatings was explained by Manson [42]. It was mentioned that in the presence of nonmetallic coating, periodic formation and departure of bubbles would take place from the antinodes, leading to liquid ingress, large fluctuations in the heat transfer process and formation of cold spots on the coated surface. The coated surface temperature would then fall to a low temperature locally to destabilize the vapour film and permit the liquid to wet the coated surface. This would result in highly localized enhanced heat transfer and improved chilldown performance.

Moreaux et al. [43] performed quenching studies with LN_2 using Nickel cylinders coated with a polymeric resin to demonstrate a concept that "larvate boiling", an intermediate mode between film boiling and nucleate boiling, was resulting in enhanced heat transfer and improved chilldown performance. It was reported that chilldown improved with coating thickness upto 90 μm and slowed down with higher thickness of 200 and 500 μm. It was mentioned that this larvate boiling is due to the alternating effect of wetting and non-wetting of the surface and this was attributed to the low effusivity of the coating. Experiments were performed using zirconium oxide coated nickel samples with water and LN_2 as simulant fluids, to capture the larvate boiling phenomenon. It was also demonstrated that with a thin layer of silver applied on top of the insulating layer, the cooling time was almost at par with the bare samples.

Experiments to evaluate the concept of early intermittent liquid wetting in the presence of a nonmetallic coating, the phenomenon responsible for enhanced heat transfer and faster chilldown, were performed by Kikuchi et al. [44]. Experiments were done with a 3 mm thick copper plate coated on one side with 14-144 μm thick Teflon coating. The reverse side of the plate was held in tight contact with acrylic plate to maintain adiabatic condition. Copper plate temperature was measured using a copper-constantan thermocouple, buried into a groove on its back side and soldered. The test specimen was vertically submerged into LN_2 and temperature data was recorded. Based on the experimental studies performed with bare and coated samples, it was reported that with thin coating, localised transition boiling phenomenon was observed with a wall superheat of 35K, when most of the region in the bulk surface was at a superheat of 105K. With thicker coating, similar phenomenon was observed, when bulk of the surface was around 149K. A theoretical model was proposed to explain the phenomenon of rapid cool down observed in the presence of an insulating layer. A good match was reported for the minimum film boiling temperature predicted by the model as compared to the experimental data.

Dreitser [45] studied the influence of flouroplastic and enamel coatings on the cooling time and film boiling crisis point. It was reported that coating thicknesses in the range of 0.04-0.1 mm enhanced the heat transfer by 2-3 times, reduced the chilldown time by 3 times and increased the film boiling crisis point, reducing the film boiling regime.

Chung et al. [46] conducted experiments to evaluate the effect of pulsed flow on transient temperature history of metal tubes during quenching process. Studies were carried out with tubes coated with low thermal conductivity Teflon layer, to study the enhancement achieved in combination with pulsed flow. Thickness of the coating employed was 64.8μm. Tests were performed with 304 stainless steel tube of 1.27 cm outer diameter, 1.168 cm inner diameter, and length 57.2 cm, held in horizontal orientation. The test section was housed inside a SS316 vacuum chamber to minimise the parasitic heat in-leak into the system. Experiments were performed for three different inlet pressure conditions, six different periods ranging from 0.5-5s and four different duty cycles ranging from 20% to 80%. It was reported that chilldown efficiency increased and coolant consumption decreased with reduction in duty cycle as compared to the reference case of continuous flow. Improvement was maximum with 20% duty cycle, chilldown efficiency improved by 65.77% and coolant consumption reduced by around 38%. With Teflon coated tube, both chilldown time and efficiency were found to be considerably improved. Reduction of cryogen consumption by around 57% was reported with teflon coating as compared to bare test section. Chilldown efficiency was reported to be higher for lower inlet pressure condition of 30psig as compared to the other two conditions of 60 and 80psig evaluated.

Experiments with uncoated and tubes coated with Teflon were conducted by Xu et al. [47] to study the effect of non-conductive coating of varying thickness on chilldown performance. Test section was made of polyurethane insulated 316L stainless steel tube of 8 mm outer diameter, 6 mm inner diameter and 200 mm length. Performance was evaluated with three different teflon coating thicknesses of 43μm, 100μm and 157μm. A significant reduction in chilldown time was observed in the presence of Teflon coating and reduction achieved was higher at around 74-78% with 157μm coating thickness as compared to bare tube. Based on the experiments, it was concluded that the presence of coating reduced the chilldown time considerably. Chilldown efficiency was also reported to be improving substantially from around 8-9% to around 54-62%, almost a six fold increase. It was also highlighted that though the chilldown process with bare line passed through film boiling to transition and then nucleate boiling as in a pool boiling study, with teflon coated tube, it entered transition boiling directly followed by nucleate boiling and wall temperature reached the steady state quickly. Heat transfer coefficient at the tube inner wall was computed using the correlation proposed by Darr et al. and the estimates were found to be closely matching with the experimental data.

Experiments were conducted by Nguyen et al. [48] using a cylindrical vessel with thick bottom section, coated with teflon coating of different thicknesses viz; 20, 50,100, 150, 200, and 300 μm to understand the influence of non-conductive coating on chilldown performance. Based on the experimental data, it was reported that the chilldown time was minimum for 100 and 150 μm Teflon coating and with higher coating thickness of 200 and 300 μm thickness, chilldown time was higher. It was mentioned that an optimum coating thickness of 100-150 μm resulted in early transition from film boiling to nucleate boiling and thereby faster chilldown. Heat flux estimation had shown that lower coating thickness in the range of 20-50 μm covered all the three boiling regimes, whereas with higher thickness of 100, 150, 200, and 300 μm, the liquid pool was in nucleate boiling almost from the beginning. Phenomenon of intermittent solid to liquid contact, as proposed by Kikuchi et al. was mentioned to explain and match the wall temperature profile observed during film boiling regime, with coating thickness upto 100 μm. Time averaged thermal resistance estimated had shown a minimum value corresponding to 150 μm coating thickness, again indicative of optimum performance. Optimum coating thickness was estimated adopting the approach proposed by Jagga et al. and it was reported the value was found to be significantly higher. Hence, a different approach was proposed with the optimum value defined as the coating thickness that would bring down the surface temperature to Leidenfrost point at the first instance of solid to liquid contact. Coating thickness estimated adopting this approach was reported to be giving a better match with the experimentally observed value.

Hartwig et al. [49] conducted experiments with three stainless steel test sections having an inner diameter of 1.27 cm, wall thickness 0.051 cm, and length 0.914 m viz; a bare one and the other two with FEP coating. Of the two coated tubes, one had 4 layers and the other had 7 layers of coating. Experiments were performed under terrestrial and micro gravity condition of 0.05-0.38g with continuous mode and pulsed mode of chilldown to evaluate the chilldown performance. LN_2 was used as test fluid and by varying the supply pressure, a wide range of mass flux and Re were simulated. Chilldown trends associated with changes in flow conditions caused by pulsed flow, coating and Re were reported to be consistent under terrestrial and microgravity conditions. In experiments performed with continuous flow at low to moderate Re, chilldown performance was reported to be higher under 1g condition for bare tube as compared to microgravity condition. It was mentioned that the performance was expected to be similar at high Re. In the case of tests with coated tube with continuous flow also, the performance was better under terrestrial as compared to low gravity condition. Further with pulsed flow, both with bare tube and coated tube, chilldown performance was better under terrestrial condition. It was also reported that the performance gain observed with higher Re was getting reduced under microgravity, as compared to terrestrial condition. Among the test conditions evaluated, chilldown was reported to be optimum for coated tube with pulsed flow at shorter duty cycles and low Re.

2.8 Numerical studies to capture the flow structure and chilldown performance

Apart from these experimental studies, very few numerical studies have been also performed in an attempt to improve the understanding on the cryogenic chilldown process. Chilldown process of a vertical test section with LH_2 was studied numerically by Hartwig and Vera [50] using the General Fluid System Simulation Program (GFSSP) software. Test section pipe was modelled using solid nodes and network connectors were modelled to connect to the nodes in fluid domain. Dittus Boelter equation was used to estimate the heat transfer for gas, liquid and two phase flows with suitable correction for two phase flow Re and Nu using Miropolski's correlation. Seven test cases were run and the simulation results were compared with experimental data. Though a good match was reported for the wall temperature for high flow rate cases, match was not so good for moderate and low flow rate conditions. Also, it was mentioned that the fluid temperature could not be predicted correctly by the model.

Guerrero et al. [51] modelled the experimental conditions reported in published literature and performed numerical simulations to capture the flow structure in vertical upward flows using both Eulerian and VOF models. Six different inlet velocity conditions for liquid and gas phases were simulated. Void fraction data from experiments was used for model validation. Number of cells was varied from a minimum of 43,400 to a maximum of 4,15,140 to assess the error observed and computation time. As the results obtained were consistent with coarser mesh, runs with Eulerian model were performed with 43,400 mesh cells. Whereas VoF runs were performed with a finer mesh with 4,15,140 cells. It was reported that Eulerian model demanded more computation time as compared to VOF model for the same number of mesh cells. VoF model had captured the flow structure more closely as compared to Eulerian model. Void fraction predictions by both the models were reported to be matching well with the experimental results for low void fraction cases, whereas for high void fraction cases, both the models had shown deviations from the experimental data.

Numerical simulations were performed by Umemura et al. [52] to capture the wall temperature, quality and flow structure in experiments carried out with vertical test sections. STAR-CCM+ software was used for the simulation and VoF based modelling technique was adopted. Mass, momentum and energy conservation equations were simultaneously solved and phase change was handled through a Heaviside function using two convection equations for gas and liquid phases. Antoine's equation was used to estimate the saturation temperature of cryogen and latent heat was estimated using the Clausius- Clapeyron equation. Bubble formation, bubble growth and phase change rates were modelled to capture boiling at the wall. Model validation was carried out using the LH_2 experimental data of Hartwig et al. for a vertical test section of outer diameter 12.7 mm and inner diameter 10.2 mm. A good match was reported for fluid and surface temperature measurements with experimental results.

Pesich et al. [53] also carried out numerical simulations of a complex geometry using START-CCM+ software to evaluate the wall temperature profile and flow features. Simulations were done, both for terrestrial and low gravity conditions and compared with experimental data. Axisymmetric model was used taking advantage of the symmetry. Simulations were performed using Eulerian multiphase and VOF models. Piece wise correlations were used for the different boiling regimes to estimate the wall heat flux in VOF model. Phase change was modelled using an empirical constant tuned to match the experimental results. Whereas in Eulerian model, the heat flux was calculated as a combination of convection, evaporation, and quench components. Convective component was estimated based on near wall fluid properties. Evaporative component had factored in terms such as nucleation site density, bubble departure diameter, and frequency. Quench component was to account for the liquid rushing in to replace the departed bubble. This was treated as a function of the time elapsed between bubble departure and nucleation of next bubble. Simulations were performed using both the models for 1g condition, whereas for low g condition, simulation was done only with VOF model. Temperature profile was reported to be captured well by both the models. However, it was mentioned that only the Eulerian multiphase model could capture the flow field in dead segments, closely matching the experimental results.

Kunniyoor et al. [54] carried out modelling studies of a horizontally held LH_2 feedline to evaluate the chilldown and heat transfer characteristics. An one dimensional model was proposed to estimate the wall temperature profile and the experimental data of Brennan et al. were used for model validation. Test section and fluid domain were discretised as nodes. The model was simplified neglecting the temperature gradient around the circumference. Transient mass, momentum and energy conservation equations were solved to capture the flow field. Dittus Boelter correlation was used to estimate single vapour phase forced convective mode heat transfer. Groeneveld's correlation was used for heat transfer prediction in film boiling region and Darr's correlation for transition and nucleate boiling regimes. Leidenfrost temperature estimated using Darr's correlation or critical temperature was used to switch from film boiling to transition boiling. Two phase pressure drop was estimated using Friedel's correlation. Five experimental cases were run and results were compared. It was reported that trend in wall temperature and pressure transient matched well with experimental results. Predominant modes of heat transfer for the cases studied were reported to be forced convection and film boiling. Complete chilldown was achieved only in experiments performed with subcooling. During the initial phase of chilldown, heat flux at locations near to inlet were higher as compared to downstream locations, whereas at far away locations, the situation was reverse. This was attributed to forced convective mode of heat transfer. Chilldown time was reported to be shorter with higher inlet pressure.

2.9 Conclusion on the aspects addressed in published literature and assessment on gap areas

As can be seen from published literature, there are several studies done to understand the chilldown performance for horizontal and vertical test sections and to estimate the wall heat flux using the measured wall temperature data. A number of correlations and methods have also been proposed to estimate the heat transfer coefficient and wall heat flux for the boiling regimes encountered during chilldown. However, studies to understand the influence of varying upward and downward orientations of test section are not many. Moreover, in the experiments performed, the inner diameter and length of the test section were limited to 11.68 mm and 572 mm respectively, whereas in rocket engines, the lines are expected to be of bigger size, both in terms of diameter and length. Visualisation studies performed so far are limited to horizontal and vertical flows only and studies to capture the flow structure in experiments with varying upward and downward orientations are absent. Studies are not attempted so far to understand the influence of thermal mass distribution of feedline on chilldown performance. Effect of metallic coating and influence of nonmetallic coatings on the chilldown performance using test sections of varying thermal mass have not been addressed so far. It is in this context, that the present experimental studies are taken up. Apart from this, numerical simulations are also attempted considering varying orientation of test section and results are compared with experimental data from the present study. Studies have brought out certain interesting findings that would help to better the understanding on the physics associated with the chilldown process. It would also help in improving the design of cryogenic systems towards achieving better performance. Details of the work carried out as part of the present study are brought out in the subsequent sections.

Chapter 3

Objectives and scope of the present study

3.1 Objectives

In cryogenic fluid transfer circuits forming part of ground storages as well as in flight stages with rocket engines, feedline routing can take different orientations, depending on the relative position of various subsystems involved. A good understanding of the influence of feedline orientation on chilldown performance is essential to optimise the relative position of subsystems, so as to achieve optimum chilldown performance. There is also a need to optimise the mass flow rate of the cryogen employed for chilldown and this is very much essential for onboard systems to minimise the propellant consumption during chilling. Influence of mass flux on chilldown performance is thus an important aspect that needs to be addressed from the mission point of view. Apart from this, there are methods like pulsed flow that can be adopted to reduce the cryogen consumption during chilldown, thereby contributing to payload advantage. Coating the inner surface of feedline with a non-conductive coating can also be solution to achieve early arrival of the liquid cryogen. Thermal mass distribution of the cryogenic subsystems like valves, pumps etc. or the relative location of entry of the cryogen into the feedline (for chilling) with respect to these lumped masses can also affect the chilldown performance considerably. Large circumferetial temperature differences observed during chilldown can induce thermal stresses and result in bowing of cryogenic feedlines. Methods that can be adopted to minimise the temperature gradients are also to be evaluated and understood. Literature survey carried out has brought out the gap areas that need to be addressed in more detail to have a better understanding of the entire chilldown process, mainly towards improving and optimising the design of cryogenic feed systems. The objectives of the present study are drawn up with due consideration to the above aspects with a focus to address experimentally and theoretically those specific areas like influence of feedline orientation, varying mass flux, thermal mass distribution of feedline, type of wall material, coatings etc. on chilldown performance of cryogenic feedlines. In summary, the main objectives can be stated as follows:

1. Understand the influence of feedline orientation and changes in mass flux of cryogen on wall

temperature and heat flux profile, chilldown time, chilldown efficacy etc.

2. Visualisation of flow structure encountered during the chilldown process, with the test section held at different upward and downward orientations, to understand the flow regimes and their effect on chilldown.

3. Bring in a better understanding on the physics associated with the pattern observed in bottom wall temperature profile in experiments with downward orientation, through numerical studies.

4. Study the effect of thermal mass distribution in the feedline on chilldown performance.

5. Capture the influence of thermophysical property of feedline material like thermal conductivity, coatings, surface finish etc. on chilldown performance.

3.2 Scope of work performed as part of the present study

Towards meeting the objectives stated above, an experimental set-up is designed and realised. Experiments are conducted and the results are analysed to bring out certain interesting findings. Major tasks performed as part of the present study are as follows:

1. Realisation of experimental setup.

2. Realisation of various test sections including their fabrication, application of coatings (wherever called for), fixing of RTDs and thermocouples, application of insulation etc.

3. Realisation of double jacketed borosilicate view glass for visualisation studies.

4. Carrying out initial trials for tuning of the facility and scheme for conduct of experiments.

5. Conduct of various experiments to meet the objectives of the study.

6. Data analysis and synthesis.

7. Carrying out 3D CFD simulations for a typical feedline configuration to bring in a better understanding on the probable reason for the pattern observed in bottom wall temperature profile in experiments with different upward and downward inclinations.

The approach for adopting different experimental and theoretical methods to meet the objectives of the present study is finalised after detailed evaluation. Experimental approach is adopted to evaluate the influence of feedline orientation on chilldown performance. Two test sections TS1 and TS2 having feedline inner diameters 30 mmm and 39 mm and 2m length are selected for the study.

Lines are insulated with poly-isocynurate foam, a material having a low thermal conductivity of around 0.018W/mK, to minimise the heat in-leak.

Selection of TS1 test section of 30mm inner diameter and 1mm wall thickness and TS2 of 42mm inner diameter and 1.5mm wall thickness is based on the fact that they represent the typical diameters and wall thickness adopted in rocket engine feed lines. Straight length of 2m is selected considering the typical configuration employed in rocket engines. Insulation thickness of 28mm is adopted for the test section considering similar values being used for rocket engine feed lines. The selected thickness would completely avoid moisture condensation on test sections during the experiments. This was ensured, as condensation and moisture ingress into the insulation can affect the transient heat in-leak into the test section.

Test section is instrumented with surface temperature measurements at top and bottom locations, at five stations along its length, to capture the wall temperature profile and chilldown performance with change in orientation. T type thermocouples are selected for surface temperature measurements, considering its high accuracy of ± 1.5K over the entire temperature range from ambient to LN_2 temperature. Apart from this, fluid temperature measurements are also introduced along the length of test section, to confirm the existence of stratified flow structure, during experiments with horizontal orientation of test section. Tests are performed for three different mass flux conditions, varying from 60 to 103 kg/m^{2}s, to understand the influence of change in mass flux on chilldown performance. Mass flux values selected for the study are in the range of 20-130 kg/m^{2}s adopted generally for rocket engine feedline chilling. Apart from this, as shown in Table 3.1, most of the studies performed so far are also for a similar range of mass flux conditions.

Table 3.1: Details of experimental studies conducted as seen in published literature

Sl. No.	Reference	Fluid employed	Range of mass flux studied (kg/m^{2}s)
1	Hu et al. [27]	LN_2	20-80
2	Darr et al. [39]	LN_2	61-1150
3	Jin et al. [30]	LN_2	19-49
4	Jin et al. [33]	LOX	15.9-75.9
5	Mohammed et al. [34]	LN_2	66-102

However, the above studies, except Darr et al. [39], had employed only horizontal and vertical orientations of test section and had used test sections of smaller diameter.

Experiments are conceived with test sections held at different upward and downward orientations of 10°, 20°, 30°, 45°, 60° and 90°, to cover the wide range of orientations encountered in practical application. Heat flux estimation by inverse heat transfer technique is adopted to have an assessment on the wall heat flux values experienced at the bottom and top locations. Number of cells considered within the wall of the test section and its insulation for heat flux estimation is finalised through a grid independence study. Finalised approach of 5 nodes within the test section wall and 28 nodes within the insulation is used for the study. Heat flux values estimated are compared to understand the influence of varying feedline orientation on wall heat flux.

Flow visualisation and numerical studies are done to bring in better understanding on the physics associated with the experimental observations with test sections held at different upward and downward orientations. A vacuum jacketed view glass made of borosilicate glass is designed and realised for carrying out the visualisation studies. Length of 250mm is selected for the view glass to provide sufficient length for flow structure visualisation. A sampling rate of 5000 frames per second is adopted for video imaging based on trial runs, to ensure adequate picture quality. In view of the issue of moisture condensation faced during initial experiments attempted with higher mass flux of 103 kg/m^2s, visualisation experiments are performed with a lower mass flux of 37 kg/m^2s. To evaluate the influence of feedline thermal mass distribution on chilldown performance, an experimental set up is suitably configured and realised. The set-up is also instrumented carefully to capture the influence precisely. Experiments are performed for two different mass flux conditions of 103 kg/m^2s and 37 kg/m^2s, to capture the influence of mass flux.

Apart from this, to study the influence of parameters like thermal conductivity of test section material, coatings, surface finish etc., an experimental approach is adopted. Evaluation sections of 250 mm length are suitably designed to simulate the required effect, with adequate instrumentation. Chilldown performance is studied for two different materials of construction namely stainless steel and copper alloy, with widely varying thermal conductivity, to evaluate the influence of thermal conductivity on chilldown performance. Effect of nonmetallic PFA coating on chilldown performance is evaluated for two different evaluation sections, having different wall thicknesses, to understand its influence on chilldown performance. PFA coating is selected as the nonconductive coating, considering its compatibility with LN_2 as well as its very low thermal conductivity (0.2W/m-K). The impact of providing a highly conductive coating on reducing the circumferential temperature gradient, is also studied by employing evaluation sections with two different thicknesses of copper coating. Cu coating is selected as the highly conductive coating considering its very high thermal conductivity and also the ease of its application on the test section by electro-chemical process. Apart from the above, effect of wall surface finish on wall wetting characteristics is also studied by carrying out experiments with surface finish varying from Ra0.3 to Ra8.4.

Test matrix for each experimental condition is finalised through a detailed thought process to cover a wide range of operating conditions and parameters. Consistency in experiments is confirmed through repeat experiments for identical conditions. Results of the experiments are analysed carefully to bring out certain interesting observations.

Details of the experimental set-up realised, experiments performed, results and findings of the study are brought out in the subsequent sections.

Chapter 4

Experimental set-up

As mentioned earlier, towards meeting the objectives of the present study, an experimental set-up consisting of a super insulated dewar for LN_2 storage, a regulated GN_2 supply for pressurisation and maintaining the required supply pressure and a feed system for supply of LN_2 at the required flow rate to the test section, are conceived and realised. This experimental set-up realised is used to conduct all the ***176*** experiments carried out to meet the objectives of the present study. Experiments carried out as part of the present study are summarised in Table 4.1.

Table 4.1: Test matrix

Sl. No.	Test description	Number of experiments performed
1	Influence of feedline orientation	69
2	Flow visualisation	11
3	Influence of thermal mass distribution	5
4	Influence of thermal conductivity coatings, surface finish etc.	34
5	Estimation of critical heat flux	57
	Total	***176***

Details of the experimental set-up realised, test sections employed for conduct of various experiments and test procedure are covered in the subsequent sections.

4.1 Description of experimental set-up

A schematic of the experimental set-up detailing the various systems and fluid components involved is shown in Figure 4.1. The set-up has a super insulated dewar of 380 litres storage capacity, to feed LN_2 to the test section during the experiments. LN_2 is filled into the dewar from the facility storage of 6,000 litre capacity, using a permanently laid foam insulated transfer line. During the experiment,

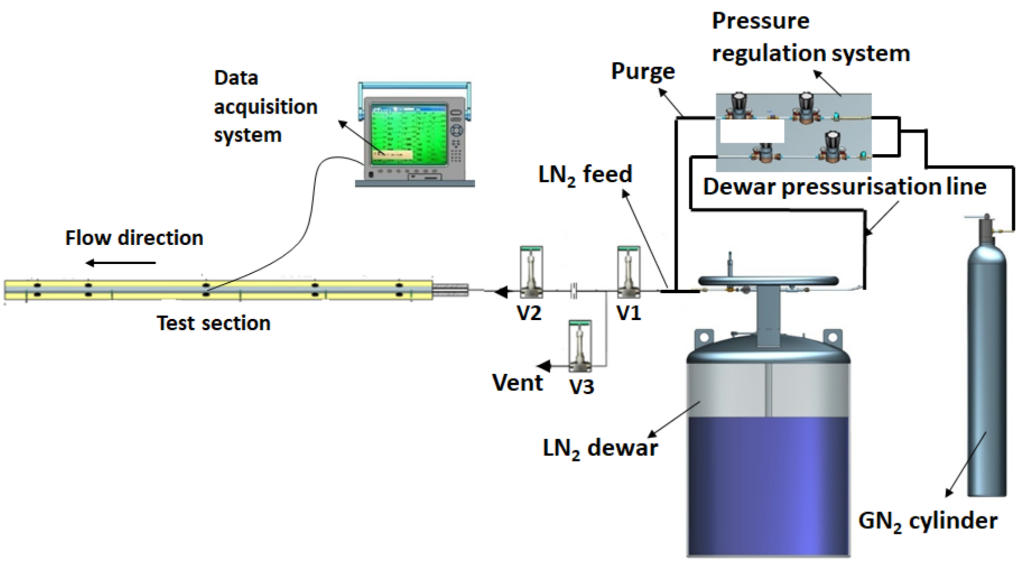

Figure 4.1: Schematic of experimental set-up

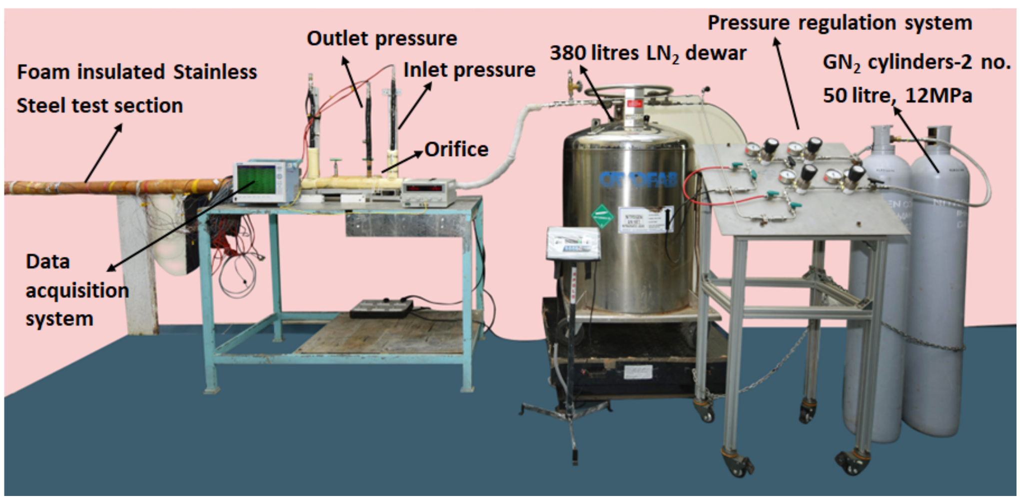

Figure 4.2: Photograph of experimental set-up

the required ullage pressure is achieved using a regulated GN_2 supply. GN_2 required for this purpose is stored in a 50litre cylinder at 12MPa pressure and fed to the dewar using a spring loaded regulator. LN_2 from the dewar is fed to the test section using a short foam insulated feedline of 10 mm inner diameter. Isolation valves V1, V2 and V3 are used to regulate the flow of LN_2 to the test section or vent circuit, as required. Required flow rate of LN_2 to the test section is achieved using a calibrated flow control orifice placed at the inlet to the test section.

Photograph of the experimental set-up realised and employed for the present study is shown in Figure 4.2.

In experiments with different upward and downward orientations of test section, the desired inclination is achieved by employing a preformed spool piece at the inlet to the test section, as shown in Figure 4.3.

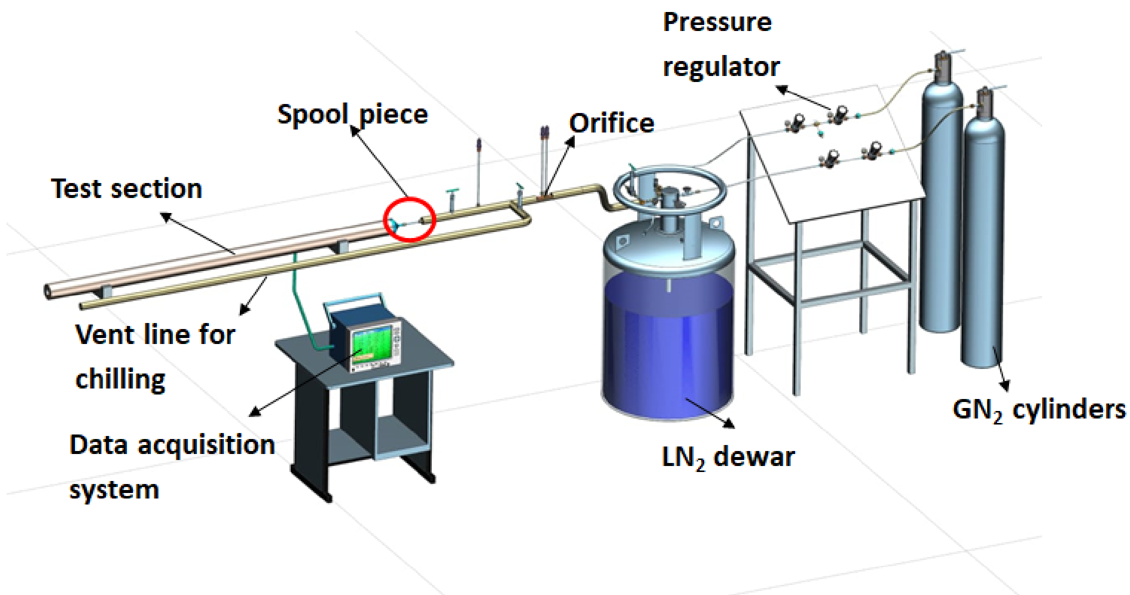

Figure 4.3: 3D view of experimental set-up

4.2 Description of test sections employed

As brought out earlier, in the present study, experiments are performed to study the influence of feedline orientation, thermal mass distribution, presence of metallic and nonmetallic coatings, surface finish, thermophysical property like thermal conductivity etc.. This demanded different types of test sections to be realised and employed to meet the desired objective of every set of experiments. Details of the various test sections employed for specific studies to meet the desired objectives are brought out in the following sections.

4.2.1 Experimental studies on the influence of feedline orientation and mass flux

The influence of feedline orientation and change in mass flux are studied using two test sections, TS1 and TS2. Test section, TS1 is of outer diameter 32 mm, inner diameter 30 mm, whereas test section, TS2 is of outer diameter 42mm and inner diameter 39 mm. Both the test sections are made of stainless steel AISI321 material and have 2 m length. Test sections are insulated with 28 mm thick poly-isocynurate foam. Insulation is first prepared as moulded foam pads, in the form of two symmetric halves, and bonded to the test section outer wall using an epoxy based adhesive. As a typical case, configuration of the test section TS1 is shown in Figure 4.4.

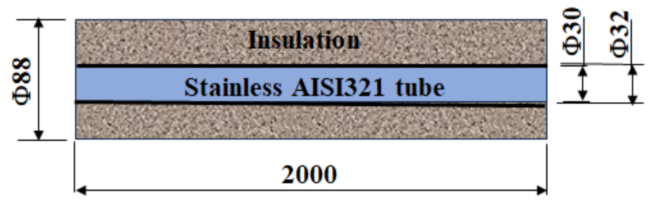

Figure 4.4: Configuration of test section TS1

Salient thermophysical properties of the test section materials at room temperature and LN_2 temperature are given in Tables 4.2 and 4.3.

Table 4.2: Thermophysical properties of Stainless steel AISI321 material at room temperature and LN_2 temperature

Sl. No.	Property	Specification	
		@ Room temperature	@ 77 K
1	Density (kg/m^3)	7950	
2	Thermal conductivity(W/mK)	16.69	8.18
3	Specific heat (kJ/kgK)	469.45	205.8

Table 4.3: Thermophysical properties of poly-isocynurate foam at room temperature and LN_2 temperature

Sl. No.	Property	Specification	
		@ Room temperature	@ 77 K
1	Density (kg/m^3)	45	
2	Thermal conductivity(W/mK)	0.018	0.008
3	Specific heat (kJ/kgK)	2009	638.7

4.2.2 Flow visualisation studies

Configuration of test section employed for flow visualisation studies is shown in Figure 4.5. Test section employed for flow visualisation has three sections viz; an inlet section, a double jacketed vacuum insulated view port for flow visualisation, which is placed just downstream of inlet section and an outlet section. Inlet section is of inner diameter 30 mm, 1 mm wall thickness, and 875 mm length, made of stainless steel AISI321 material and insulated with poly-isocynurate foam of 28 mm thickness. Outlet section is of 30 mm inner diameter, 1 mm wall thickness and 250 mm length.

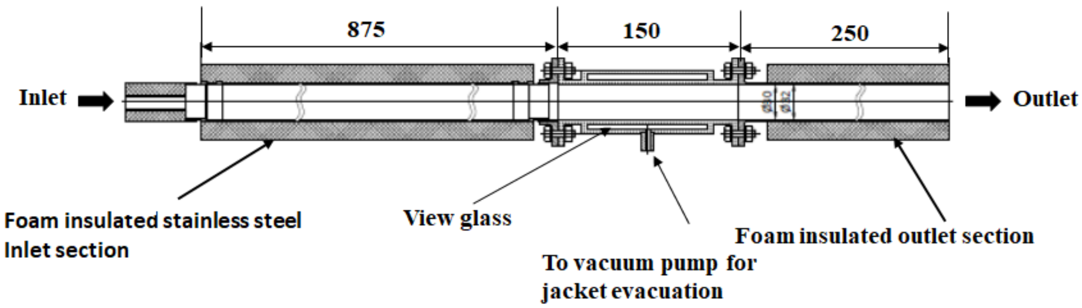

Figure 4.5: Configuration of test section employed for flow visualisation

View glass is provided with flanged interfaces to connect to the inlet and outlet sections upstream and downstream. Split and loose flanges are used to interface the view glass with upstream and downstream sections. These parts are made of Teflon to minimise the associated thermal effects. A calibrated flow control orifice of diameter 1.50 mm is placed upstream of the inlet section to control and achieve the required flow rate of LN_2 during the experiments.

View glass used for flow visualisation has an inner diameter of 30 mm and length 150 mm. It is made of borosilicate glass, which is a mixture of silica, boric oxide, alumina etc. View glass is conceived with a vacuum jacket to minimise the heat in-leak and associated moisture condensation, thereby ensuring good image quality. It is realised by manual blowing process. The vacuum jacketed section and end flanges are realised separately and fused to make it integral. The process of joining is done by locally heating the regions to be fused to a temperature of around 800°C, using a gas flame of liquified petroleum gas mixed with oxygen. After fusing, the unit is stress relieved at a temperature of 550°C for a duration of about 20-30 minutes. The end faces of the flanges are then ground using emery powders to achieve the required surface finish. Photograph of the view glass employed for flow visualisation is shown in Figure 4.6. During the experiment, the vacuum jacket of the view glass is evacuated and maintained at 1Pa vacuum, employing a vacuum pump.

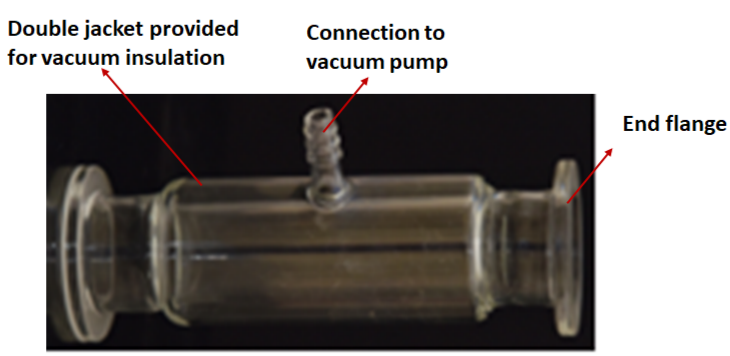

Figure 4.6: Photograph of view glass used for flow visualisation

4.2.3 Experiments to understand the influence of thermal mass distribution

Influence of thermal mass distribution of test section on chilldown performance is studied by employing three different configurations of test section viz; configurations 1, 2, and 3, as shown in Figures 4.7, 4.8, and 4.9. Feedline configuration-1 shown in Figure 4.7, is the same as the test section TS1 used for evaluating the influence of feedline orientation and has a thermal mass of 1.53 kg. Feedline configuration-2 is shown in 4.8. This simulates the condition in which the additional thermal mass is placed near to the inlet of test section. This additional thermal mass simulator is made of stainless steel AISI321 material, weights 4.05kg approximately and simulates the presence of lumped mass like valves, pumps etc.. Figure 4.9 shows the details of feedline configuration-3 that simulates a case in which the same additional thermal mass weighing 4.05kg is located near to the exit of the test section.

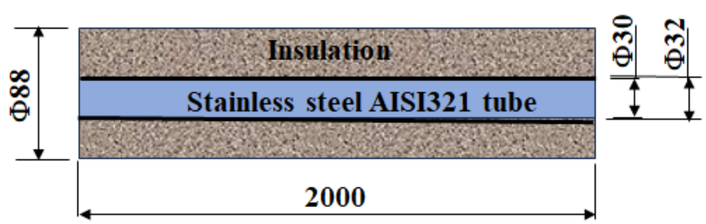

Figure 4.7: Feedline configuration-1, used for thermal mass distribution study, as reference for comparison

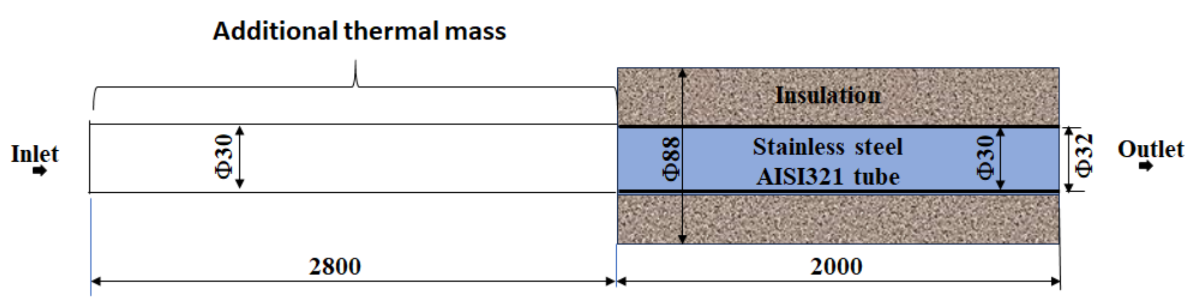

Figure 4.8: Feedline configuration-2 with additional thermal mass placed near to the test section inlet

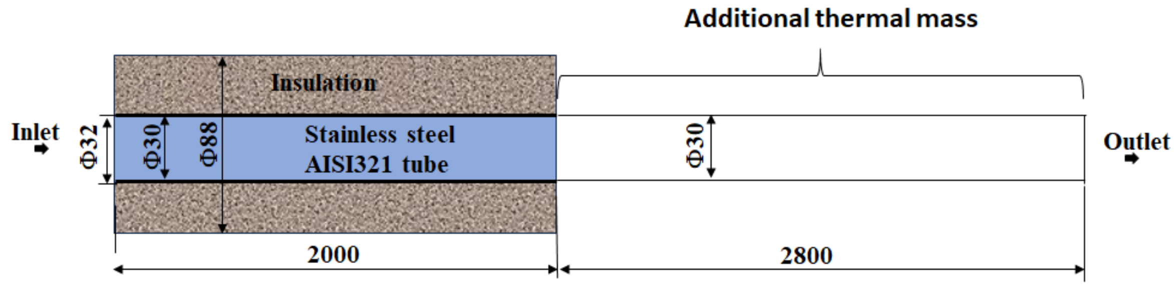

Figure 4.9: Feedline configuration-3 with additional thermal mass placed near to the test section outlet

4.2.4 Experiments to study the effect of thermal conductivity of test section material, coatings, surface finish etc.

Influence of parameters like thermal conductivity of test section material, coatings, surface finish etc. is studied using an evaluation section of 250 mm length, in which the influencing parameter is simulated. Effect of location on the influence of these sensitive parameters is studied by placing this evaluation section at two locations along the feedline of 2 m length viz; at 875 mm and 1500 mm from inlet. As a typical case, the configuration of test article employed for experiments with the evaluation section placed at 875 mm from inlet is shown in Figure 4.10.

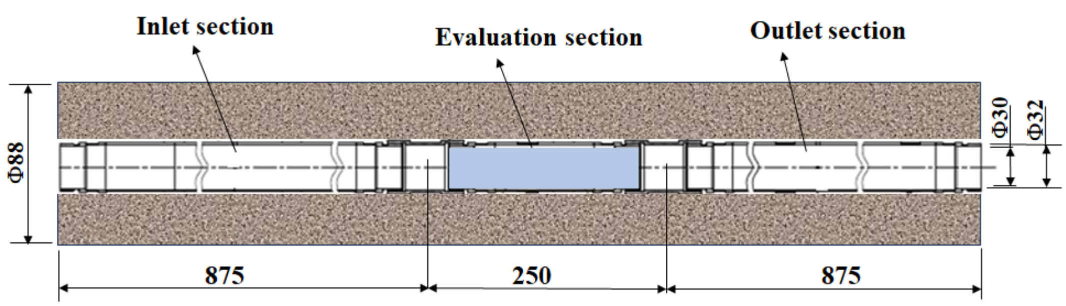

Figure 4.10: Configuration of test article employed to study the influence of thermal conductivity, coatings, surface finish etc

Test article employed has three sections viz; an inlet section, an evaluation section, which is placed just downstream of inlet section and an outlet section. Inlet and outlet sections are of inner diameter 30 mm, 1 mm wall thickness, and 875 mm length, made of stainless steel AISI321 material. Evaluation section is also of the same inner diameter of 30 mm and 250 mm length. Test conditions that need to be examined are simulated here. The following are the parameters simulated to study the influence on chilldown performance.

1. Thermal conductivity of wall material, studied by using materials having widely different

thermal conductivity, stainless steel and copper

2. Presence of high conductivity metallic coating (Copper coating)

3. Presence of nonmetallic coating (Perfluoroalkoxy Alkane)

4. Surface finish

Ten types of evaluation sections are realised, details of which are covered in the subsequent sections. All the three sections viz; inlet, outlet and evaluation sections are provided with poly-isocynurate foam insulation of 28 mm thickness to minimise the heat in-leak from ambient. As described earlier, the foam pads are bonded to the evaluation section outer wall using an epoxy based adhesive. The inlet and outlet sections are interfaced with the evaluation sections using teflon adapters to minimise the addition of thermal mass into the system. The evaluation sections employed are conceived, realised and inspected to ensure that they meet the desired objective. The manufacturing process adopted for realising the evaluation sections of various types are covered here.

Test article configuration employed for experiments performed with the evaluation section placed at 1500 mm from the inlet is also similar except for the changes with regard to lengths of the inlet and outlet sections; length of the inlet section is increased to 1500 mm, whereas length of the outlet section is reduced to 250 mm.

4.2.4.1 Evaluation section with high thermal conductivity material

The material selected to study the influence of thermal conductivity is Cu-Cr-Zr-Ti alloy, in view of its high thermal conductivity as compared to stainless steel AISI321 material. Thermophysical properties of the two materials are compared in Table 4.4.

Table 4.4: Comparison of thermophysical properties of stainless steel AISI321 and Cu alloy

Sl. No.	Thermophysical property	AISI321	Cu alloy
1	Thermal conductivity at room temperature, W/mK	16.69	279
2	Specific heat at room temperature, kJ/kgK	469.45	383
3	Density (kg/m^3)	7850	8950

A cross sectional view of the evaluation section made of Cu-Cr-Zr-Ti alloy is shown in Figure 4.11. It is realised from a forged rod by conventional machining route and provided with poly-isocynurate foam insulation to minimise the heat in-leak from ambient.

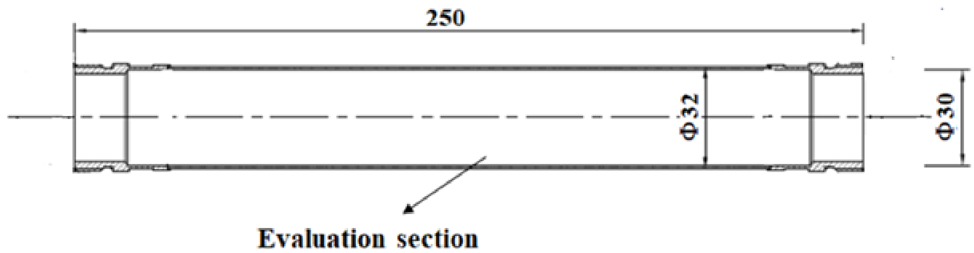

Figure 4.11: Evaluation section used to study the influence of thermal conductivity

4.2.4.2 Evaluation section with metallic copper coating of different thicknesses

The influence of metallic coating on chilldown performance is studied by employing copper coating on the inside surface of evaluation section. The performance is studied for two coating thicknesses viz; 100 μm and 200 μm. Bare evaluation section is realised by welding the end adapters made of stainless steel AISI321 material to a tubular section of inner diameter 30 mm and outer diameter 32 mm. Copper coating on inside surface of evaluation section is achieved by electroplating process. The required coating thickness is achieved by suitable selection of coating process parameters based on previous experience. To ensure that the required coating thickness is achieved in actual hardware, coating thickness is inspected and verified on annular specimens coated along with the evaluation section, as shown in Figure 4.12.

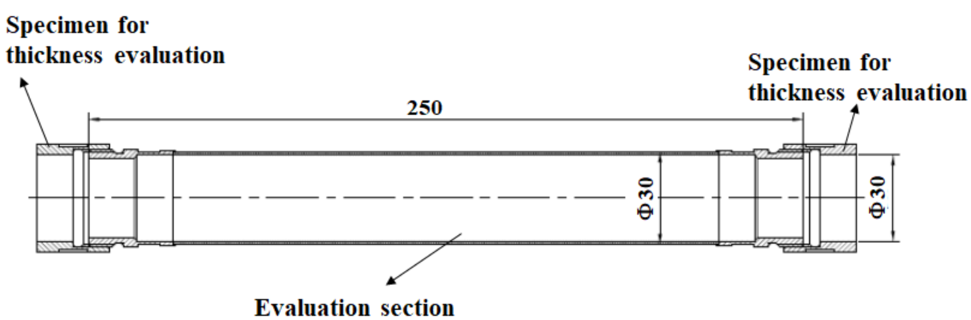

Figure 4.12: Evaluation section used to study the influence of metallic coating

4.2.4.3 Evaluation sections having different wall thicknesses with Perflouroalkoxy Alkane coating

To study the influence of non-conductive coating, the material selected is Perflouroalkoxy Alkane (PFA), which is very similar to Teflon, having a low thermal conductivity of 0.2W/mK. Performance is evaluated using evaluation sections having two different section thickness of 1 mm and 5 mm, both of 30 mm inner diameter. As mentioned for metallic coating, bare evaluation sections are realised first by welding the end adapters, on which PFA coating is applied in the form of multiple layers. PFA in the form of a slurry is poured into the evaluation section to be coated and tumbled to get a uniform coating on the inside surface. Excess slurry is then drained out and evaluation section is sintered to get a solid coating. The process is repeated multiple times to get the required coating thickness. Coating thickness achieved is inspected and verified using a 3 point micrometer on the evaluation section and the cylindrical specimens coated along with the actual sections employed for the present study. The cyindrical specimens are also put through a cut open study to reconfirm the coating thickness.

4.2.4.4 Evaluation section with varying surface finish

Effect of surface finish is studied by employing three evaluation sections having surface finish of Ra0.3, Ra3, and Ra8.4. Evaluation sections of varying surface finish are realised through an elaborate manufacturing process involving realisation of a tubular section, wire cutting to make into two equal halves, grit blasting, stress relieving and electron beam welding. A tubular section of inner diameter 30 mm, outer diameter 35 mm and length 190 mm, as shown in Figure 4.13, is realised first by conventional machining, from a rod of stainless steel AISI321 material.

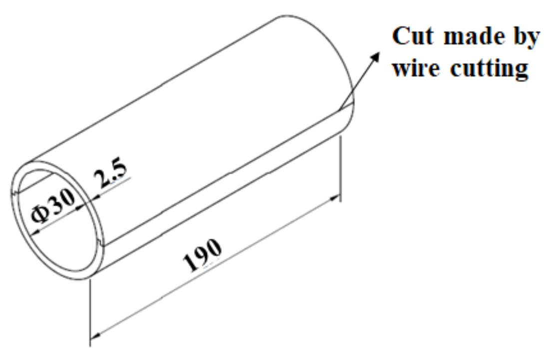

Figure 4.13: Tubular sections realised for evaluation of influence of surface finish

This is cut into two halves, along the length, by wire cutting process. Each of the two halves is subjected to electropolishing (for achieving a surface finish of Ra0.3) or grit blasting (for achieving a surface finish of Ra3 and Ra8.4).

Grit blasting can induce a large amount of stress in the material and can cause serious dimensional changes, posing difficulties in electron beam welding in the subsequent stage. To overcome this, the tube half is rigidly clamped in a fixture shown in Figure 4.14, during grit blasting and subsequent stress relieving. After grit blasting, to remove the stresses induced, stress relieving is

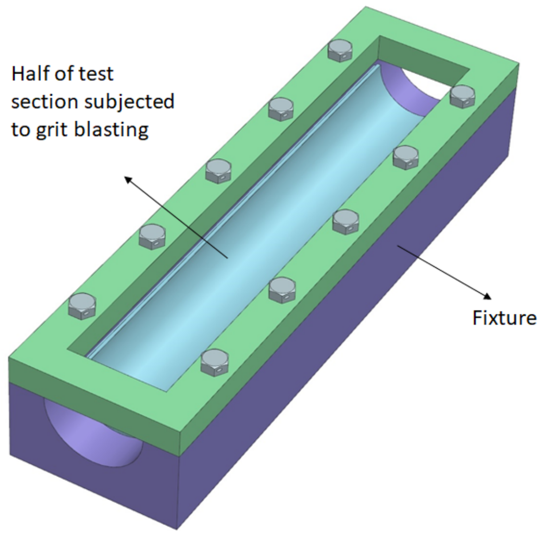

Figure 4.14: Fixture employed for grit blasting and stress relieving

performed, at 350°C for a duration of 60minutes. Surface finish achieved is measured using a taly-surf, for a length of 10 mm from either ends of both the halves and the average value is reported. Both the halves are then joined together by electron beam welding followed by end adapter welding to realise the complete test section.

4.3 Instrumentation and measurement uncertainty

In the present study, chilldown performance is evaluated by analysing the wall temperature and heat flux profile at various stations along the length of the test sections employed in the experiments. Towards this, test sections are equipped with temperature sensors to measure the fluid and wall temperature at different stations along the length of the test section. 100Ω Platinum RTD and T type thermocouples are used for fluid and surface temperature measurements. As mentioned earlier, cryogen flow rate to the test section is controlled using a calibrated flow control orifice placed at the inlet to the test section and the set-up is equipped with strain gauge type pressure sensors, of 0-0.5MPa range, to measure the pressure at orifice inlet, orifice outlet and test section inlet. During the experiments, these pressure and temperature values are recorded using a portable data acquisition system, at a sampling rate of 1 Hz or 10Hz, depending on the requirement. The instrumentation scheme to meet each of the objective is different in view of the test requirements and therefore details of scheme adopted are brought out in detail in the subsequent chapters, while explaining each of these experiments.

In view of the uncertainties associated with the surface temperature data due to measurement inaccuracy and scatter expected in various other parameters like thermophysical properties of test section material and physical dimensions of test section, there are uncertainties expected in the wall heat flux estimates. Also uncertainties are expected in chilldown efficiency parameter defined as CPI. A detailed assessment is made on the above and details are covered in section 5.5 of Chapter 5.

4.4 Test procedure

Experiments are performed following a standard procedure for media substitution of the supply line and test section and chilldown of the supply line. As part of test preparation, the test section and inlet feedline to the test section are media substituted by purging with GN_2. This process of purging and media substitution is an essential preparatory activity while handling cryogen, to avoid freezing of moisture, which can result in clogging at the orifice location, affecting the cryogen flow to the test section. This purging action ensures that air and moisture traces in the line are completely removed and segment gets media substituted with GN_2. This is achieved by feeding GN_2 to the feedline through a purge line at a supply pressure of 0.5MPa. Purging of vent line and test section is carried out for a duration of 15 minutes each. The feedline to the test section is then chilled with LN_2 by opening the isolation valve V1 and vent valve V3. Schematic shown in Figure 4.1 may be referred for clarity on valve nomenclature. During this chilling process, cold GN_2 vapour is vented out through vent valve V3. Vent line surface temperature is monitored continuously and feedline chilling is stopped by closing the vent valve V3, when the vent line surface temperature reaches 82K. LN_2 is then admitted into the test section by opening the test section isolation valve V2. This marks the start of chilldown of the test section. Every experiment is done till steady values are read by the surface temperature sensors mounted at various stations along the length of the test section. The data read by pressure and temperature sensors are acquired using a portable Yokogawa system. Cryogen exiting from the test section is freely let out into the atmosphere.

As described here, the experimental set-up and six different types of test sections are realised. Two types namely TS1 and TS2 of inner diameters 30mm and 39mm are realised to study the influence of feedline orientation on chilldown performance. Test section with visualisation window is realised to study the flow structure observed during experiments with different feedline orientation. Two types are test sections with additional thermal mass placed near the inlet and exit of test section, realised to understand the influence of thermal mass distribution on chilldown performance. A test section with provision to introduce an evaluation section is realised to study the influence of test section material with high thermal conductivity, coatings, surface finish etc. Experiments are performed employing these test sections to meet the objectives described in Chapter 3 of the thesis.

The experiments done for each of the objectives stated and their salient results are discussed in detail in the subsequent chapters.

Chapter 5

Experiments to study the influence of test section orientation and change in cryogen mass flux on chilldown performance

The influence of feed line orientation and change in mass flux on chilldown performance of cryogenic feedline are studied by conducting experiments with LN_2 as test fluid. Towards this, a test set-up as described in chapter 4 is conceived & realised. Experiments are performed for different orientations of the test section viz; horizontal and upward and downward inclinations of 10^o, 20^o, 30^o, 45^o, 60^o, and 90^o. The procedure followed for the experiments is also covered in chapter 4. Evaluation is done for three mass flux conditions of 103 kg/m^{2}s, 83 kg/m^{2}s and 60 kg/m^{2}s. As explained earlier, two test sections TS1 and TS2 are used for the experiments viz; TS1 of inner diameter 30 mm and 1 mm wall thickness is employed for achieving a mass flux condition of 103 kg/m^{2}s and 83 kg/m^{2}s, whereas TS2 of inner diameter 39 mm and 1.5 mm wall thickness is used for simulating a mass flux of 60 kg/m^{2}s. Details of the instrumentation scheme adopted, test matrix, experimental results and findings of the study are brought out in the subsequent sections.

5.1 Instrumentation scheme

Instrumentation scheme employed for the test section TS1 is shown in Figure 5.1, whereas the one employed for test section TS2 is almost similar and is shown in Figure 5.2. Both the set-ups are equipped with three pressure sensors (P1, P2 and P3) for pressure measurement and nine thermocouples for surface temperature measurement. Pressure sensors used are of strain gauge type of operating range 0-0.5MPa and have an accuracy of $\pm 0.7\%$ of the full scale range. Measurements P1 and P2 read the orifice inlet and outlet pressures, whereas the sensor P3 measures the test section inlet pressure. Fluid temperature measurements are made using 100Ω Platinum RTD, placed at various stations along the length of the test section as shown in Figures 5.1 and 5.2. RTDs used have an accuracy of ±0.55 K at 73 K (close to LN_2 temperature). Five RTDs are used for fluid temperature measurement in TS1 and two numbers are used in TS2 test section. T type thermocouples used for measuring the test section outer wall temperature have an accuracy of ±1.5K. Nine thermocouples are placed at five stations 1 to 5 along the length of test section, station 1 has only one surface temperature at the bottom, whereas stations 2, 3, 4, and 5 have two measurements each, placed 180^o apart, one each at bottom and top locations. Alphabets 'D' and 'U' in the legend represent the measurements at bottom and top locations respectively.

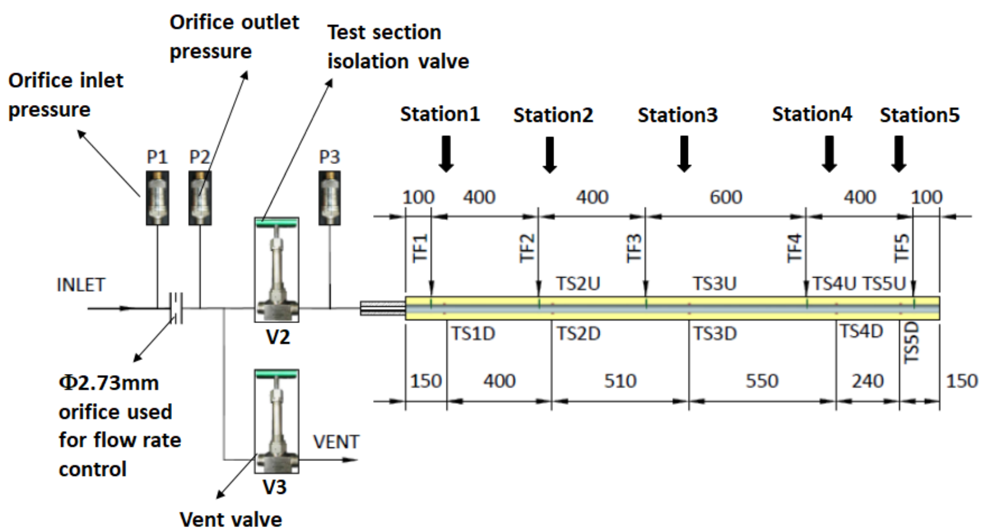

Figure 5.1: Instrumentation scheme employed for TS1 test section

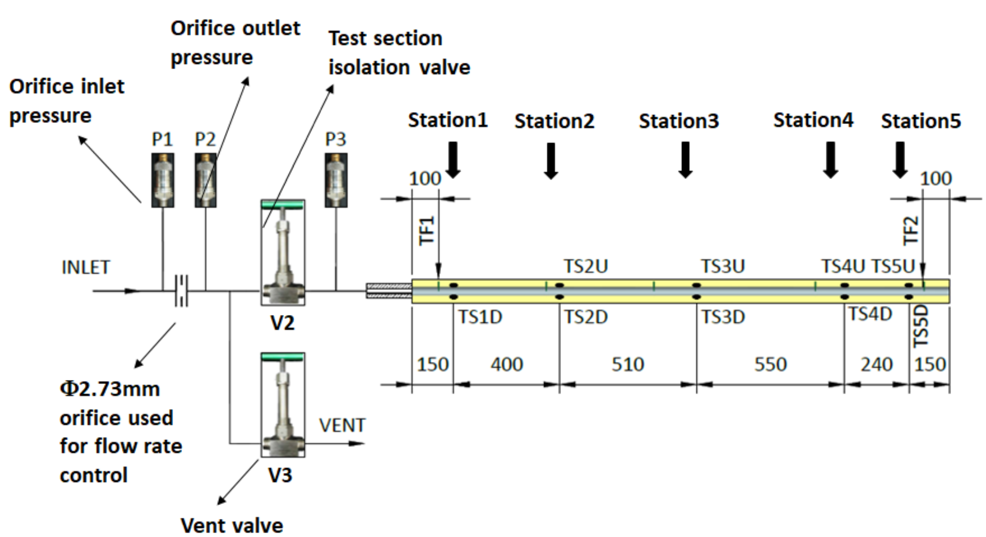

Figure 5.2: Instrumentation scheme employed for TS2 test section

The data read by pressure and temperature sensors are acquired using a portable Yokogawa data acquisition system. Sampling rate employed for the initial set of experiments is 1Hz, as this is adequate enough to evaluate the trend in surface temperature and heat flux pattern in the film boiling regime (which mostly decides the chilldown time) and assess the chilldown performance. However based on the suggestion made by one of the reviewers of the paper titled "Chilldown of Cryogenic feedlines- An insight into the influence of feedline orientation and mass flux", it is felt that a higher sampling rate is needed to have a closer estimate of the critical heat flux. Based on this, the experiments with varying test section orientations are repeated with a higher sampling rate of 10Hz and used for critical heat flux evaluation.

5.2 Test Matrix

As mentioned earlier, experiments are performed with the test sections TS1 and TS2 held at different upward and downward orientations with respect to horizontal. The orientations covered are horizontal, 10°, 20°, 30°, 45°, 60°, and 90° upward and downward inclinations with respect to horizontal using TS1 test section, whereas experiments with TS2 test section covered horizontal and upward and downward inclinations of 10°, 20°, 30°, 45° and 60°. Tests are performed for three mass flux conditions of 103, 83, and 60 kg/m^2s. A set of forty eight experiments are carried out with Test section TS1, twenty six are performed for a mass flux condition of 103 kg/m^2s and twenty two for a lower mass flux of 83 kg/m^2s. Whereas with test section TS2, twenty one experiments are performed for a mass flux condition of 60 kg/m^2s.

Experiments performed with test sections TS1 and TS2 are listed in Tables 5.1 and 5.2.

5.3 Experiments performed with different test section orientations to establish consistency

The experiments listed in tables 5.1 and 5.2 are repeated to establish consistency in the data used for evaluation. As a typical case, wall temperature profiles obtained in one set of experiments performed with TS1 and TS2 test sections, for the three mass flux conditions of 103 kg/m^2s, 83 kg/m^2s and 60 kg/m^2s, are shown in Figures 5.3, 5.4, and 5.5, to show the consistency achieved between tests.

The variation seen in the wall temperatures at different stations during repeat experiments is found to be well within 5K and the maximum dispersion seen in chilldown time is well within 10%. This consistency check is done for all the data points generated as part of the present study.

Table 5.1: Experiments performed with TS1 test section to study the influence of feedline orientation on chilldown performance

Sl. No.	Test section	No of tests (Mass flux 103 kg/m^{2}s)	No. of tests (Mass flux 83 kg/m^{2}s)
1	Horizontal	3	1
2	10° down	2	2
3	20° down	3	1
4	30° down	2	2
5	45° down	3	1
6	60° down	2	3
7	90° down	2	2
8	10° up	1	1
9	20° up	1	2
10	30° up	1	2
11	45° up	2	1
12	60° up	2	2
13	90° up	2	2
	Total	***26***	***22***

Table 5.2: Experiments performed with TS2 test section to study the influence of feedline orientation on chilldown performance

Sl. No.	Test section	No. of tests (Mass flux 60 kg/m^{2}s)
1	Horizontal	2
2	10° down	2
3	20° down	2
4	30° down	2
5	45° down	3
6	60° down	1
7	10° up	2
8	20° up	1
9	30° up	2
10	45° up	2
11	60° up	2
	Total	***21***

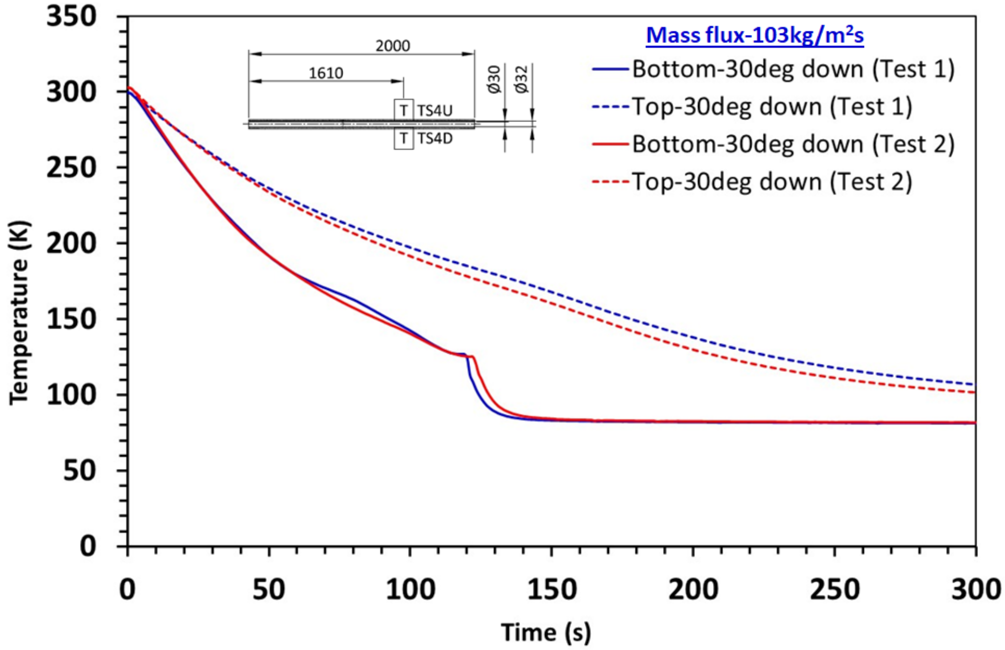

Figure 5.3: Wall temperature profile at station 4 during repeat experiments with 30° downward orientation of TS1 test section simulating a mass flux of 103 $\mathrm{kg/m^2s}$

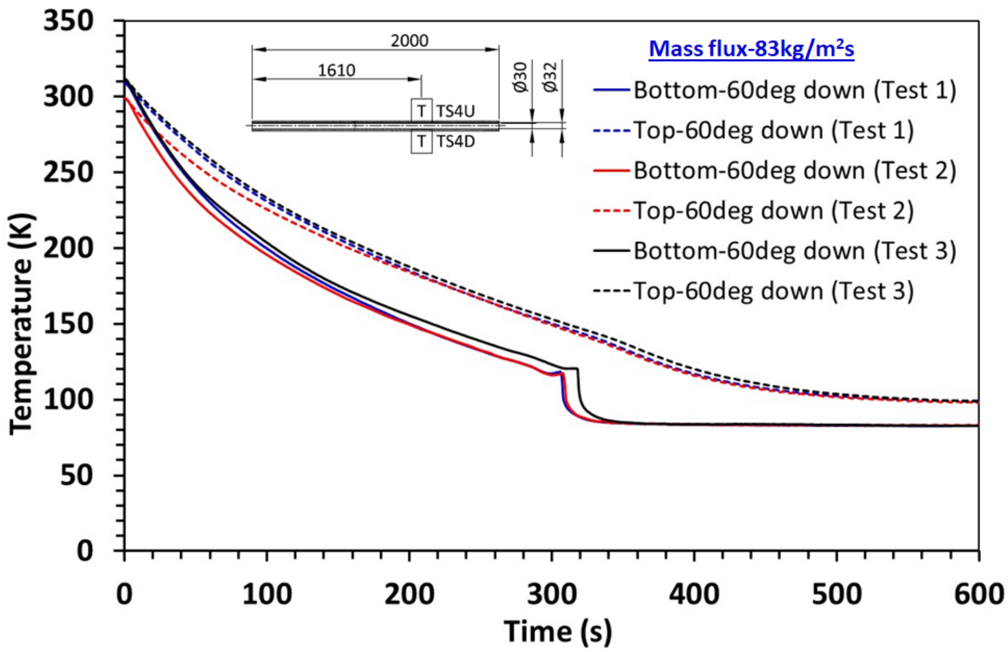

Figure 5.4: Wall temperature profile at station 4 during repeat experiments with 60° downward orientation of TS1 test section simulating a mass flux of 83 $\mathrm{kg/m^2s}$

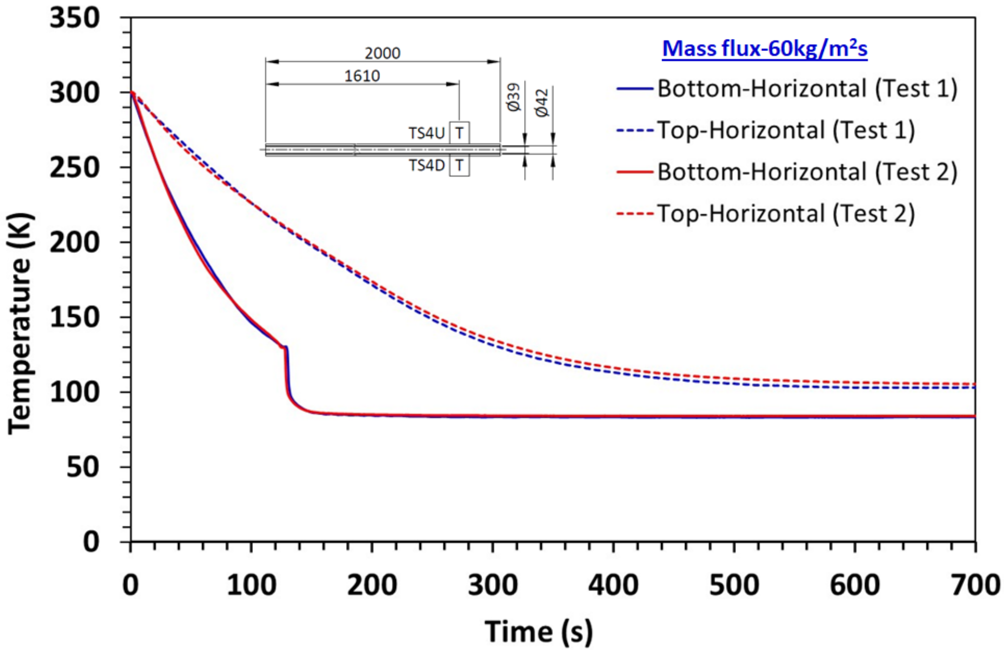

Figure 5.5: Wall temperature profile at station 4 during repeat experiments with horizontal orientation of TS2 test section simulating a mass flux of 60 kg/m^{2}s

5.4 Results and discussions

Surface temperature measurements made during the experiments are analysed in detail to bring out a better understanding on the chilldown pattern and the influence of test section orientation and mass flux on chilldown performance. Re for the experiments conducted is in the range of 1.9×10^4. Typically for high Re flows, a distance of 10 times tube diameter is to be considered for avoiding entrance effects and this works out to be 300 mm for the present study. Based on this, surface temperature measurements at stations 2, 3, and 4 placed beyond a distance of 300 mm from the entry point only are considered for the analysis. Measurements at station 5 are not included, being close to the outlet. Findings of the analysis are brought out in the subsequent sections.

5.4.1 Wall temperature profile observed in experiments with TS1 and TS2 test sections

As mentioned earlier, the chilldown performance of cryogenic feedlines is evaluated by studying the pattern of wall temperature fall at different stations along its length. Since the test section is not flowing full, the pattern of wall temperature fall is expected to be different for bottom and top locations. Detailed analysis of the wall temperature profiles at station 2, 3, and 4 is done for all the experiments performed to gather a complete understanding of the influence of test section orientation on chilldown performance. Results and findings are of the study are brought out here.

A typical plot of surface temperature measurement at station 2 during tests with TS1 test section employing a mass flux of 103 kg/m^{2}s is shown in Figure 5.6.

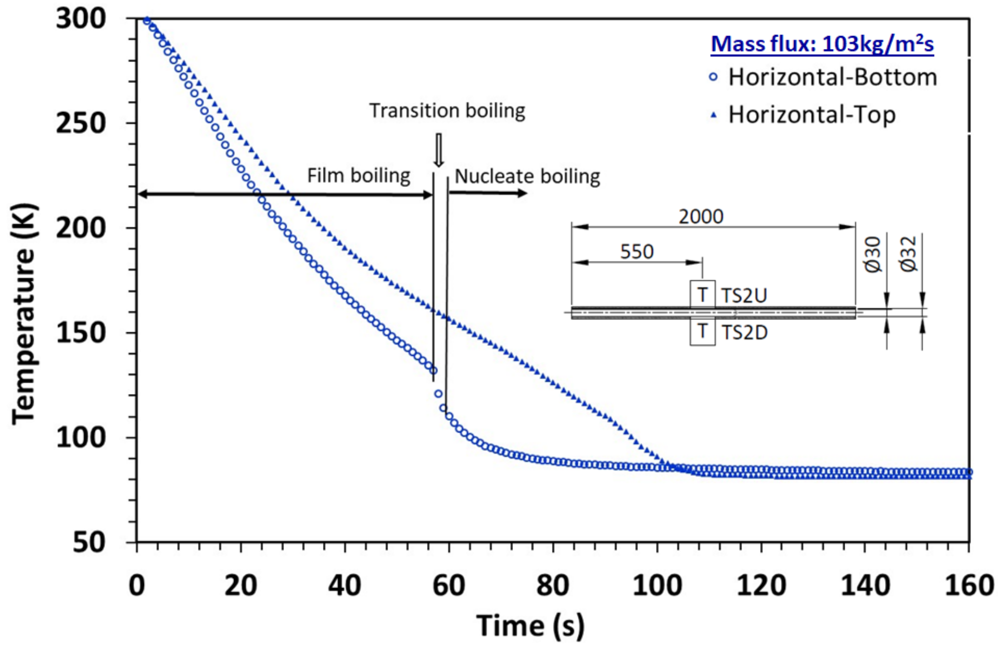

Figure 5.6: Boiling regimes observed in surface temperature measurement at bottom location at station 2 during experiment with test section TS1 held in horizontal orientation (mass flux - 103 kg/m^{2}s)

Chilldown pattern for the bottom location shows signature of all the three boiling regimes, namely film boiling, transition and nucleate boiling, indicative of cooling by liquid, whereas the top region does not show any signature of wetting by liquid and is cooled only by vapour. This data along with the fluid temperature measurements at stations 1 to 5 have confirmed that the flow structure is stratified in experiments with horizontal orientation of test section. As a typical case, the temperature profile observed in fluid temperature sensors TF1 to TF5, during experiments with 83 kg/m^{2}s is shown in Figure 5.7.

Figures 5.8 and 5.9 show the wall temperature profile observed at bottom and top locations at stations 3 and 4 during experiments with downward orientation of test section. Pattern of fall of wall temperature and heat transfer regimes observed at stations 2, 3, and 4 are similar to the ones observed with horizontal orientation of test section. Bottom wall shows signature of liquid wetting whereas the top wall is cooled only by vapour. Wall temperature profiles are almost similar up to 45° downward inclination. Beyond this, at 60° downard inclination, chilldown is seen to be improving for the top wall and further improvement is seen at 90° downward inclination due to all around

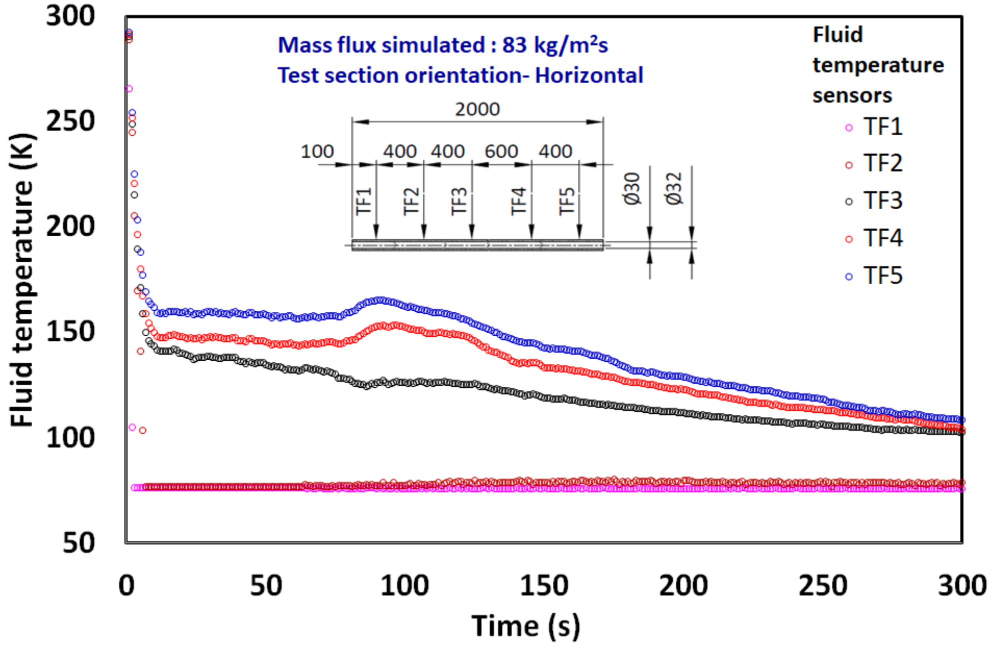

Figure 5.7: Trend observed in fluid temperature measurements placed at five stations along the length of test section during experiment with test section TS1 held in horizontal orientation (mass flux - 83 kg/m^{2}s)

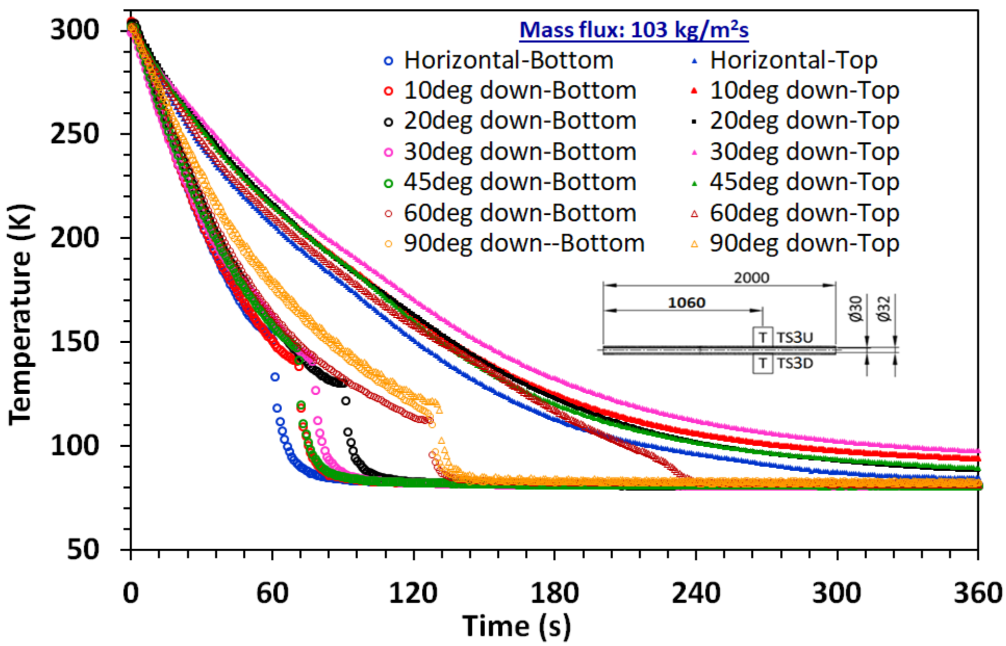

Figure 5.8: Wall temperature profile at station 3 during experiments with test section TS1 held in horizontal & downward orientation (mass flux - 103 kg/m^{2}s)

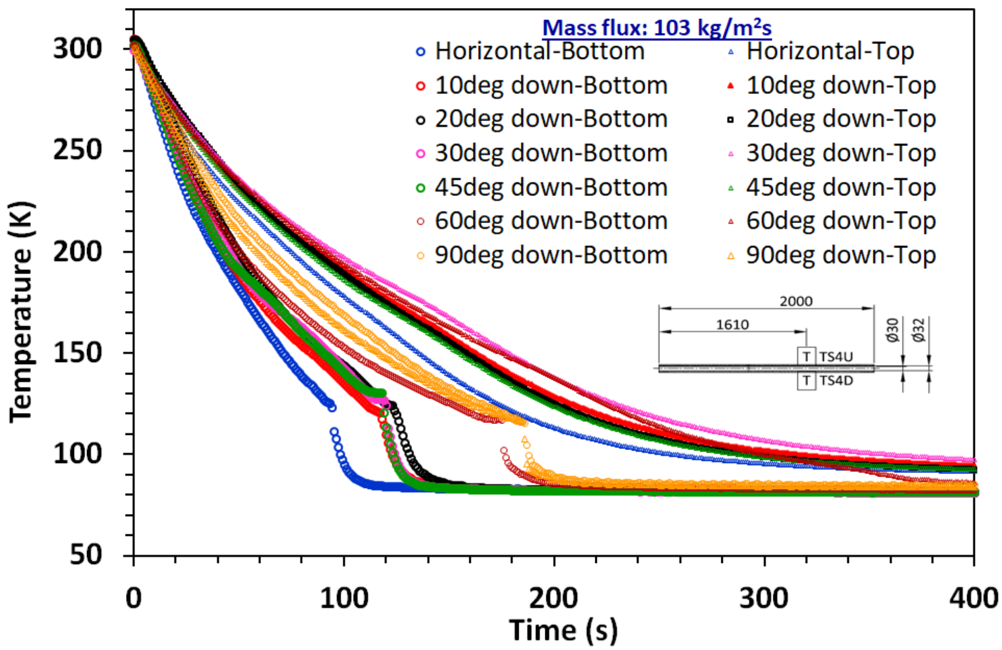

Figure 5.9: Wall temperature profile at station 4 during experiments with test section TS1 held in horizontal & downward orientation (mass flux - 103 kg/m^{2}s)

wetting of the test section wall by the liquid.

It is also seen that the fall rate of bottom wall temperature decreases with downward orientation of test section viz; fall rate is higher with horizontal orientation and decreases as downward orientation increases from 10° to 60°. This trend can be attributed to reduction in the extent of liquid wetting of the tube wall in downward inclination experiments as compared to the ones with horizontal orientation. This observation is in contrast to the general expectation that with increase in downward inclination, the fluid velocity at the wall and hence the transfer is expected to be higher, resulting in a faster bottom wall temperature fall rate. A better understanding on the physics associated with this reduced wall temperature fall rate could be obtained in the present study through flow visualisation and numerical studies, details of which are covered in Chapters 6 and 7.

Whereas in the case of top wall temperature, fall rate reduces till around 30° downward orientation and beyond this at 45° downward inclination, there is minor improvement seen. This improves further with 60° and 90° downward orientation of test section.

Figures 5.10 and 5.11 show the wall temperature profile at stations 3 and 4 during experiments with upward orientation of test section. The trend in top wall temperature is significantly different as compared to experiments with horizontal and downward orientation. As can be seen, the bottom wall temperature profile shows signature of all the three boiling regimes and wetting by liquid as observed in experiments with horizontal and downward inclination. Top wall also shows signature of all the three boiling regimes and wetting by liquid. This results in a much faster drop rate of the

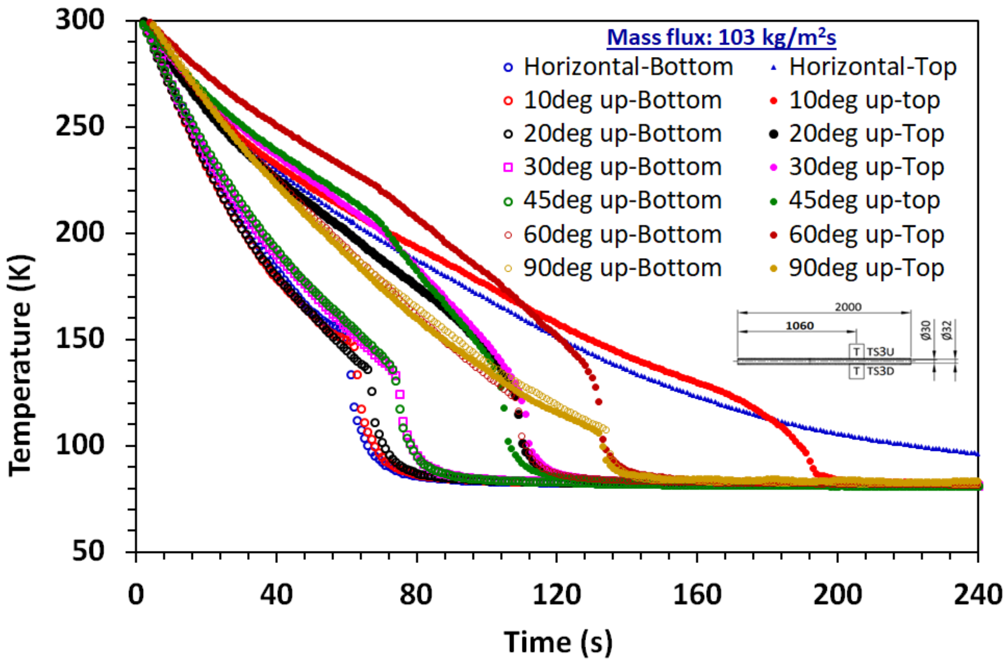

Figure 5.10: Wall temperature profile at station 3 during experiments with test section TS1 held in horizontal & upward orientation (mass flux - 103 kg/m^2s)

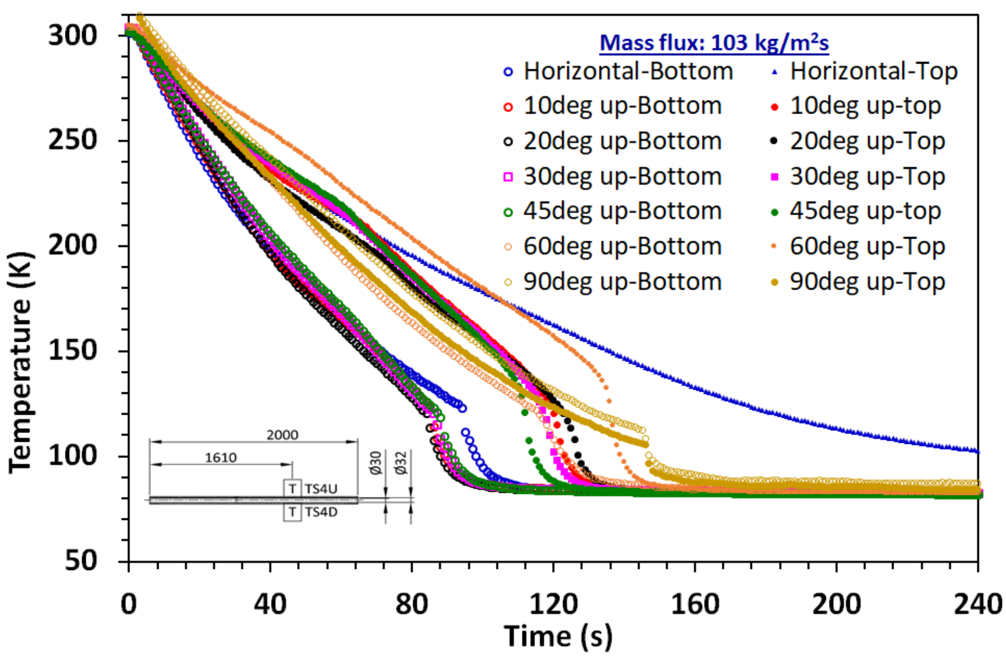

Figure 5.11: Wall temperature profile at station 4 during experiments with test section TS1 held in horizontal & upward orientation (mass flux - 103 kg/m^2s)

top wall temperature. This improved fall rate in top wall temperature is observed with 10° upward inclination itself. This trend continues further up to 45° upward inclination of test section, beyond which the fall rate reduces.

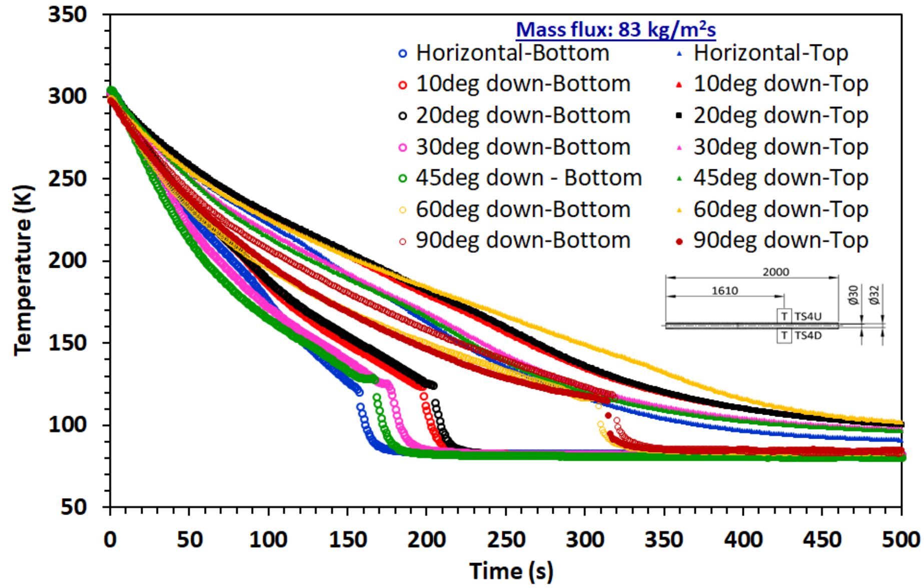

Figure 5.12: Wall temperature profile at station 4 during experiments with test section TS1 held in horizontal & downward orientation (mass flux - 83 kg/m^{2}s)

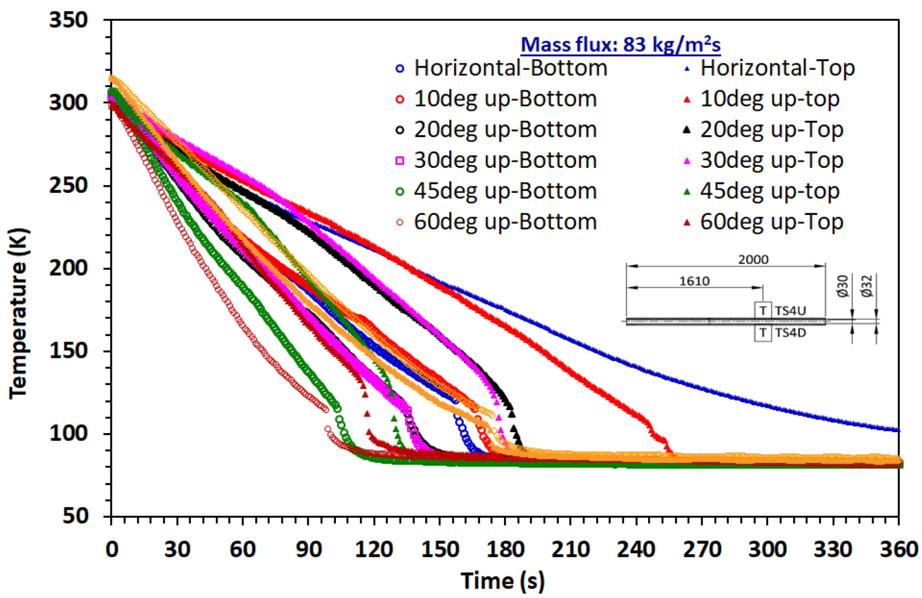

Figure 5.13: Wall temperature profile at station 4 during experiments with test section TS1 held in horizontal & upward orientation (mass flux - 83 kg/m^{2}s)

Observations in experiments with lower mass flux of 83 kg/m^{2}s are similar. As a typical case, wall temperature profile observed at station 4 in experiments with this lower mass flux condition is shown in Figures 5.12 and 5.13.

Trend of wall temperature fall is experiments with mass flux of 83 kg/m^{2}s is very much similar to the observations with mass flux of 103 kg/m^{2}s. In experiments with downward orientation, bottom wall temperature fall rate is seen to be decreasing with increase in downward inclination. A minor improvement in top wall temperature fall rate is seen beyond 20° downward orientation of test section, as compared to 30° downward inclination with 103 kg/m^{2}s mass flux. However, with 60° downward orientation, a trend change is seen again and the fall rate is observed to be lower, which could be due to flow structure change and needs to be investigated. Further with 90° downward orientation, the temperature fall rate improves as seen with 103 kg/m^{2}s mass flux.

Observations during experiments with TS2 test section with mass flux of 60 kg/m^{2}s are similar. As a typical case, the profile of wall temperature measurements at station 4 are shown in Figures 5.14 and 5.15.

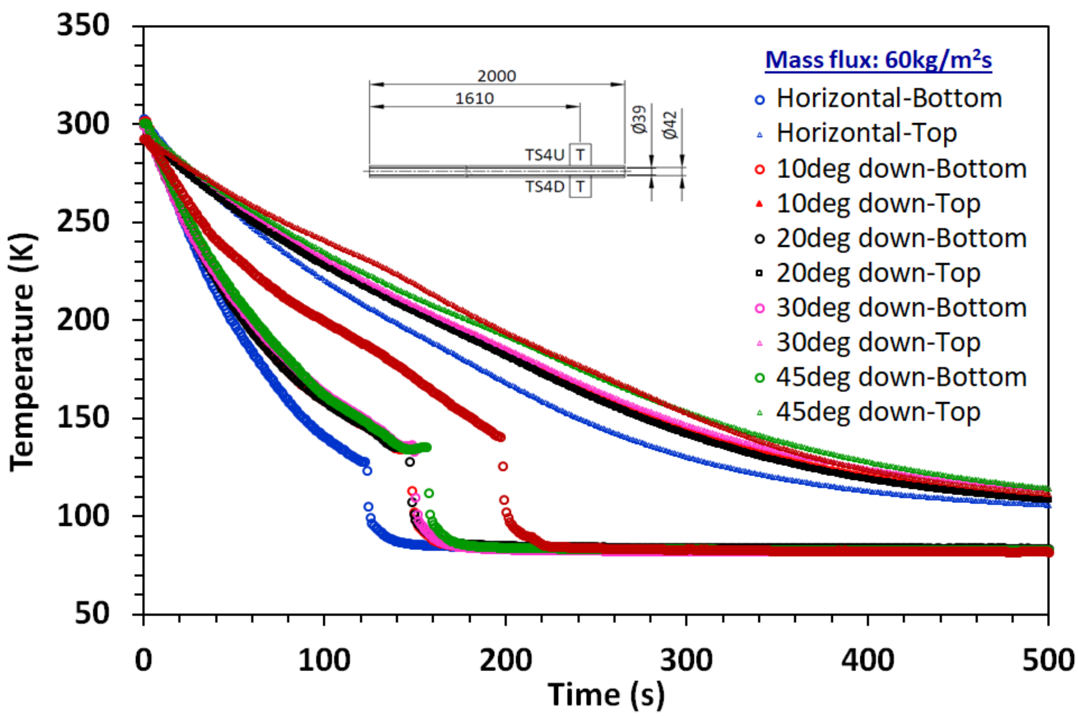

Figure 5.14: Wall temperature profile at station 4 during experiments with test section TS2 held in horizontal & downward orientation (mass flux - 60 kg/m^{2}s)

In experiments with downward orientation of TS2 test section, observation of reduction in fall rate of bottom wall temperature with increase in downward inclination is similar. Improved fall rate is observed in top wall temperature only from 60° downward inclination. It is felt that this improved fall rate in top wall temperature could be due to droplet formation due to higher shear at

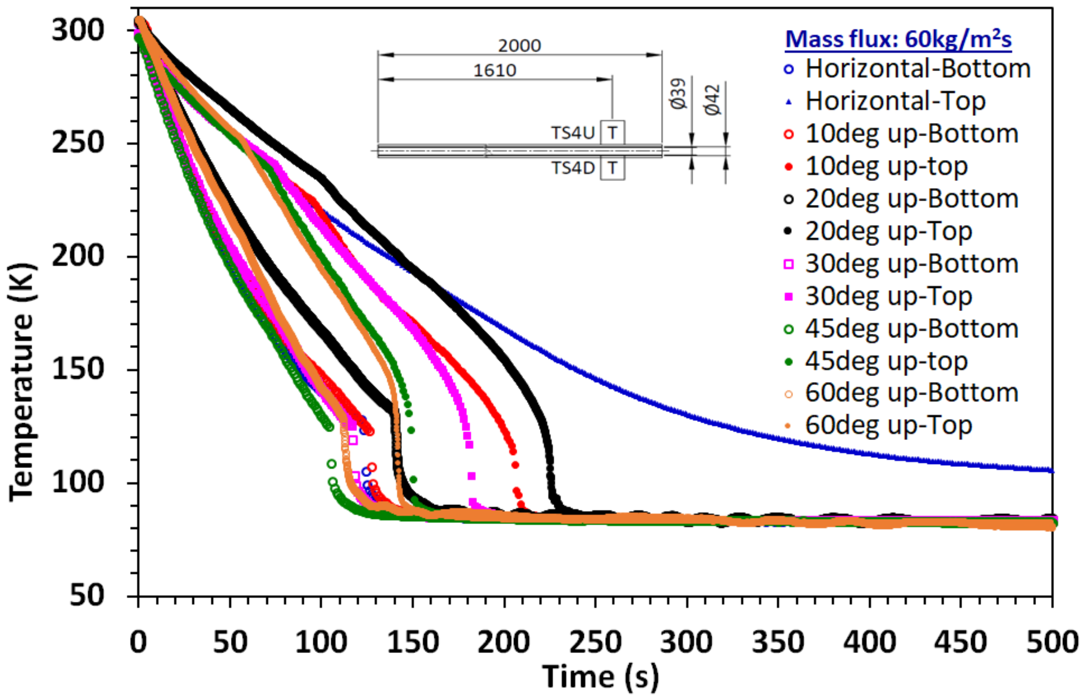

Figure 5.15: Wall temperature profile at station 4 during experiments with test section TS2 held in horizontal & upward orientation (mass flux - 60 kg/m^{2}s)

liquid vapour interface and its impingement with the top wall. With TS2 test section, higher drop rate in top wall temperature is seen only with a higher downward inclination and could be due to its larger diameter as compared to TS1 test section.

Variation of feedline temperature along the length of the test section for different orientations of test section is also studied. Figure 5.16 shows the typical plot of bottom wall temperature profile, at stations 2, 3 and 4, during experiments with horizontal orientation, plotted for every 10s interval. Whereas Figure 5.17 shows the trend at stations 2, 3 and 4 in top wall temperature, in the same experiment. As can be seen, upstream locations get chilled faster as compared to locations downstream and this trend observed is similar for all the orientations studied. Falling trend in bottom wall temperature measurements is almost similar irrespective of the orientation of the test section. Whereas the trend in top wall temperature is distinctly different in experiments with upward orientation, as compared to experiments with horizontal and downward orientation. This trend change observed in experiments with upward orientation of test section is captured in Figures 5.17 and 5.18. In experiments with upward inclination, top wall gets chilled faster, as compared to horizontal and downward inclination, due to its wetting by the liquid. This results in faster chilldown in experiments with upward orientation, as compared to horizontal and downward orientation.

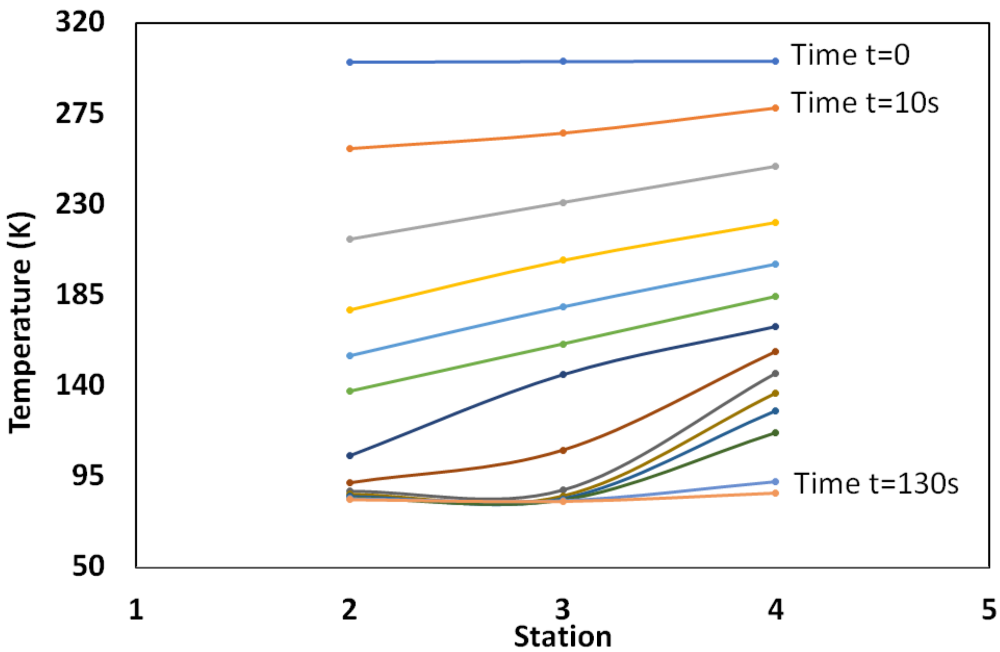

Figure 5.16: Trend of bottom wall temperature at different stations along the length of test section during experiments with TS1 held in horizontal orientation (mass flux - 103 kg/m^2s)

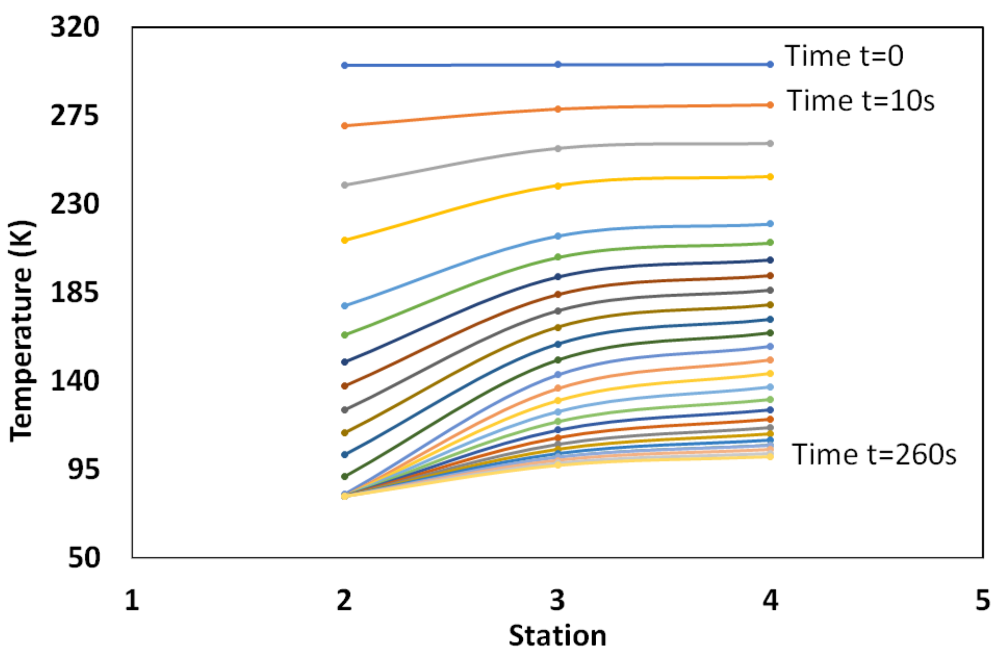

Figure 5.17: Trend of top wall temperature at different stations along the length of test section during experiments with TS1 held in horizontal orientation (mass flux - 103 kg/m^2s)

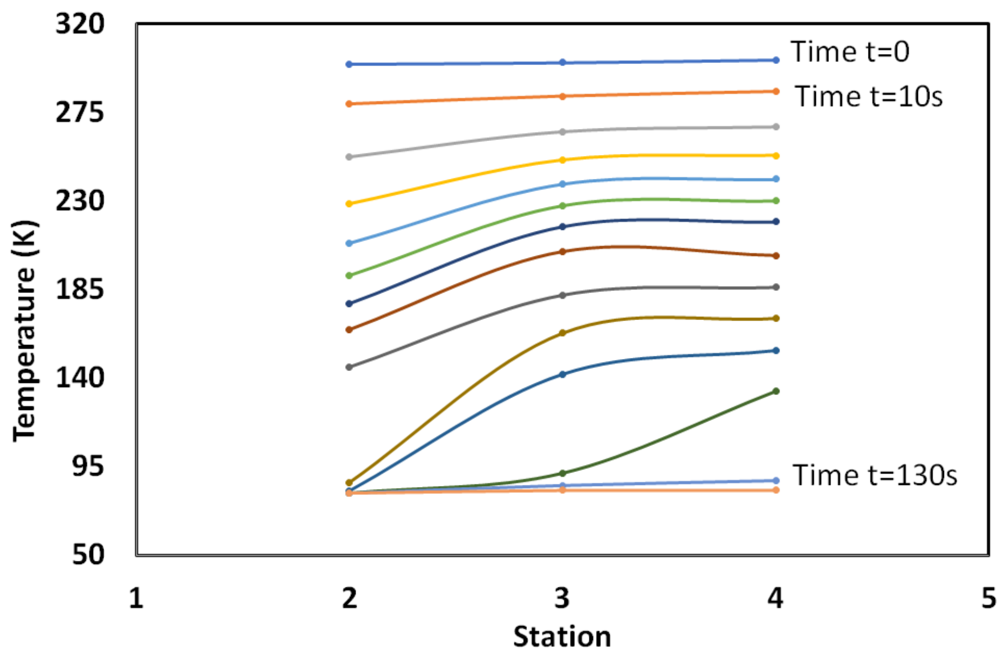

Figure 5.18: Trend of top wall temperature at different stations along the length of test section during experiments with TS1 held at 45° upward orientation (mass flux - 103 kg/m^{2}s)

5.4.2 Influence of test section orientation on chilldown time and Chilldown Performance Index, as observed during experiments with TS1 and TS2 test sections

Average wall temperature at each of the three stations 2, 3 and 4 is estimated using the bottom and top surface temperature measurements made during the experiment. Trend of fall of average wall temperature at stations 3 and 4 with varying test section orientation are studied to evaluate qualitatively the influence of feedline orientation on chilldown performance. Average surface temperature at stations 3 and 4 during experiments with varying test section downward orientation and mass flux of 103 kg/m^{2}s are shown in Figures 5.19 and 5.20.

Trend of average temperature fall in experiments with downward inclination as compared to horizontal is similar at stations 3 and 4. As can be seen, among the horizontal and downward inclinations tested (excepting 90° downward orientation), chilldown performance is the best for horizontal orientation of test section. Chilldown performance is inferior for all downward orientations of test section as compared to horizontal till it reaches 90^o inclination. This is mainly due to the variation seen in the top wall temperature fall rate with increase in downward inclination.

Whereas in experiments with upward orientation, chilldown performance is seen to be improving significantly as compared to horizontal as shown in Figures 5.21 and 5.22. Performance improves significantly with 10° upward inclination itself and continues to improve till 45^o orientation

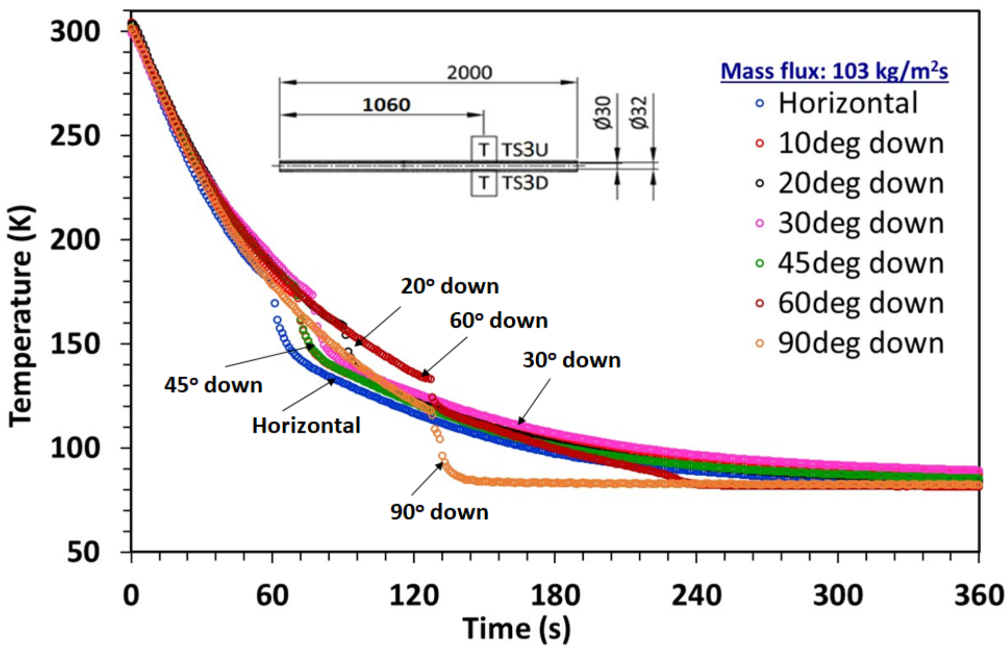

Figure 5.19: Average wall temperature at station 3 during experiments with test section TS1 held in horizontal & downward orientation (mass flux - 103 kg/m^{2}s)

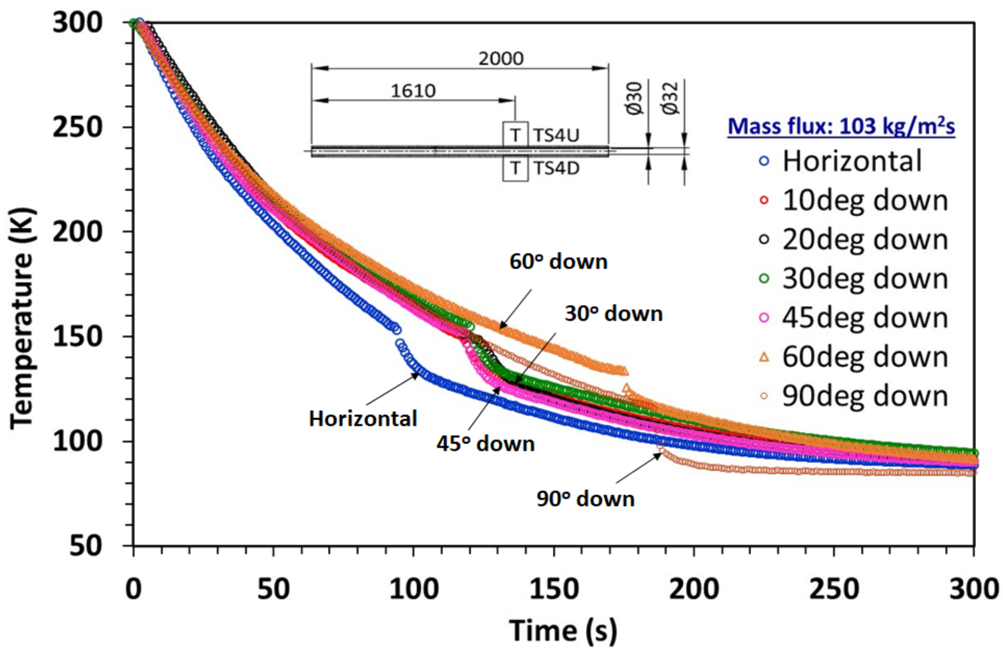

Figure 5.20: Average wall temperature at station 4 during experiments with test section TS1 held in horizontal & downward orientation (mass flux - 103 kg/m^{2}s)

is reached. This is mainly due to earlier fall in top wall temperature with increase in upward inclination. Beyond this, though minor reduction is seen in chilldown performance for 60° and 90° upward orientation, it is still better than horizontal.

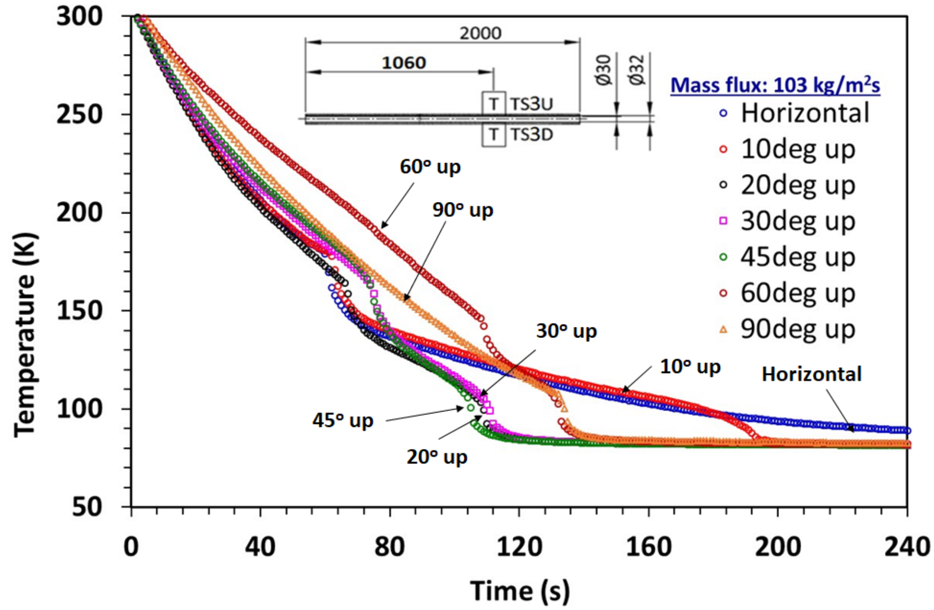

Figure 5.21: Average wall temperature profile at station 3 during experiments with test section TS1 held in horizontal & upward orientation (mass flux - 103 kg/m^{2}s)

Observations in experiments with TS1 section at a lower mass flux of 83 kg/m^{2}s are also similar as shown in Figures 5.23 and 5.24.

Average surface temperature fall is better for horizontal orientation of test section as compared to other downward orientation (excepting 90° downward inclination). It decreases with increase in downward inclination up to 20° and thereafter improves slightly. Trend observed with 60° downward inclination is different and needs to be addressed. Improved trend with 90° downward inclination could be due to better wall wetting by the liquid. Whereas in experiments with upward inclination, average wall temperature fall improves with 10° upward inclination itself and continues to improve up to 45° upward inclination. Drop rate reduces thereafter, as observed in experiments with mass flux of 103 kg/m^{2}s.

Observations in experiments with TS2 test section for 60 kg/m^{2}s mass flux condition are shown in Figures 5.25 and 5.26.

In experiments with downward orientation, average temperature fall rate is inferior as compared to horizontal. Whereas in experiments with upward orientation, reduction in average temperature is seen to be improving with 10° upward inclination itself and continues to improve till 45-60° upward inclination. Thus the observations with mass flux of 60 kg/m^2s are similar to other mass flux conditions evaluated.

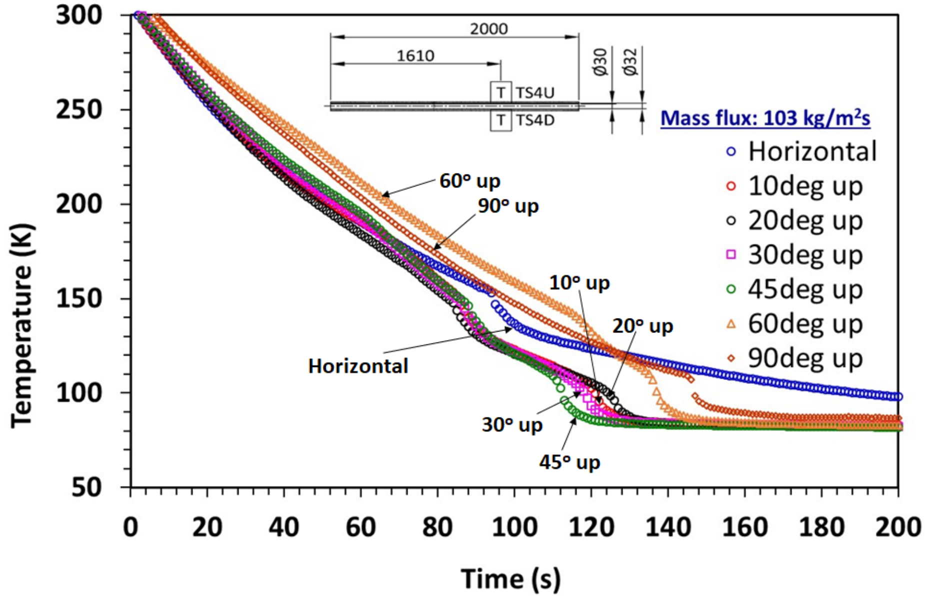

Figure 5.22: Average wall temperature profile at station 4 during experiments with test section TS1 held in horizontal & upward orientation (mass flux - 103 kg/m^{2}s)

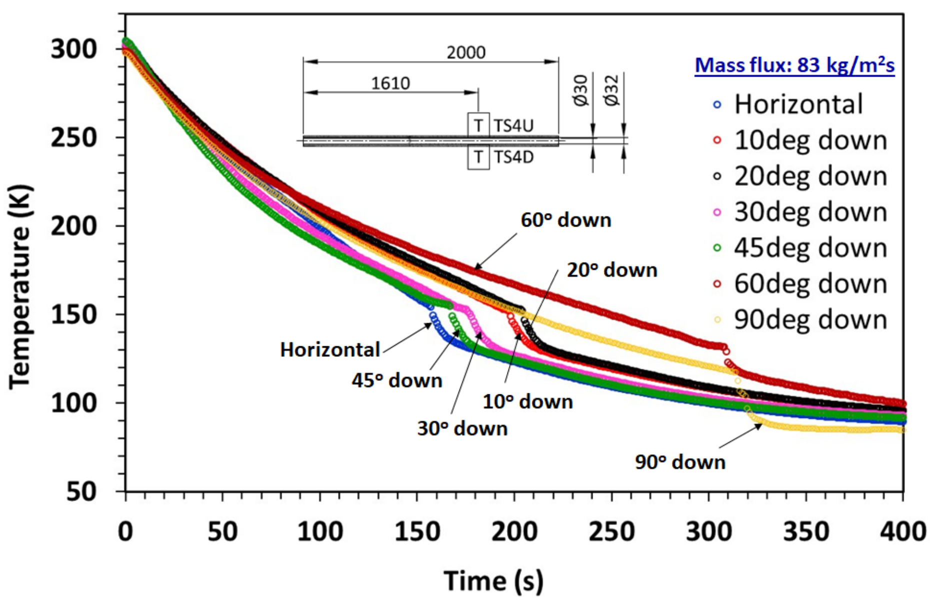

Figure 5.23: Average wall temperature profile at station 4 during experiments with test section TS1 held in horizontal & downward orientation (mass flux - 83 kg/m^{2}s)

Chilldown performance of cryogenic systems can be evaluated on the basis of chilldown time, which is defined as the time required to chill the system to a steady temperature, close to the saturation temperature of the cryogen. This temperature value targeted for chilldown completion in

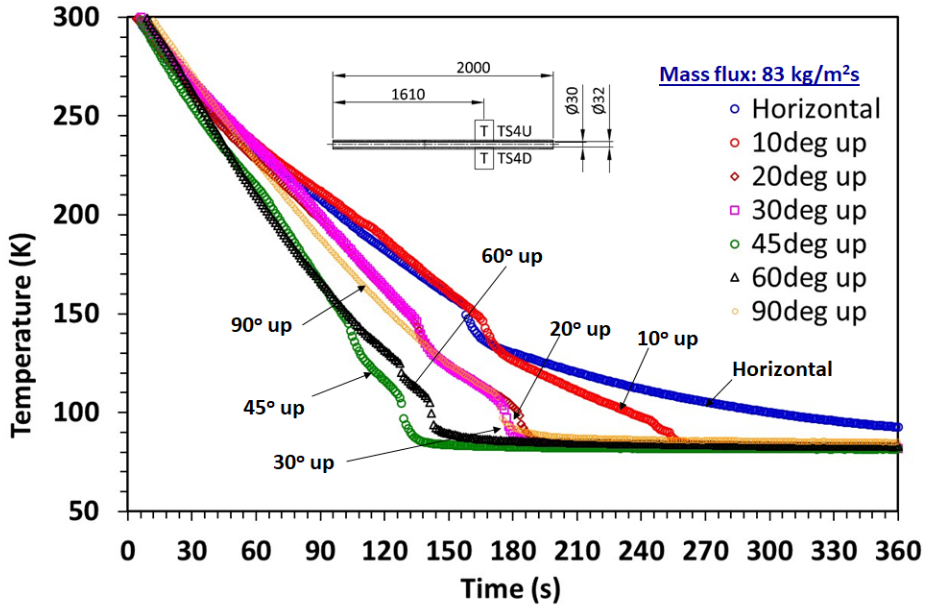

Figure 5.24: Average wall temperature profile at station 4 during experiments with test section TS1 held in horizontal & upward orientation (mass flux - 83 kg/m^{2}s)

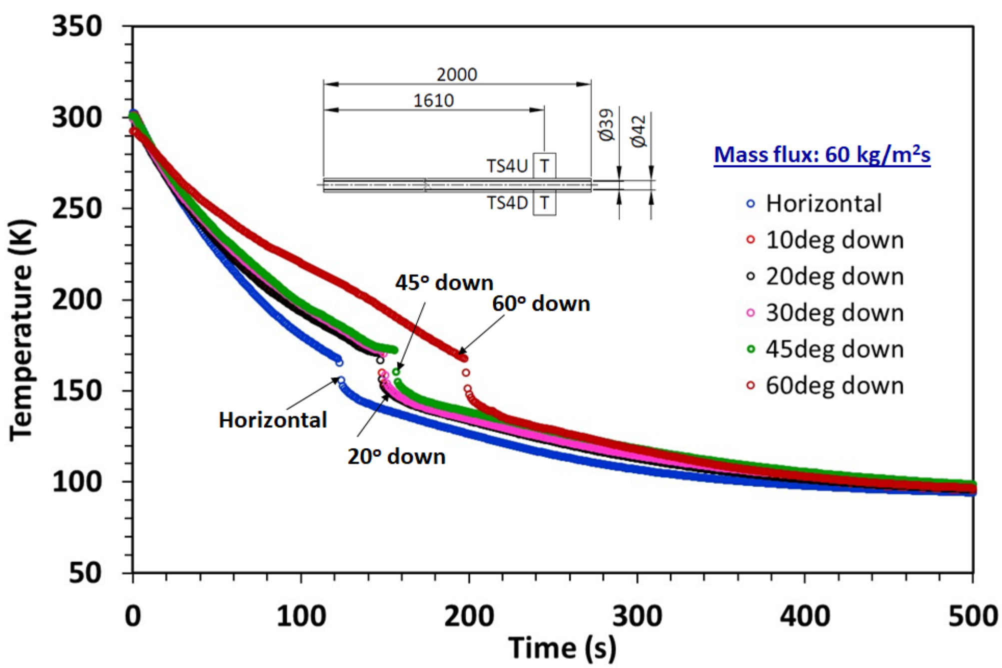

Figure 5.25: Average wall temperature profile at station 4 during experiments with test section TS2 held in horizontal & downward orientation (mass flux - 60 kg/m^{2}s)

the present study is 92 K for experiments with TS1 test section and 97 K for experiments with TS2 test section. A higher temperature is chosen for the TS2 test section in view of the inferior

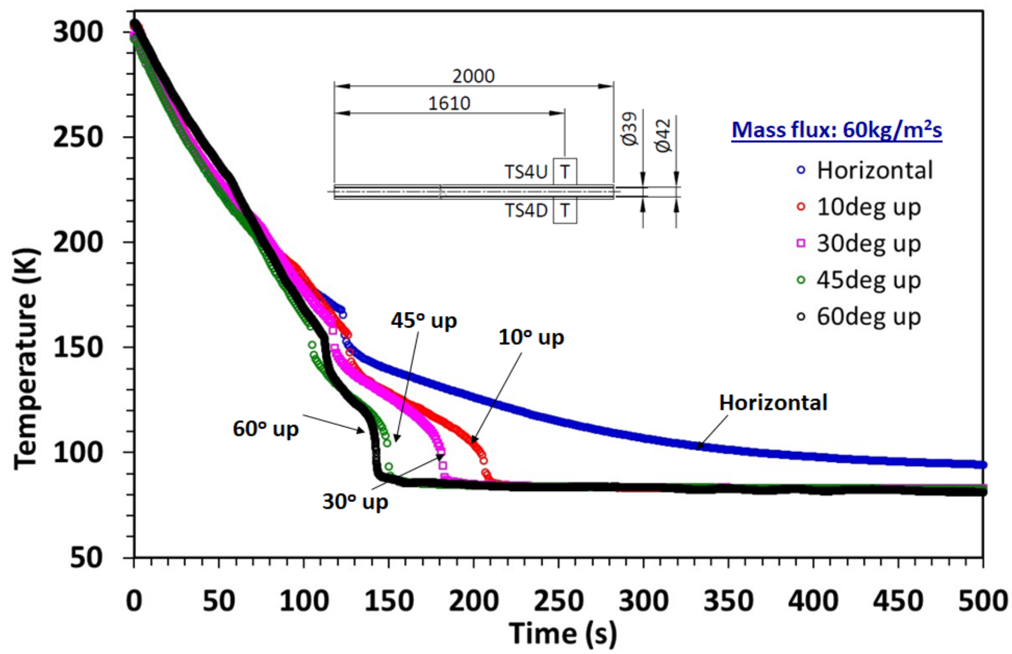

Figure 5.26: Average wall temperature profile at station 4 during experiments with test section TS2 held in horizontal & upward orientation (mass flux - 60 kg/m^{2}s)

chilldown performance seen for the lower mass flux condition simulated. The time taken for the average surface temperature at station 4 to fall below this specified value is defined as the chilldown time. Trend of chilldown time variation with respect to test section orientation, as observed during the experiments performed using TS1 test section with mass flux of 103 kg/m^{2}s and 83 kg/m^{2}s is shown in Figures 5.27 and 5.28.

Chilldown time is higher in experiments with downward inclination as compared to horizontal and is found to be significantly reduced with upward inclination. In experiments with mass flux of 103 kg/m^{2}s, with increase in downward inclination up to 30°, chilldown time is increasing by around 22%. A reduction of around 16% is seen with 45° downward orientation and with further increase to 60° inclination, chilldown time is increasing marginally. With 90° downward orientation, chilldown time decreases and becomes almost comparable with horizontal or even better. Whereas in experiments with upward orientation, about 50% reduction in chilldown time is seen with 10° change and beyond this, the reduction is not so significant up to 45° upward inclination. Chilldown time increases with 60° upward orientation and with further increase to 90° upward inclination, an increase in chilldown time by around 12% is observed. Observations in experiments with reduced mass flux of 83 kg/m^{2}s are almost similar, except for the following:

- Trend of minor reduction in chilldown time is seen beyond 20° downward inclination in experiments with 83 kg/m^{2}s mass flux condition, whereas this is observed beyond 30° downward orientation, in experiments with mass flux of 103 kg/m^{2}s.

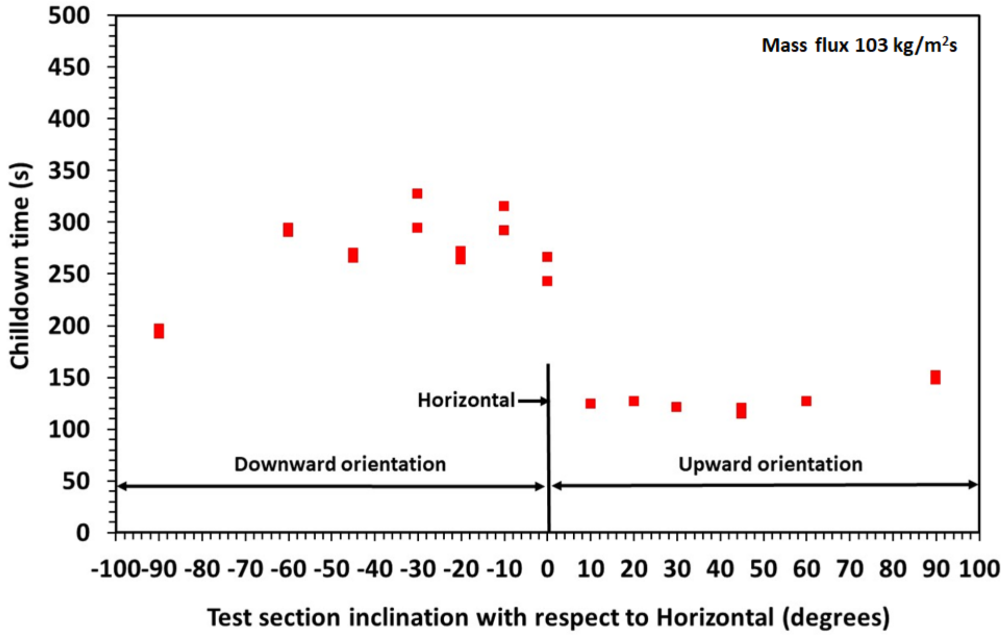

Figure 5.27: Variation of chilldown time with respect to test section orientation as observed during experiments with TS1 test section (mass flux - 103 kg/m^{2}s)

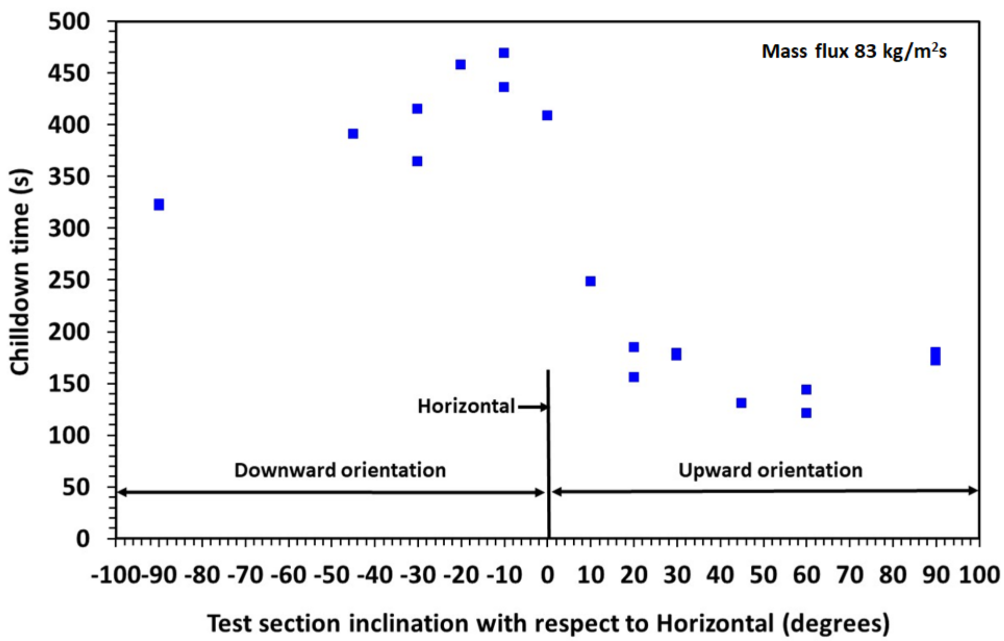

Figure 5.28: Variation of chilldown time with respect to test section orientation as observed during experiments with TS1 test section (mass flux - 83 kg/m^{2}s)

- In experiments with upward inclination, up to upward 30° inclination, improvement in chilldown time is less as compared to the one observed with mass flux of 103 kg/m^{2}s. However, the values become comparable to 103 kg/m^{2}s mass flux condition at 45° upward orientation.

The observations in experiments with upward inclination could be attributed to the lower mass flux condition simulated, as compared to experiments with 103 kg/m^{2}s.

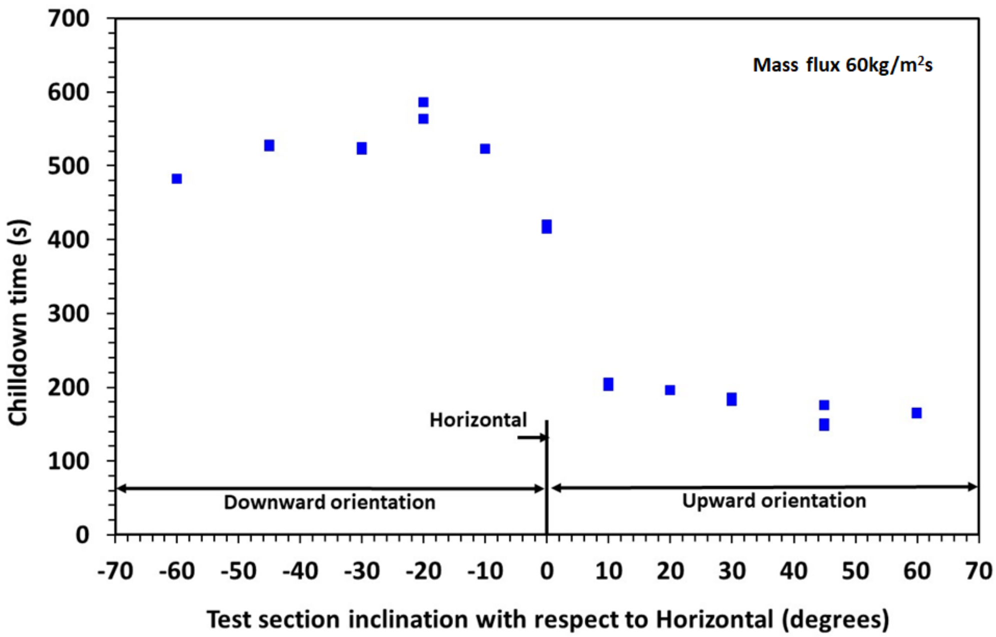

Figure 5.29: Variation of chilldown time with respect to test section orientation as observed during experiments with TS2 test section (mass flux - 60 kg/m^{2}s)

Variation of chilldown time in experiments performed with TS2 test section employing a mass flux of 60kg/m^{2}s is shown in Figure 5.29. Observation in experiments with TS2 test section are almost similar to the ones performed with TS1 test section employing a mass flux of 103kg/m^{2}s, except for the minor difference in experiments with downward orientation of test section. A significant reduction in chilldown time is observed beyond 45° downward orientation (at 60° downward inclination) as compared to beyond 30° downward orientation in experiments with TS1 test section and the probable reason for the same has been stated earlier.

Chilldown performance can also be expressed as a non dimensionalised parameter termed as "Chilldown Performance Index" (CPI). As shown in expression 5.1, CPI is defined as the ratio of enthalpy that need to be removed from the test section while being cooled to the specified temperature targeted for chilldown completion to the latent heat content of LN_2 consumed during the chilldown process.

$$CPI = \frac{m_{ts}Cp_{ts}\Delta T}{m_c t h_{fg}} \tag{5.1}$$

CPI values estimated for the experiments performed using TS1 test section for mass flux conditions of 103 kg/m^{2}s and 83 kg/m^{2}s are plotted in Figures 5.30 and 5.31. CPI values estimated for experiments with mass flux of 60 kg/m^{2}s are shown in Figure 5.32.

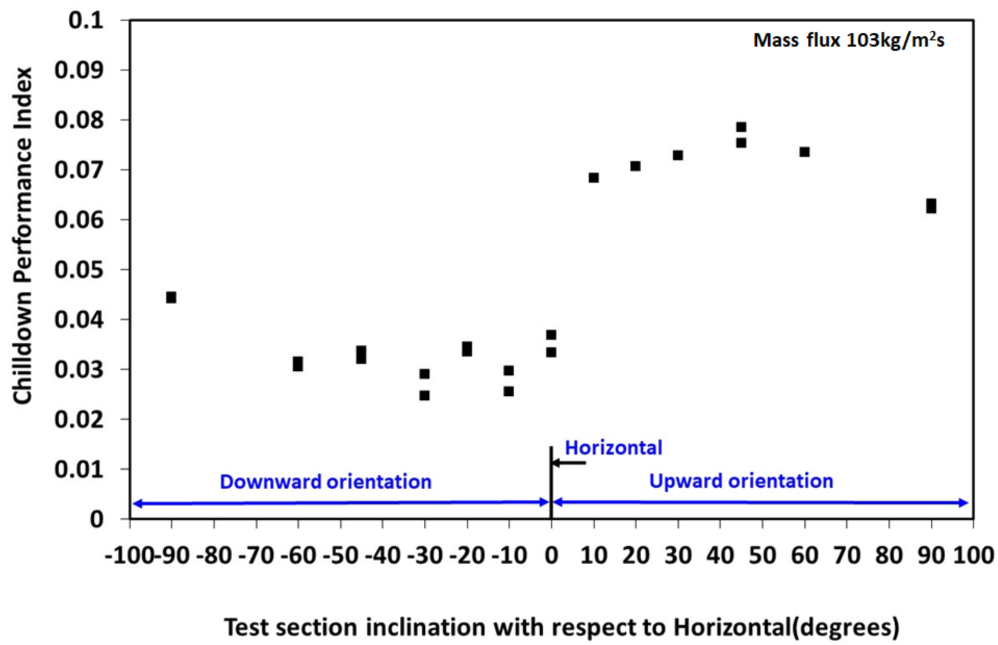

Figure 5.30: Variation of CPI with respect to test section orientation as observed during experiments in TS1 test section with mass flux of 103 kg/m^{2}s

As seen here, CPI is low for experiments with downward orientation of test section and significantly higher with upward orientation. In experiments with downward orientation, CPI reduces till around 20-30° downward inclination and improves thereafter. Among the downward orientations, 90° downward gives the maximum CPI. Whereas in experiments with upward orientation, CPI increases till around 45° upward inclination. Beyond this, CPI decreases for 60° and 90° upward orientations, but still the performance is better as compared to horizontal. Between 90° downward and upward orientations, performance is better for 90° upward orientation, probably due to the buoyancy effects, which is absent in the former.

Inferior performance in experiments with downward orientation as compared to horizontal is mainly attributed to reduced fall rate of top wall temperature. This could be due to reduced wetting of the bottom wall and lesser heat extraction from the wall. This assessment is mainly based on the observations made in flow visualisation and numerical studies, that are covered in more detail in Chapters 6 and 7. Whereas improved performance in experiments with upward orientation is due

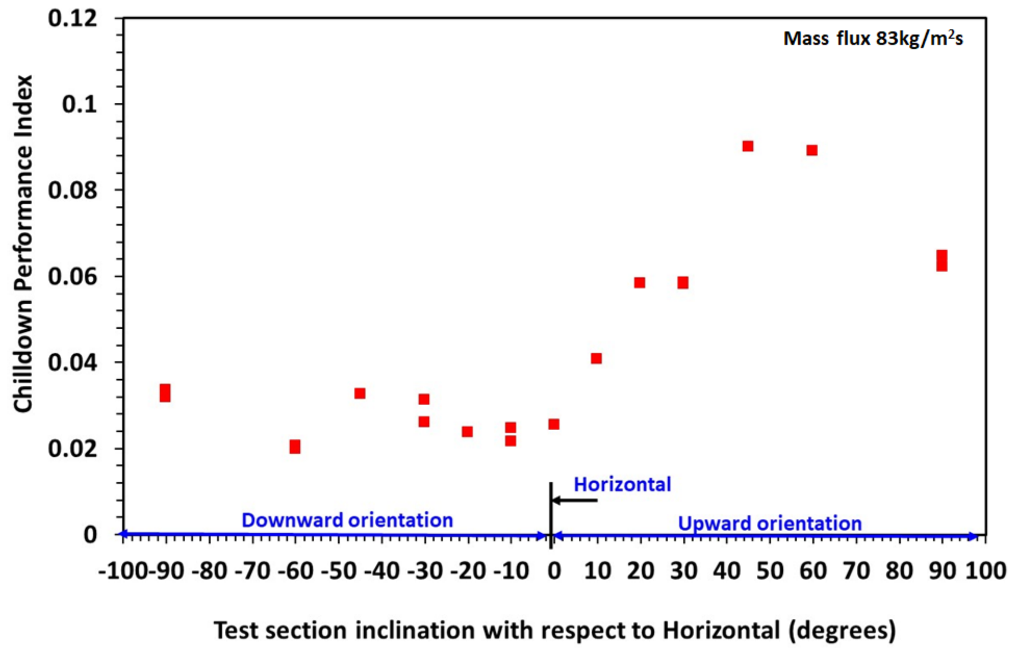

Figure 5.31: Variation of CPI with respect to test section orientation as observed during experiments in TS1 test section with mass flux of 83 kg/m^{2}s

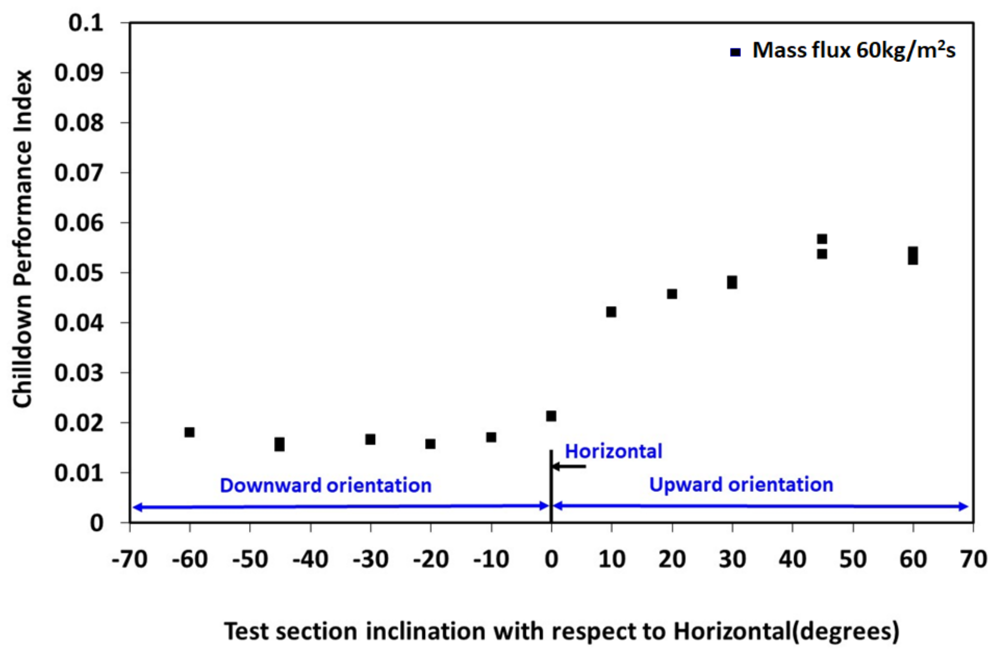

Figure 5.32: Variation of CPI with respect to test section orientation as observed during experiments in TS2 test section with mass flux of 60kg/m^{2}s

to wetting of the top wall by the liquid. This is attributed to the presence of slug or plug flow, as observed in flow visualisation studies, the results of which are covered in Chapter 6.

Experiments performed with TS1 test section for two different mass flux conditions of 103 kg/m^{2}s and 80 kg/m^{2}s, show CPI is not highly sensitive to mass flux.

5.4.2.1 Heat flux estimation by inverse technique -Methodology adopted

The following four transient conduction equations 5.2, 5.3, 5.4 and 5.5 are solved iteratively to estimate the heat flux at the inner wall of test section. Equation 5.2 represents the heat transfer at the outside surface of the test section insulation. Whereas equations 5.3 and 5.4 refer to the heat conduction within the insulation and test section wall respectively. Equation 5.5 reflects the heat transfer at the test section inner wall with the cryogen.

$$\frac{\Delta r_{ins}}{2}\rho_{ins}Cp_{ins}\frac{\delta T_{ins}}{\delta t} = h_{out}[T_{\infty} - T_{ins}] - k_{ins}\frac{\delta T_{ins}}{\delta r_{ins}} \tag{5.2}$$

$$\rho_{ins}Cp_{ins}\frac{\delta T_{ins}}{\delta t} = \frac{1}{r_{ins}}\frac{\delta[k_{ins}r_{ins}\frac{\delta T_{ins}}{\delta r_{ins}}]}{\delta r_{ins}} \tag{5.3}$$

$$\rho_{ss}Cp_{ts}\frac{\delta T_{ss}}{\delta t} = \frac{1}{r_{ss}}\frac{\delta[k_{ss}r_{ss}\frac{\delta T_{ss}}{\delta r_{ss}}]}{\delta r_{ss}} \tag{5.4}$$

$$\frac{\Delta r_{ss}}{2}\rho_{ss}Cp_{ts}\frac{\delta T_{ss}}{\delta t} = h_{in}[T_w - T_f] - k_{ss}\frac{\delta T_{ss}}{\delta r_{ss}} \tag{5.5}$$

Where r$_{ins}$ and r$_{ss}$ refer to the radius of insulation and test section wall at the respective nodes.

The influence of axial heat conduction is expected to be negligible and hence neglected. Heat transfer coefficient at the outside surface of insulation is estimated using Churchill-Chu correlation for natural convection.

Temperature dependent thermo-physical properties of test section material like specific heat and thermal conductivity, as shown in Figures 5.33 and 5.34 are also considered.

A computational code is developed in matlab software using the algorithm shown in Figure 5.35.

Discretisation methodology adopted for solving considered 5 equi-spaced nodes in the test section wall and 28 nodes within the insulation. To confirm that the number of nodes considered is adequate, case is run with double the number of nodes. No significant change is seen in the heat flux values as shown in Figure 5.36. Variation seen in heat flux is only around 3.4% and hence the number of nodes taken is considered adequate.

Using the experimental data, wall heat flux values are computed for stations 2, 3, and 4 and compared to understand the influence of test section orientation and mass flux on chilldown performance. Apart from comparison of heat flux profile, minimum and critical heat flux values are also compared. Findings of the study are brought out in the subsequent sections.

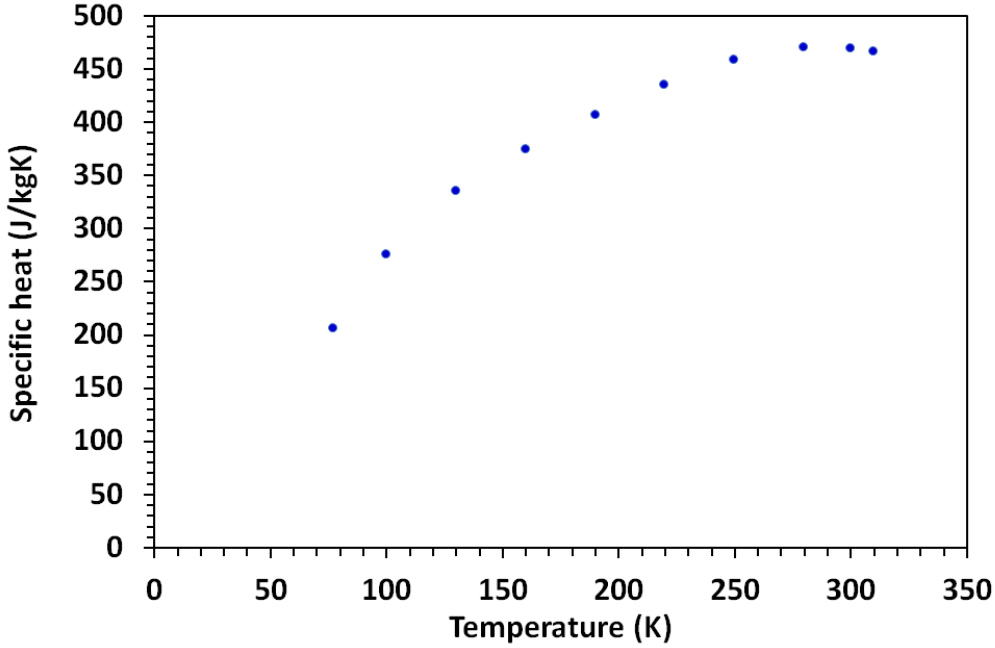

Figure 5.33: Variation of specific heat of stainless steel AISI321 with temperature

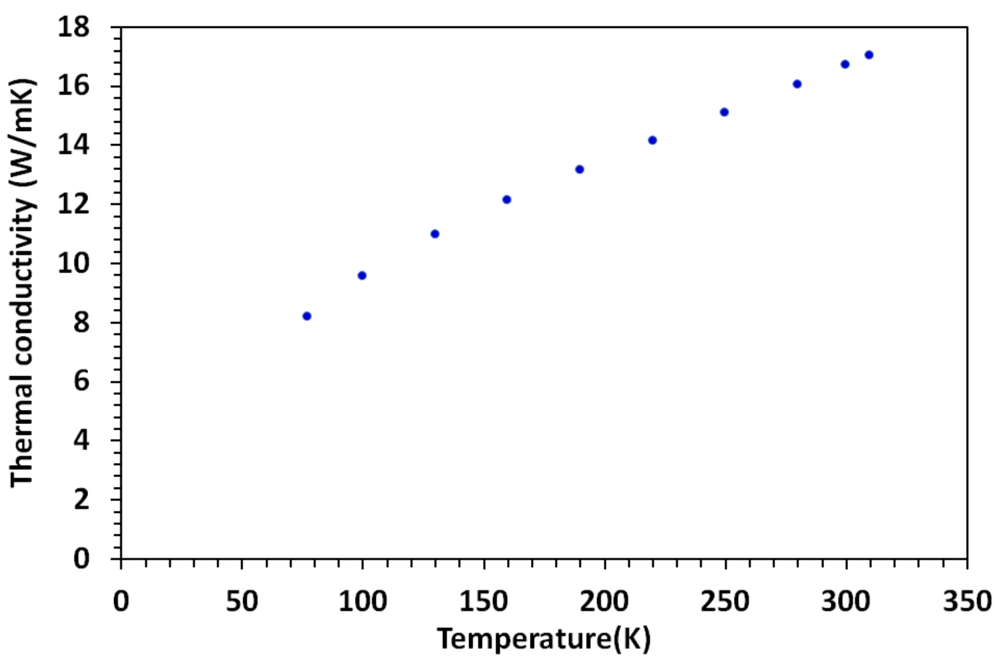

Figure 5.34: Variation of thermal conductivity of stainless steel AISI321 with temperature

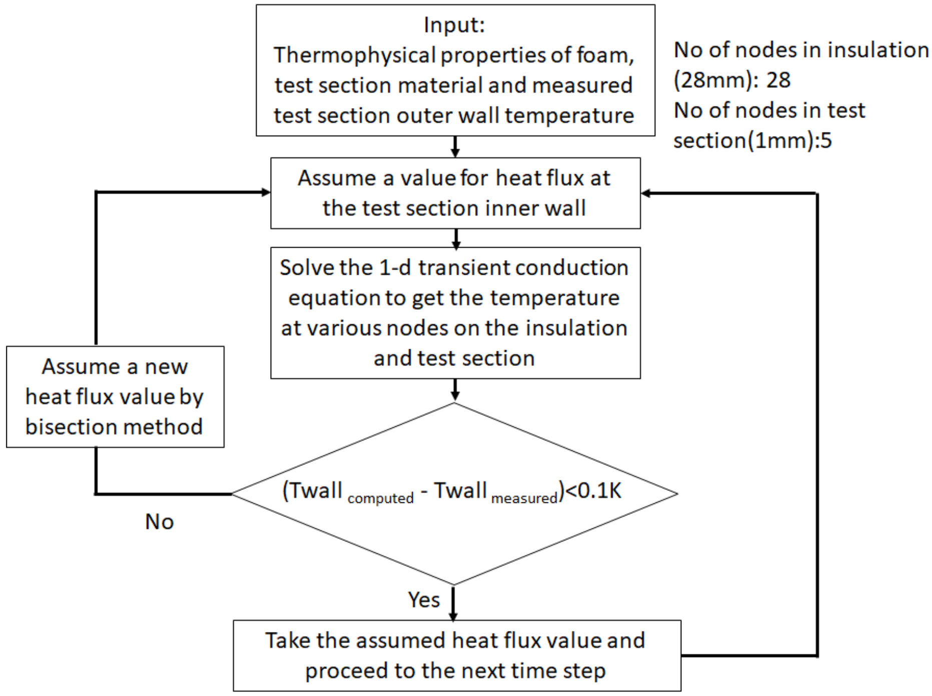

Figure 5.35: Flow chart of the algorithm used for wall heat flux computation

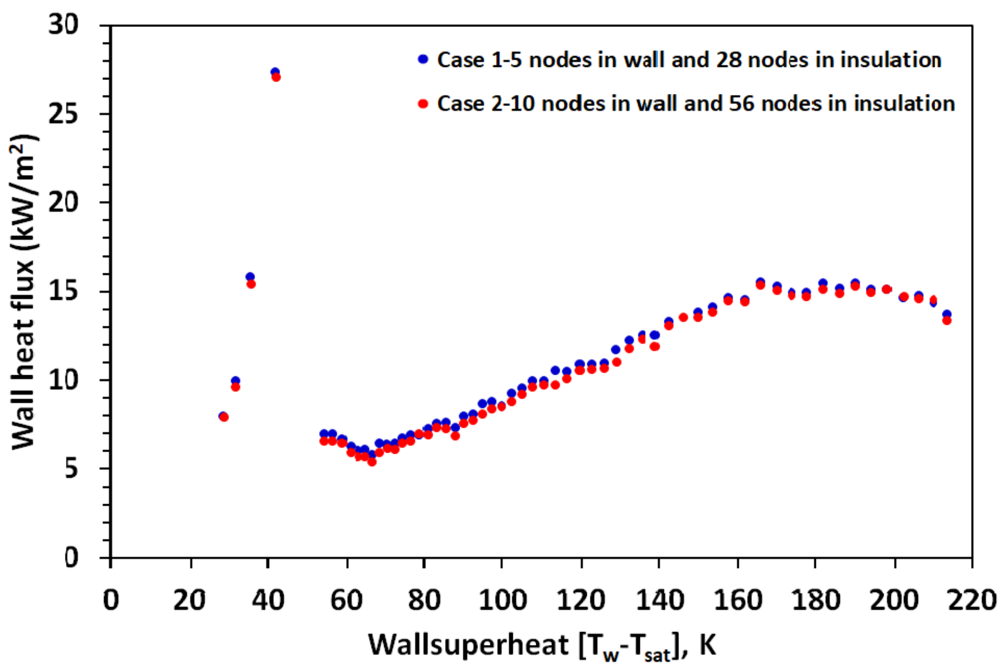

Figure 5.36: Comparison of wall heat flux values computed with double the number of nodes in wall and insulation

5.4.2.2 Comparison of bottom and top wall heat flux profiles

Figures 5.37 and 5.38 show the pattern of variation of bottom and top wall heat flux in the film boiling regime, at stations 3 and 4, during experiments performed on TS1 test section with downward orientation up to 60° and mass flux of 103 kg/m^{2}s.

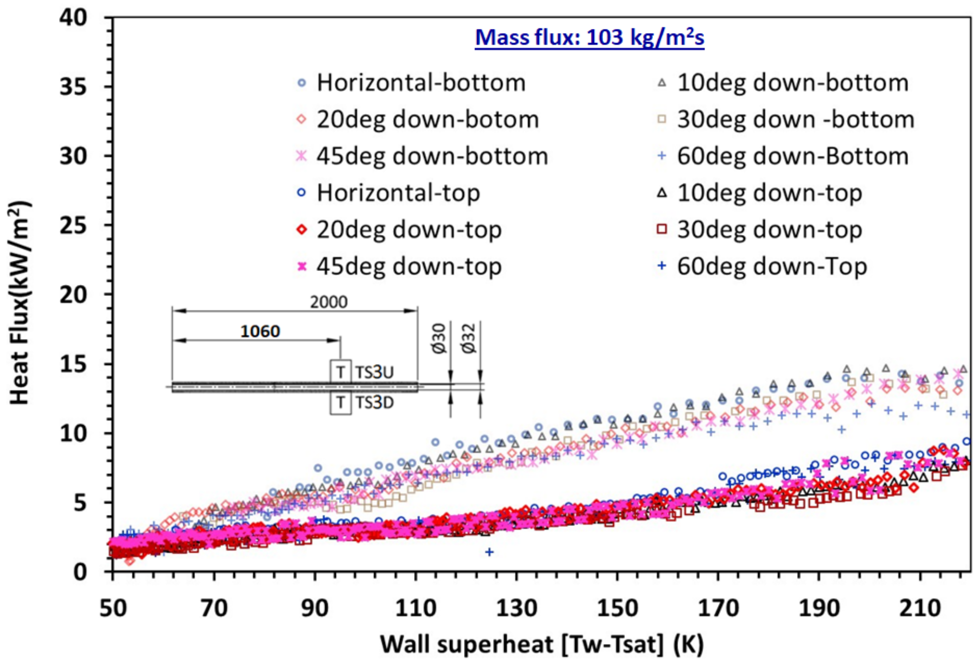

Figure 5.37: Variation of wall heat flux at bottom and top location at station 3 during experiments performed up to 60° downward orientation with TS1 test section (mass flux - 103 kg/m^{2}s)

Being the most dominant phase that decides the chilldown time, heat flux values in the film boiling regime are considered for comparison. In the experiments with different downward inclination, pattern of heat flux is similar. Bottom wall heat flux values are higher as compared to the ones reported for top wall, due to close vicinity of the liquid present. Whereas the top region is predominantly cooled by vapour only. Minor variations are seen in the magnitude of heat flux at the top wall with different test section orientation, which is also in line with the drop rate of top wall temperature.

Pattern of variation of heat flux at the top wall, at stations 3 and 4, in experiments with upward orientation up to 60° and mass flux of 103 kg/m$^2 s$ using test section TS1 is shown in Figures 5.39 and 5.40. The pattern of variation of bottom wall heat flux is similar to experiments with horizontal or downward orientation. Whereas the pattern of variation of top wall heat flux is distinctly different. A jump in top wall heat flux is seen when the wall superheat reaches a threshold value of around 130K. Top wall heat flux increases and becomes at par with the values reported for the bottom wall and this is attributed to the wall wetting by liquid.

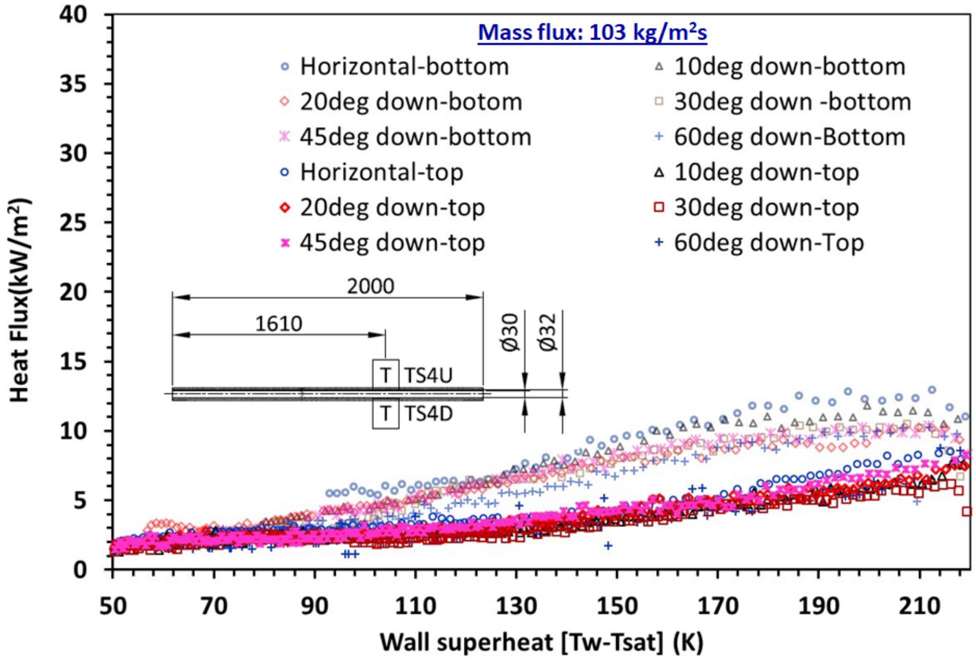

Figure 5.38: Variation of wall heat flux at bottom and top locations at station 4 during experiments performed up to 60° downward orientation with TS1 test section (mass flux - 103 kg/m^{2}s)

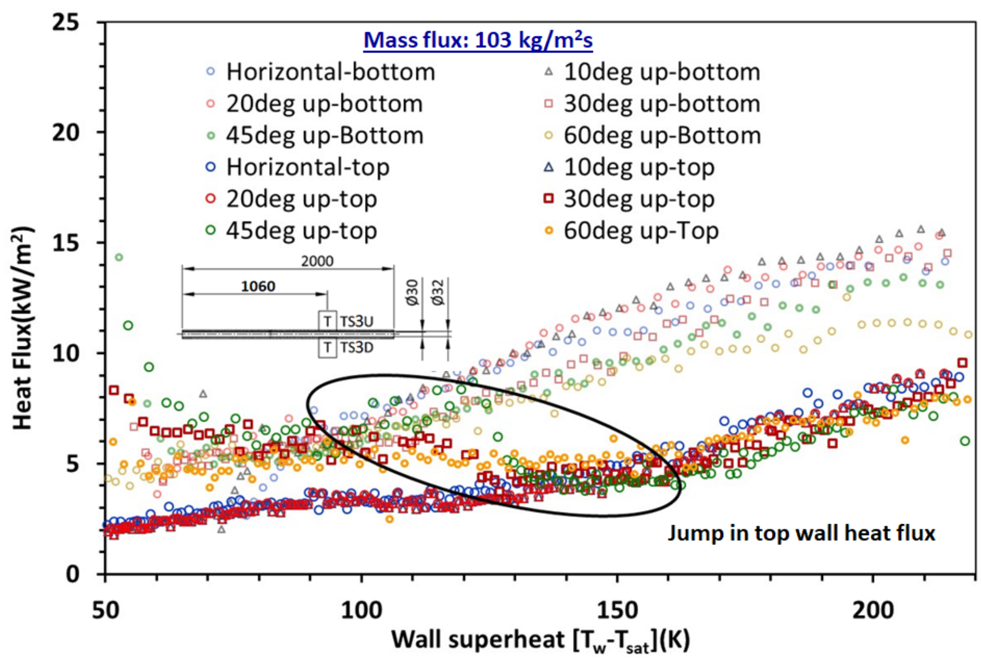

Figure 5.39: Variation of wall heat flux at bottom and top locations at station 3 during experiments up to 60° upward orientation with TS1 test section (mass flux - 103 kg/m^{2}s)

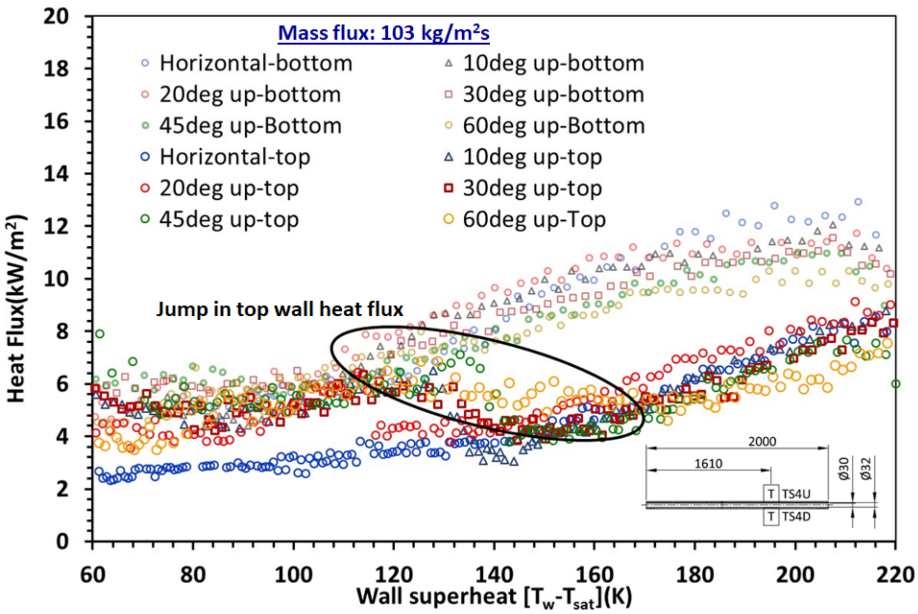

Figure 5.40: Variation of wall heat flux at bottom and top locations at station 4 during experiments up to 60° upward orientation with TS1 test section (mass flux - 103 kg/m^{2}s)

Wall heat flux profile at station 3, estimated for experiments with TS1 test section for downward and upward orientation up to 60° and mass flux condition of 83 kg/m^{2}s, are shown in Figures 5.41 and 5.42.

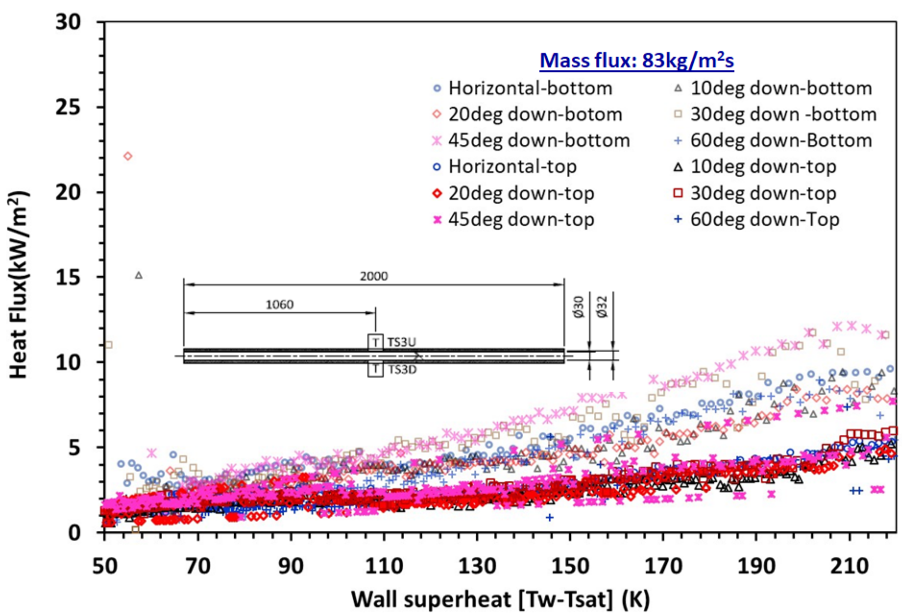

Figure 5.41: Variation of wall heat flux at bottom and top locations at station 3 during experiments up to 60° downward orientation with TS1 test section (mass flux of 83 kg/m^{2}s)

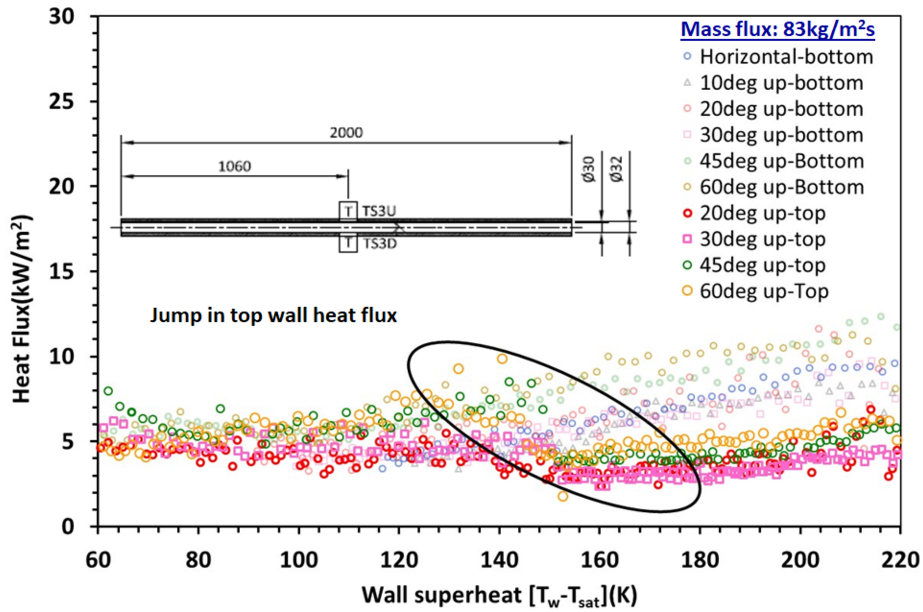

Figure 5.42: Variation of wall heat flux at bottom and top locations at station 3 during experiments up to 60° upward orientation with TS1 test section (mass flux of 83 kg/m^{2}s)

Heat flux profile at station 4, with TS2 test section for downward and upward inclination up to 60° and mass condition of 60 kg/m^{2}s, are shown in Figures 5.43 and 5.44.

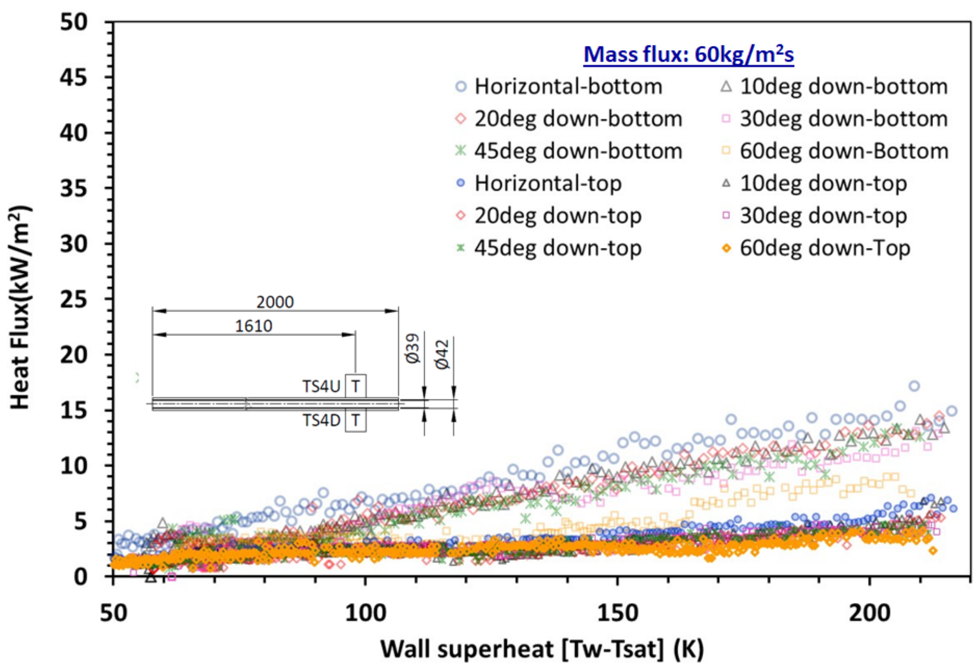

Figure 5.43: Variation of wall heat flux at bottom and top locations at station 4 during experiments with downward orientation with TS2 test section (mass flux - 60 kg/m^{2}s)

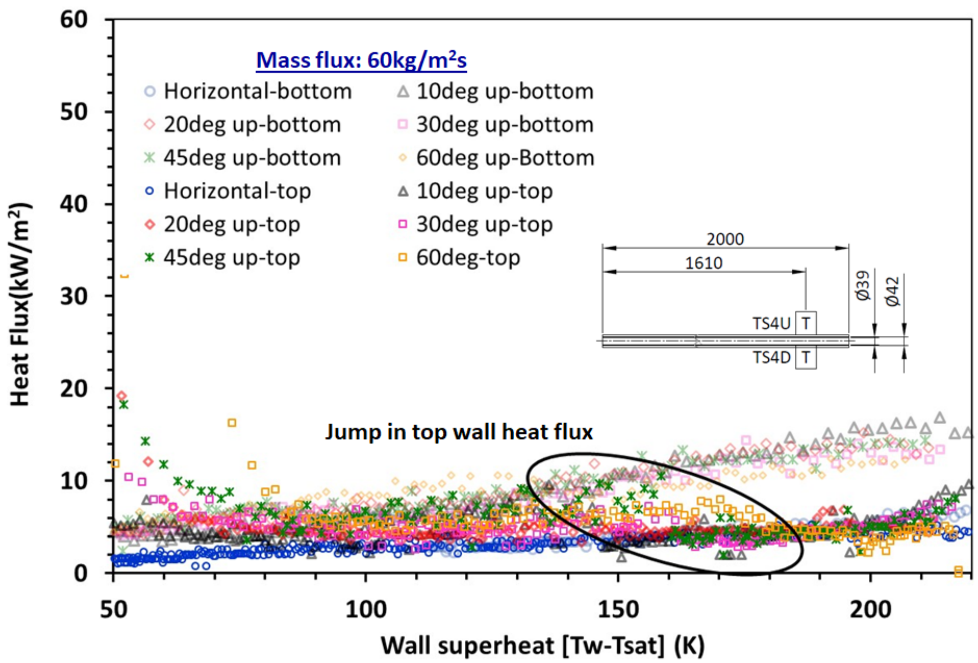

Figure 5.44: Variation of wall heat flux at bottom and top locations at station 4 during experiments with upward orientation with TS2 test section (mass flux - 60 kg/m^{2}s)

They also show a similar trend of higher bottom wall heat flux in experiments with downward inclination as compared to the values reported for top wall. In experiments with upward orientation, bottom wall heat flux is higher than top wall values, till a threshold is reached for the wall superheat. Thereafter a jump is seen, and the top wall heat flux almost becomes comparable with that of the bottom wall. This coincides with the signature of wall wetting by the liquid, as reflected by the wall temperature profile. The observations are almost similar to the ones reported with TS1 test section with mass flux of 103 kg/m^{2}s.

Wall heat flux profile at station 4, observed with 90° downward and upward inclination of TS1 test section during experiments with mass flux of 103 kg/m^{2}s, are shown in Figures 5.45 and 5.46.

As can be seen, wall heat flux at the bottom location is slightly lower in experiments with 90° orientation of test section as compared to horizontal. Whereas heat flux at the top region is higher as compared to horizontal. This is mainly due to improved wetting of the test section wall by the liquid and is the primary reason for improved chilldown performance in experiments with 90° downward and upward orientation.

Observations in experiments with TS1 test section and lower mass flux of 83 kg/m^{2}s are similar as shown in Figures 5.47 and 5.48.

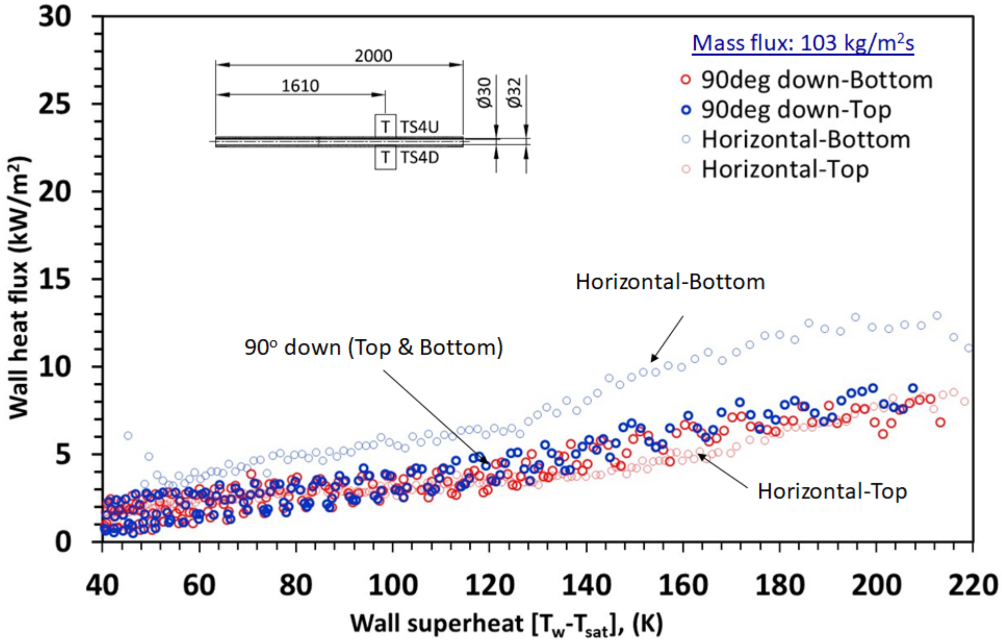

Figure 5.45: Variation of wall heat flux at bottom and top locations at station 4 during experiments with 90° downward orientation of TS1 test section (mass flux - $103\,\mathrm{kg/m^2s}$)

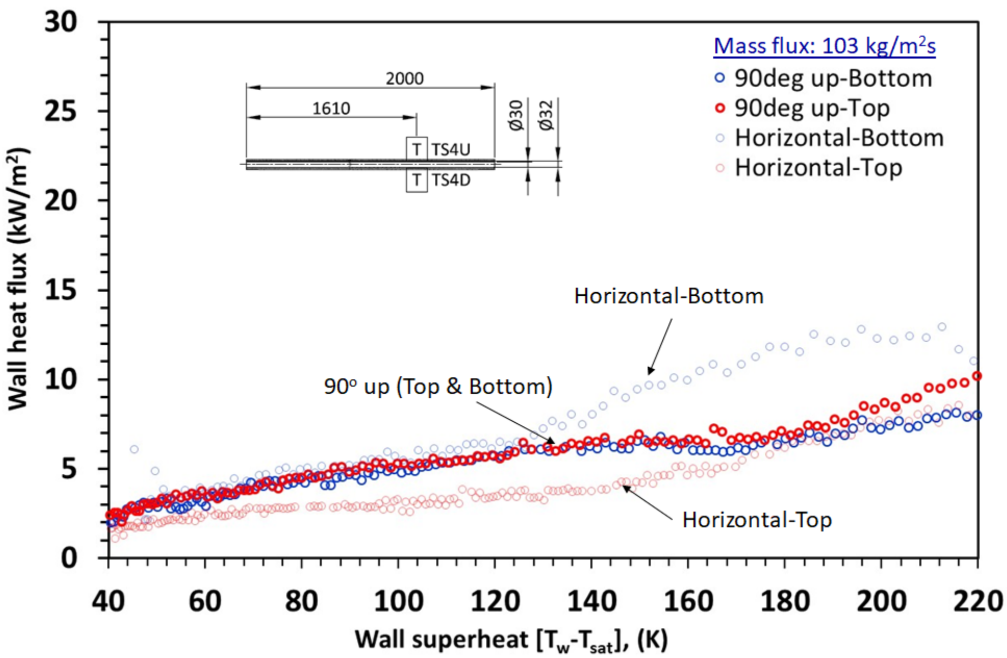

Figure 5.46: Variation of wall heat flux at bottom and top locations at station 4 during experiments with 90° upward orientation of TS1 test section (mass flux - $103\,\mathrm{kg/m^2s}$)

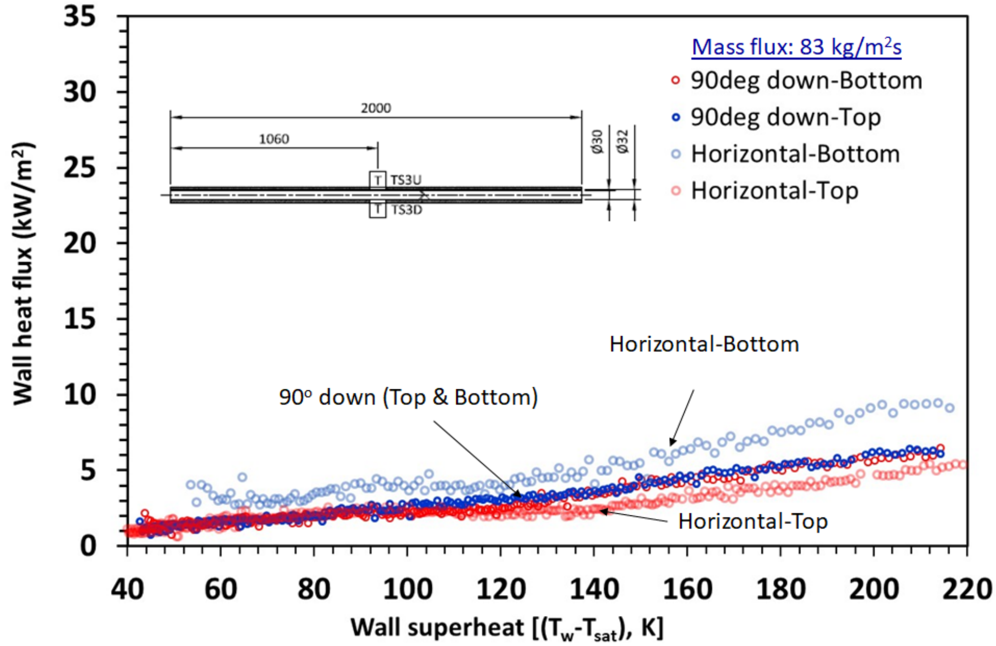

Figure 5.47: Variation of wall heat flux at bottom and top locations at station 3 during experiments with $90°$ downward orientation of TS1 test section (mass flux - 83 kg/m^{2}s)

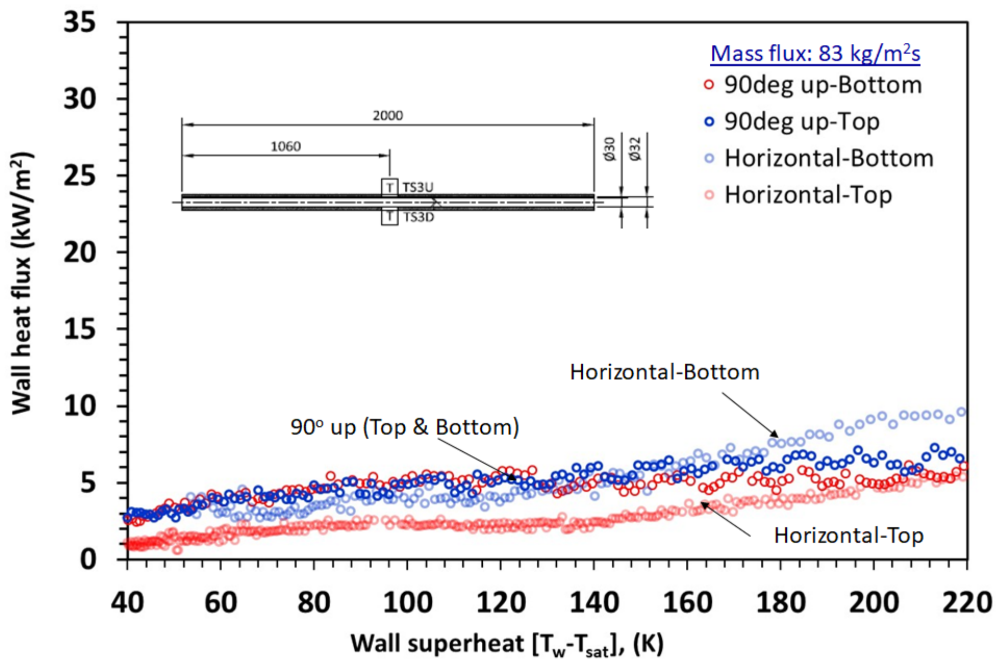

Figure 5.48: Variation of wall heat flux at bottom and top locations at station 3 during experiments with $90°$ upward orientation of TS1 test section (mass flux - 83 kg/m^{2}s)

5.4.2.3 Comparison of minimum heat flux and critical heat flux

The heat flux values estimated by inverse heat transfer technique have been used to compare the minimum heat flux and critical heat flux as well. Data acquired with 1s sampling rate is used for estimation of minimum heat flux, being a slow process, whereas 0.1s sampling rate is used for critical heat flux estimation, being a fast changing process. As generally observed in a chilldown process, in the film boiling regime, heat flux decreases as chilldown proceeds and wall superheat decreases. It then goes through a point of minimum heat flux before entering into transition boiling followed by nucleate boiling regime. Minimum heat flux is the heat flux at the point of change over from film boiling to transition boiling and critical heat flux is the maximum heat flux experienced by the wall in nucleate boiling regime. Minimum heat flux point and critical heat flux points are shown in Figure 5.49, which is a typical heat flux profile for station 3 of TS1 test section, as observed during experiment with mass flux of 103 kg/m^{2}s.

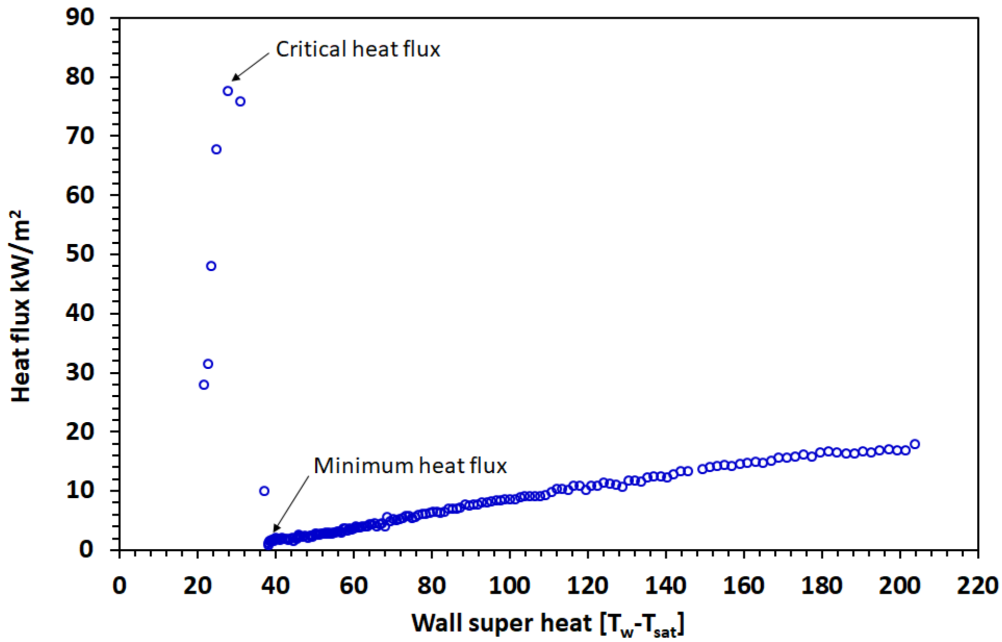

Figure 5.49: Typical wall heat flux profile observed at station 3 during experiment performed with TS1 test section held in horizontal orientation (mass flux - 103 kg/m^{2}s)

Variation of average minimum heat flux at the bottom location with respect to test section orientation as observed during experiments with TS1 test section employing a mass flux of 103 kg/m^{2}s is shown in Figure 5.50.

Average minimum heat flux values at the bottom location are estimated by taking the average of the values reported at stations 2, 3, and 4. Minimum heat flux values are observed to be lower for downward and horizontal orientation of test section. It is seen to be decreasing up to 60° downward

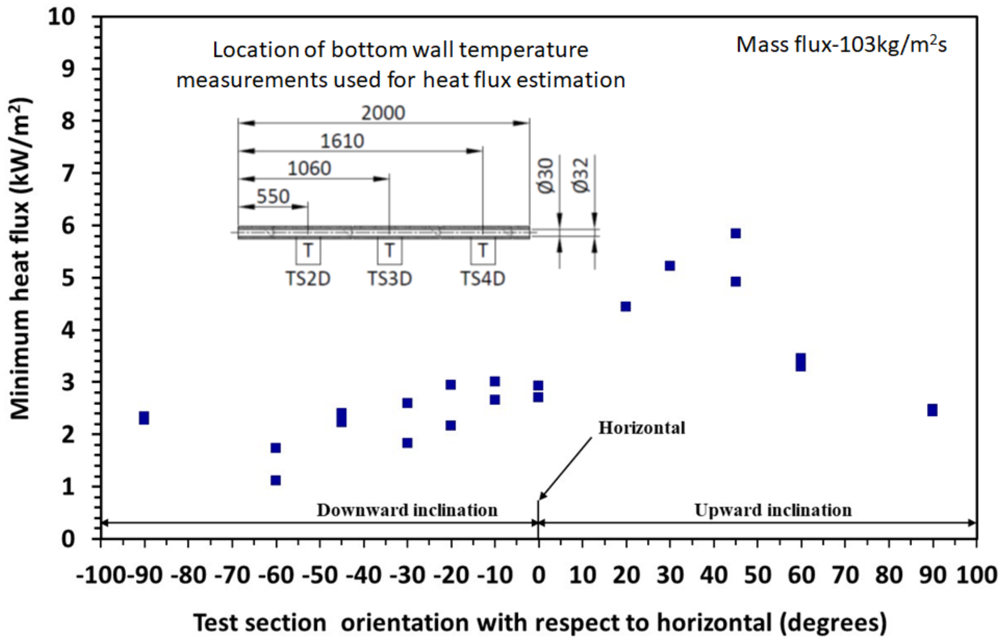

Figure 5.50: Variation of average minimum heat flux at bottom during experiments with TS1 test section (mass flux - 103 kg/m^{2}s)

inclination and beyond that a minor increase is seen at 90° downward orientation. In experiments with upward orientation, it increases up to 45° upward inclination, beyond which it reduces to a value similar to horizontal or downward inclination. The values observed for 90° upward and downward orientations are almost similar. The trend of variation in minimum heat flux is almost following the pattern of variation of CPI.

Observation with regard to variation of minimum heat flux with change in test section orientation are almost similar in experiments with mass flux of 83 and 60 kg/m^{2}s as well with some minor differences. Results are shown in Figures 5.51 and 5.52. In experiments with mass flux of 83 kg/m^{2}s, with downward orientation, the decreasing trend of minimum heat flux continues up to 60° and the trend with upward orientation is similar.

Whereas in experiments with mass flux of 60 kg/m^{2}s, trend with downward orientation is similar and the increasing trend with upward orientation continues up to 60° inclination.

As mentioned earlier, to evaluate the critical heat flux, sixty two experiments are performed, twenty two each for mass flux conditions of 103 kg/m^{2}s and 83 kg/m^{2}s with TS1 test section and eighteen tests for a mass flux condition of 60 kg/m^{2}s with TS2 test section. List of experiments performed for different test section orientations are given in Table 5.3.

Experiments repeated have shown very good consistency in the wall temperature profile. As mentioned earlier, the variation in top and bottom wall temperatures between repeat experiments is well within 5K and the dispersion in chilldown time is well within acceptable limits. As a typical

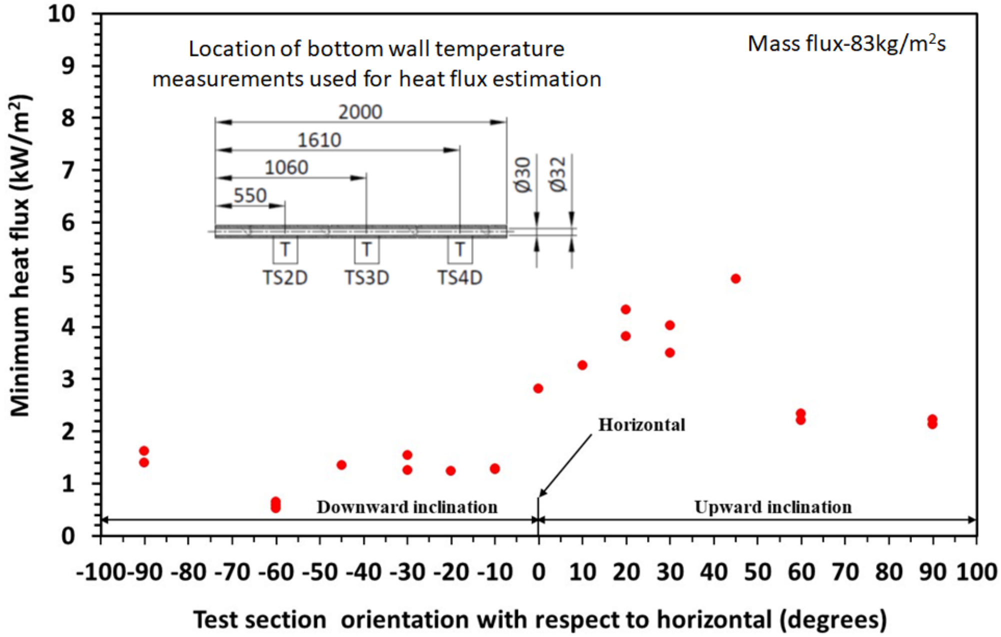

Figure 5.51: Variation of average minimum heat flux at bottom during experiments with TS1 test section (mass flux - 83 kg/m^{2}s)

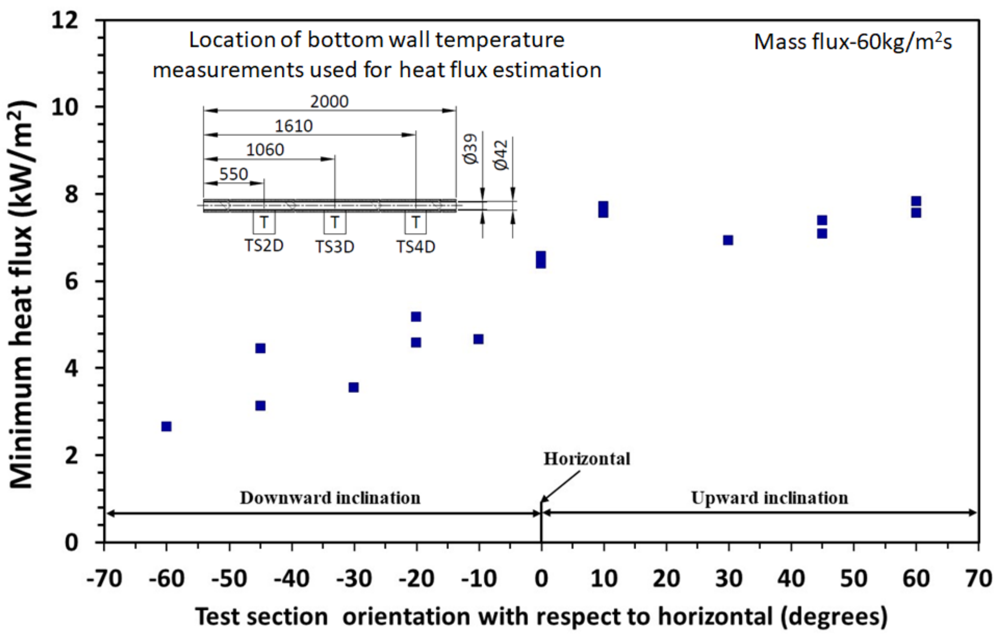

Figure 5.52: Variation of average minimum heat flux at bottom during experiments with TS2 test section (mass flux - 60 kg/m^{2}s)

Table 5.3: Experiments performed with TS1 and TS2 test sections for critical heat flux estimation

Sl. No.	Test section	Mass flux/Number of tests		
		103 kg/m^{2}s	83 kg/m^{2}s	60 kg/m^{2}s
1	Horizontal	2	1	2
2	10° down	1	1	2
3	20° down	2	2	1
4	30° down	2	2	2
5	45° down	1	2	2
6	60° down	2	2	1
7	90° down	2	2	–
8	10° up	2	2	1
9	20° up	2	2	1
10	30° up	1	1	2
11	45° up	2	2	2
12	60° up	1	2	2
13	90° up	2	2	–
	Total	***22***	***22***	***18***

case, wall temperature profile observed at station 4 during repeat experiments performed for three different test section orientations and mass flux conditions are shown in Figures 5.53 5.54, and 5.55.

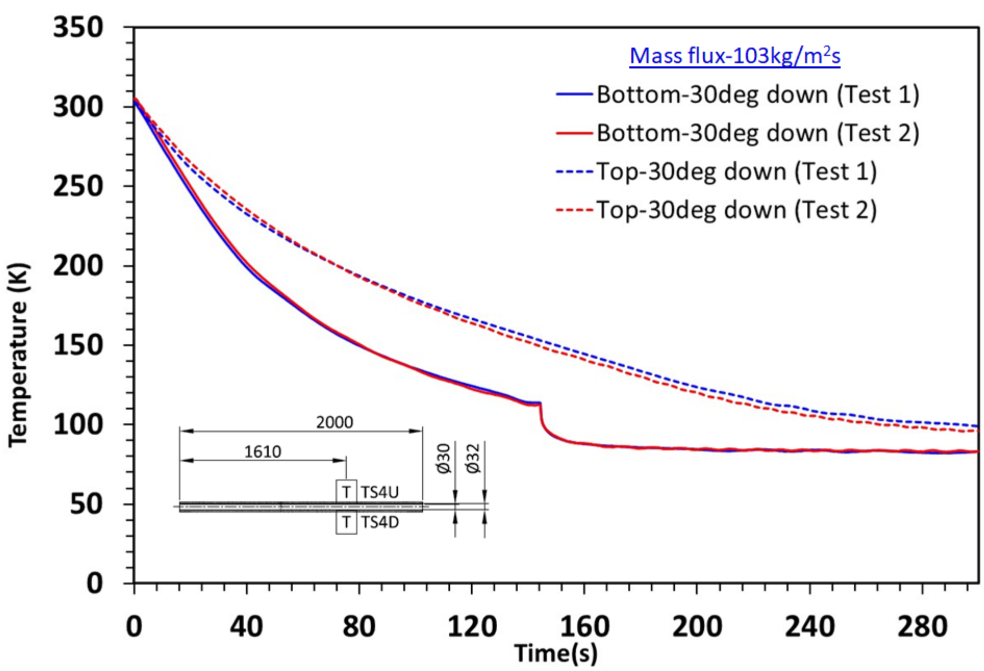

Figure 5.53: Comparison of wall temperature profile observed at station 4 during experiments with 30° downward orientation of TS1 test section (mass flux - 103 kg/m^{2}s)

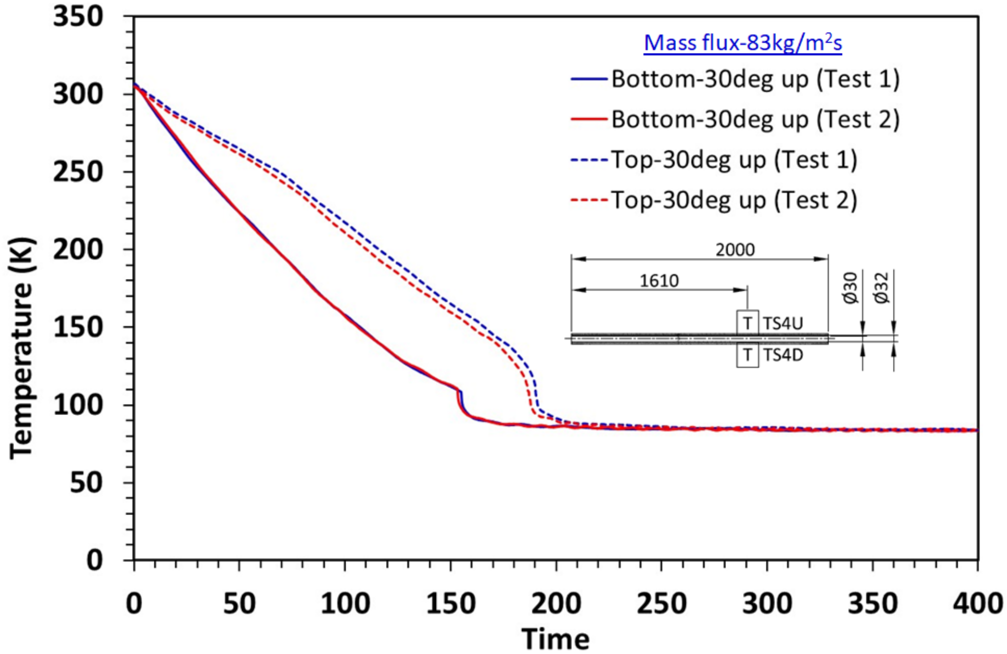

Figure 5.54: Comparison of wall temperature profile observed at station 4 during experiments with 30° upward orientation of TS1 test section (mass flux - 83 kg/m^{2}s)

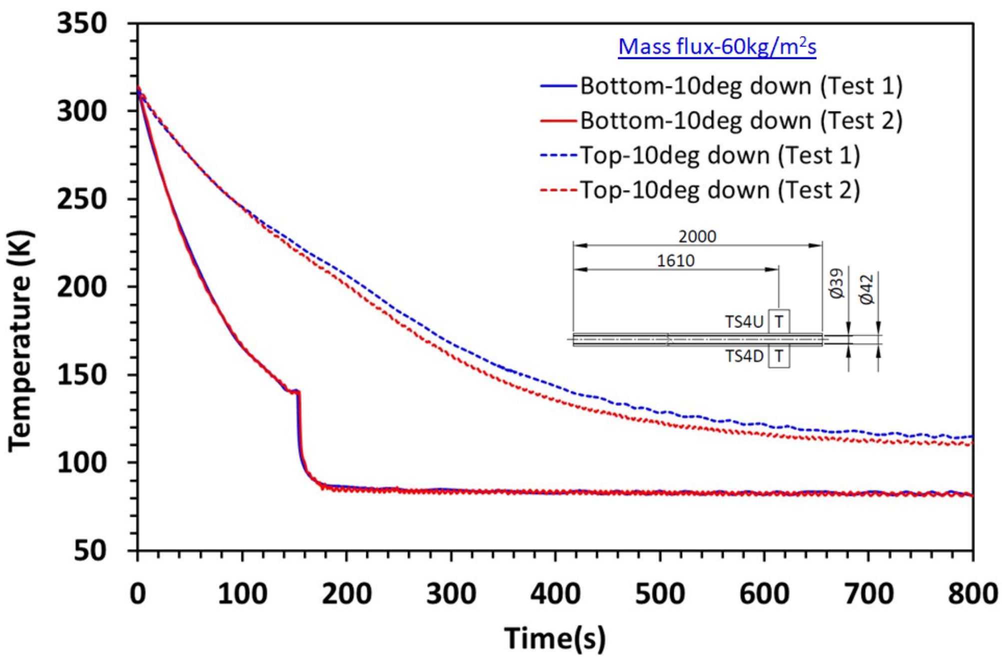

Figure 5.55: Comparison of wall temperature profile observed at station 4 during experiments with 10° downward orientation of TS2 test section (mass flux - 60 kg/m^{2}s)

Heat flux at the inner wall is estimated from the measured outer wall temperature using the inverse heat transfer technique as described in section 5.4.2.1. Data acquired with a sampling rate of 10Hz is used for the heat flux estimation. Data is smoothened with a sampling rate of 2Hz for the film boiling regime and 5Hz in transition and nucleate boiling regimes, as a higher sampling rate of 10Hz is found crashing and not giving consistent results. Critical heat flux is estimated using the heat flux values computed. Variation of average critical heat flux at stations 2, 3, and 4 with test section orientation, as observed in experiments with TS1 test section for a mass flux condition of 103 kg/m^{2}s, is shown in Figure 5.56. In experiments with downward orientation, up to 60° inclination, critical heat flux values are found to be generally higher. Whereas the values are lower in experiments with upward orientation. In experiments with 90° upward and downward orientation, the values are almost similar. This trend of critical heat flux variation with test section orientation follows a reverse pattern of chilldown performance and is probably decided by the heat capacity left with the test section wall on reaching the critical heat flux point. Heat capacity will be lower, if chilldown performance is better and will be higher, if performance is inferior.

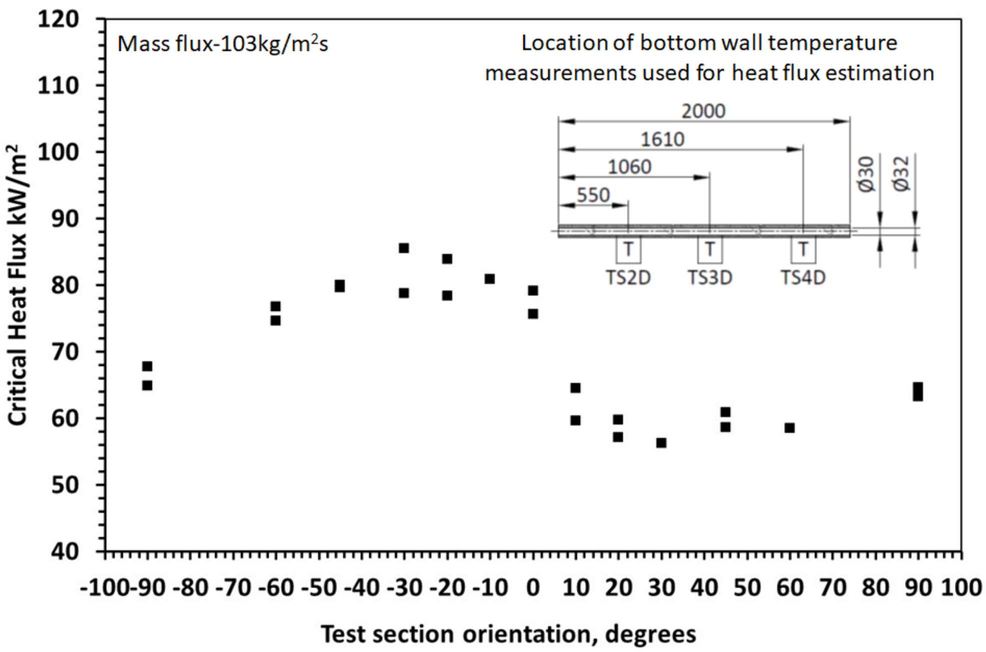

Figure 5.56: Variation of average critical heat flux at bottom during experiments with TS1 test section (mass flux 103 kg/m^{2}s)

Trend of variation of critical heat flux with change in test section orientation is almost similar in experiments with mass flux of 83 and 60 kg/m^{2}s as well. Results are shown in Figures 5.57 and 5.58. Critical heat flux is higher for experiments with downward orientation and lower in experiments with upward orientation. Probable reason for this trend is the same as the one mentioned earlier for mass flux condition of 103 kg/m^{2}s.

Minimum and critical heat flux values are estimated using the various correlations available in

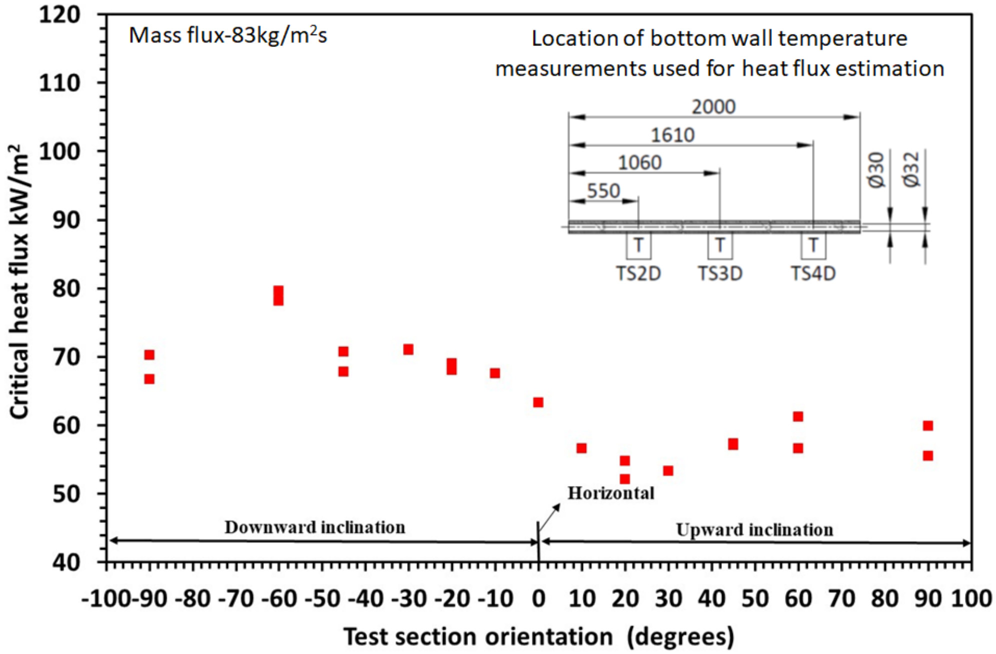

Figure 5.57: Variation of average critical heat flux at bottom during experiments with TS1 section (mass flux 83 kg/m^{2}s)

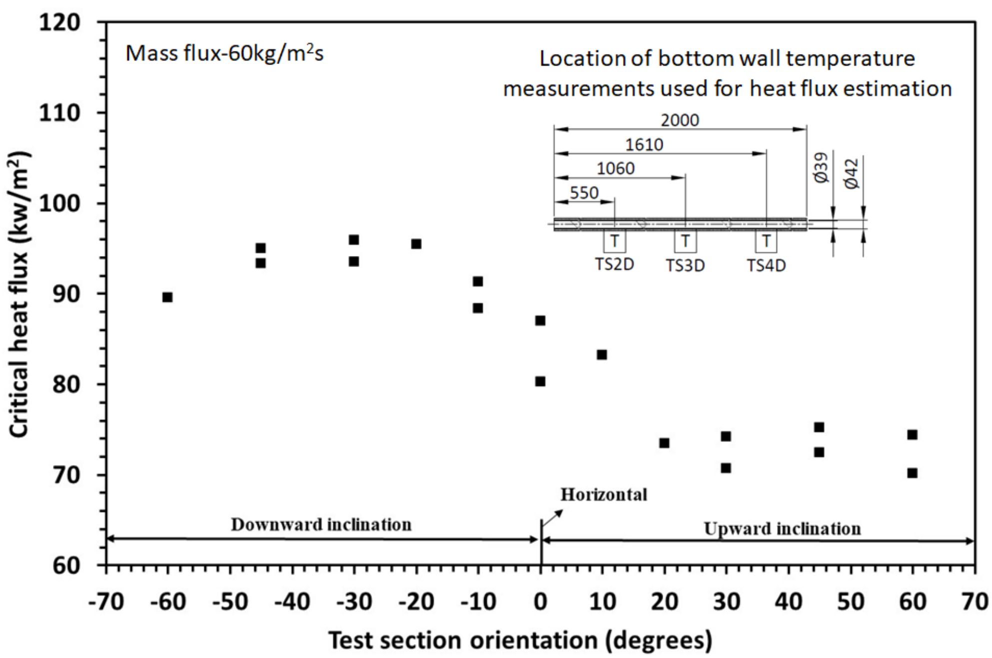

Figure 5.58: Variation of average critical heat flux at bottom during experiments with TS2 section (mass flux 60 kg/m^{2}s)

published literature and compared with the experimental values. Correlations used for minimum and critical heat flux values are listed in Tables 5.4 and 5.5.

Table 5.4: Empirical correlations proposed by various authors and available in published literature for estimation of minimum heat flux

Sl. No.	Author	Correlation
1	Zuber [55]	$q_{MHF} = 0.176\rho_v h_{fg}\left[\frac{\sigma g(\rho_l-\rho_v)}{(\rho_l+\rho_v)^2}\right]^{0.25}$
2	Berenson [56]	$q_{MHF} = 0.091\rho_v h_{fg}\left[\frac{\sigma g(\rho_l-\rho_v)}{(\rho_l+\rho_v)^2}\right]^{0.25}$

Table 5.5: Empirical correlations proposed by various authors and available in published literature for estimation of critical heat flux

Sl. No.	Author	Correlation
1	Zuber [57]	$q_{CHF} = 0.131\rho_v h_{fg}\left[\frac{\sigma g(\rho_l-\rho_v)}{{\rho_v}^2}\right]^{0.25}$
2	Lienhard and Dhir [58]	$q_{CHF} = 0.149\rho_v h_{fg}\left[\frac{\sigma g(\rho_l-\rho_v)}{{\rho_v}^2}\right]^{0.25}$
3	Katto and Ohno [13]	$q_{CHF} = 0.186Gh_{fg}\left[\frac{\rho_v}{\rho_l}\right]^{0.559}{We_l}^{-0.264}$
4	Mudawar and Maddox [59]	$q_{CHF} = 0.161Gh_{fg}\left[\frac{\rho_v}{\rho_l}\right]^{\frac{15}{23}}{We_l}^{-\frac{8}{23}}\left[\frac{L}{D}\right]^{\frac{1}{23}}$
5	Darr et al. [29]	$q_{CHF} = 0.0527Gh_{fg}{We_l}^{-0.2894}$

Minimum heat flux values estimated using these are correlations are compared with the experimental values observed in the present study in Table 5.6. The values estimated using the correlations are very high compared to the experimental values observed in the present study and the difference could be attributed to the fact that these correlations are either based on pool boiling studies or heat flux controlled experiments and hence may not be directly applicable for such quenching studies with flow boiling.

Table 5.6: Comparison of minimum heat flux values predicted with the experimental data generated as part of present study

Sl. No.	Author	Mass flux/Average minimum heat flux (kW/m^2)		
		103 kg/m^{2}s	83 kg/m^{2}s	60 kg/m^{2}s
1	Zuber [55]	16.32		
2	Berenson [56]	8.44		
3	Present study	3.03	2.19	5.75

Critical heat flux values estimated using Zuber [57] and Lienhard and Dhir [58] correlations are very high and the reason could be due to the fact that these correlations are based on pool boiling

Table 5.7: Comparison of critical heat flux values predicted with the experimental data generated as part of present study

Sl. No.	Author	Mass flux/Average critical heat flux (kW/m^2)		
		103 kg/m^{2}s	83 kg/m^{2}s	60 kg/m^{2}s
1	Zuber [57]	161.38		
2	Lienhard and Dhir [58]	183.55		
3	Katto and Ohno [13]	25.7	23.18	19.89
4	Mudawar and Maddox [59]	8.42	7.88	7.06
5	Darr et al. [29]	106.71	97.35	84.89
6	Present study	70.39	63.97	83.70

data, whereas the values estimated using the correlations proposed by Katto and Ohno [13] and Mudawar and Maddox [59] are lower as compared to experimentally observed values. Estimates worked out using the correlation proposed by Darr et al. [29] are closer and error compared to experimental data is around 33%.

5.4.2.4 Pattern of variation of heat transfer coefficient with wall superheat

In the flim boiling regime, heat flux shows a gradual reduction with decrease in wall superheat, as can be seen in the typical graphs shown earlier. Whereas heat transfer coefficient shows an increasing trend with wall superheat. A typical plot showing the variation of heat transfer coefficient with wall superheat, during experiment with TS1 test section with horizontal orientation and mass flux of 103 kg/m^{2}s is shown in Figure 5.59.

5.5 Experimental errors and uncertainty in heat flux and CPI estimates

As mentioned earlier, the inner wall heat flux values are computed using the measured surface temperature data. Physical dimensions of test section like its diameter and wall thickness and the thermophysical properties of the test section material like thermal conductivity, specific heat etc. are also used for this heat flux estimation. Similarly CPI is estimated using the experimental data on chilldown time, total mass of cryogen consumed during chilldown, thermal mass of test section, latent heat of cryogen etc. Errors, if any, in any of these parameters, can affect the accuracy of wall heat flux and CPI estimation. An assessment has been made on the extent of uncertainty that can exist in the heat flux and CPI values estimated and are brought out in the subsequent sections.

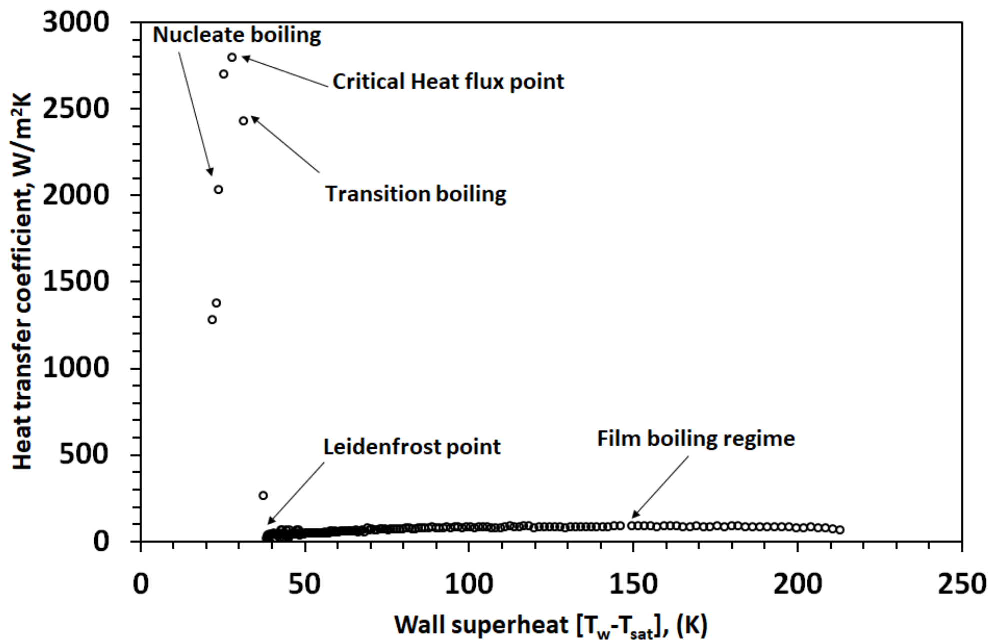

Figure 5.59: Graph showing the variation of heat transfer coefficient with wall superheat at station 3 during experiments with TS1 test section held in horizontal orientation (mass flux 103 kg/m^{2}s)

5.5.1 Uncertainty in heat flux estimate

Heat flux is estimated using the transient conduction-convection equations 5.2 to 5.5 and the code developed for heat flux estimation as described in section 5.4.2.1. Measured surface temperature data, test section dimensions and thermophysical properties of test section material are considered for this estimation. Hence the estimate is sensitive to the uncertainties associated with the test section dimensions like tube diameter, wall thickness etc. and the thermophysical properties of the materials involved. Sensitive parameters that can affect the heat flux estimates and the maximum possible error or deviation in these parameters considered for the present study are given in Table 5.8. Expected variation in tube dimensions like diameter and wall thickness, thermophysical property of materials like thermal conductivity and specific heat of the test section and insulation material are seelected based on previous experience.

The variation expected in heat flux due to variation in each of these parameters is assessed by plugging in these parametric variations into the code developed. Root sum square of these variations are thus arrived at individually, which are brought out in Table 5.9.

Table 5.8: Error or deviation in sensitive parameters considered for wall heat flux estimate uncertainty analysis

Sl. No.	Parameter	Error or deviation
1	Surface temperature	±1.5K
2	Test section diameter	±0.5%
3	Test section wall thickness	±5.0%
4	Thermal conductivity of Stainless steel	±1.5%
5	Specific heat of Stainless steel	±1.5%
6	Thermal conductivity of Insulation	±1.5%
7	Specific heat of Insulation	±1.5%

Table 5.9: Outcome of sensitivity study to assess the uncertainty in wall heat flux estimate

Sl. No.	Parameter	Uncertainty in heat flux estimate
1	Surface temperature	±2.2%
2	Test section diameter	±0.9%
3	Test section wall thickness	±5.6%
4	Thermal conductivity of Stainless steel	±1.5%
5	Specific heat of Stainless steel	±3.0%
6	Thermal conductivity of Insulation	±1.0%
7	Specific heat of Insulation	±1.5%

$$\sigma_{HF} = \{\sigma_T^2 + \sigma_d^2 + \sigma_t^2 + \sigma_{cpss}^2 + \sigma_{kss}^2 + \sigma_{cpins}^2 + \sigma_{kss}^2\}^{0.5} \tag{5.6}$$

Maximum uncertainty in heat flux estimate is then worked out using equation 5.6 taking the root sum square of the uncertainty values reported for all these parameters considered and this works out to 7.17%. Thus it is declared that the uncertainty in the heat flux values estimate is expected to be well within $\pm 8\%$.

5.5.2 Uncertainty in CPI estimate

CPI is estimated using the experimental data on chilldown time, estimated thermal mass of test section, total mass of the cryogen consumed during chilldown and latent heat of cryogen. The maximum possible error or deviation in the sensitive parameters that is considered for this study is given in Table 5.10.

Taking into account the above, the uncertainty in CPI works out to $\pm 11.27\%$. Based on this, it is declared that the uncertainty in CPI is well within $\pm 12\%$.

Influence of feedline orientation on chilldown performance has been extensively studied using

Table 5.10: Error or deviation in sensitive parameters considered for CPI estimate uncertainty analysis

Sl. No.	Parameter	Error or deviation
1	Chilldown time	$\pm 10\%$
2	Thermal mass of test section	$\pm 1\%$
3	Mass of cryogen consumed	$\pm 5\%$
4	Latent heat of cryogen	$\pm 1\%$

two test section configurations, varying the orientation from 90° downward to 90° upward inclination. As reported, chilldown performance becomes inferior with downward inclination and improves significantly with upward inclination. Best chilldown performance is achieved around 45° upward inclination. Heat flux pattern for different downward and upward orientations of test section has been studied. It is seen to be similar at the bottom wall for different inclinations of test section. Whereas at the top wall, it is similar for horizontal and downward orientation of test section and significantly different in experiments with upward orientation. A significant jump is seen in the top wall heat flux when the wall superheat reduces below a threshold value. Experiments have also brought out a typical pattern in the variation of minimum and critical heat flux with the feedline orientation.

Chapter 6

Flow visualisation experiments

Based on the experiments carried out as part of the present study with varying test section orientation, it is very much evident that feedline orientation has a significant impact on the chilldown performance. A need was then felt to perform experiments with a visualisation window to capture and understand the flow structure during tests with varying feedline inclination and also study its effect on chilldown performance. Vacuum jacketed view glass made of borosilicate glass, as described in Chapter 4 is realised and used for flow visualisation.

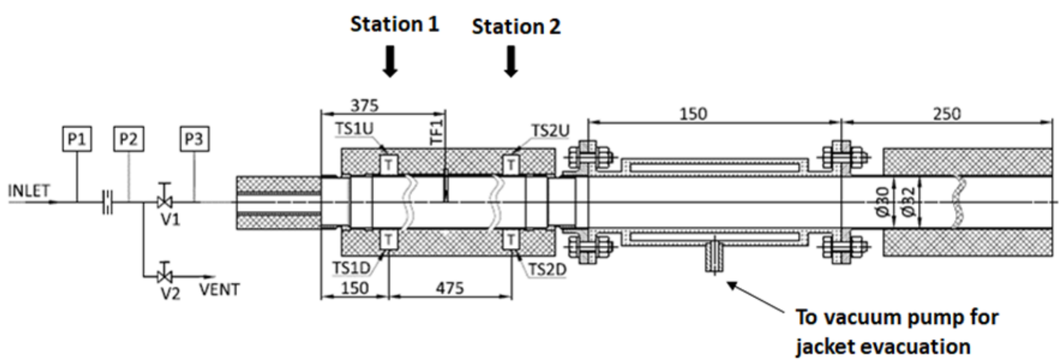

Sensors	Type, range and accuracy	Quantity	Legend
Pressure	Strain gauge type, 0-0.5MPa range, ±0.7%	3	P1, P2 and P3
Fluid temperature	100Ω Platinum RTD, ±0.55K at 73K	1	TF1
Surface temperature	T type Thermocouple, ±1.5K at 77K	4	TS1D, TS1U, TS2D, TS2U

Figure 6.1: Instrumentation scheme employed for flow visualisation studies

Details of the experimental set-up has already been brought out in Chapter 4. Instrumentation scheme employed for flow visualisation studies is shown in Figure 6.1. The set-up is provided with three pressure sensors P1, P2 and P3 which are used to measure orifice inlet, orifice outlet and test section inlet pressures respectively, as mentioned earlier. Test section is provided with 4 numbers of T type thermocouples, two numbers each at two stations along the length of test section to measure its outside wall temperature and have an accuracy of ±1.5K. Stations 1 and 2 have two surface temperature measurements each, one each at the bottom and top location, placed 180° apart. Measurements provided at bottom and top location are identified by the alphabets D and U in the legend. Fluid temperature measurement is also made using one number of 100Ω Platinum RTD (TF1) placed at a distance of 375 mm from inlet. RTD probe is provided only to get an assessment of the fluid temperature and not used directly for any computation. RTD has an accuracy of ±0.55K at 73K. During the experiments, measurements are acquired using a portable data acquisition system at a sampling rate of 1 Hz. A PHANTOM make V2012 model camera, is used to videograph and capture the flow structure during the experiments and the scanning rate employed is 5000 frames per second.

6.1 Test Matrix

Test procedure followed is already described in Chapter 4. Flow visualisation experiments are performed with test sections held at eight different orientations as listed in Table 6.1, which includes horizontal, and upward and downward orientations upto 90° with respect to horizontal. Mass flux simulated during the experiments is 37 kg/m^{2}s.

Table 6.1: Experiments performed for flow visualisation

Sl. No.	Test section	No. of tests
1	Horizontal	2
2	20° down	1
3	30° down	1
4	45° down	2
5	90° up	2
6	20° up	1
7	45° up	1
8	90° up	1

Though attempts are made to carry out experiments with a higher mass flux of 103 kg/m^{2}s, clear images of flow structure could not be obtained due to condensation of moisture on the double jacketed view glass. Experiments performed as part of the study have shown that the trend in wall temperature profile at bottom and top locations are similar even with a lower mass flux of 60 kg/m^{2}s as compared to those with 103 kg/m^{2}s and 83 kg/m^{2}s mass flux conditions. Based on this, experiments with flow visualisation are performed with a lower mass flux of 37 kg/m^{2}s. With this lower mass flux, the issue of moisture condensation on the double jacketed view glass could be almost avoided completely. Poor image quality with higher mass flux of 103 kg/m^{2}s can be seen as a limitation of the present experimental set-up and can be improved by placing the entire experimental set-up inside a vacuum chamber.

Experiments are repeated for certain orientations of test section to establish consistency. High speed video images are analysed in detail and studied in conjunction with surface temperature measurements made at station 2. An attempt is made to corroborate the changes in flow structure observed with the changes in wall temperature profile and chilldown performance with varying feedline orientation. Findings of the present study are brought out in the subsequent section.

6.2 Results and discussions

As mentioned earlier, experiments are performed for eight different orientations of test section. The flow structure is observed to be stratified in experiments with horizontal orientation of test section. As can be seen in Figure 6.2, liquid is flowing along the bottom and vapour along the top of the test section.

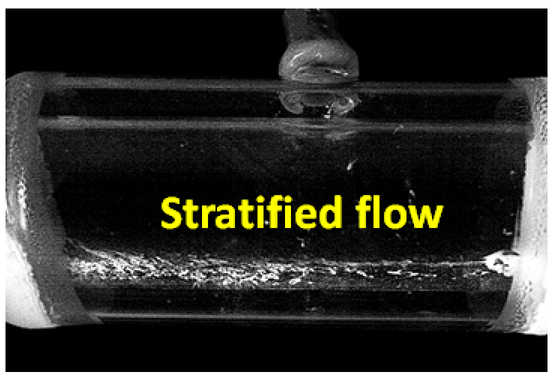

Figure 6.2: Flow structure observed in experiment with test section held horizontal

The images captured during experiments with 20° and 45° upward orientation of test section are shown in Figures 6.3 and 6.4 respectively.

Flow is seen to be periodic and the flow structure keeps changing from stratified to plug or slug flow. Plug or slug is seen to be emerging from the inlet side and slowly filling up the entire length of the view glass. It moves along the direction of flow in the axial direction and leaves the viewing section, after which the flow structure changes to stratified again. This cycle is seen to be repeating. Test section is flowing almost full with liquid wetting the top wall at instances of slug or plug flow. This flow structure induces liquid wetting at the top wall, making it cool down faster as compared to horizontal and downward inclination. Thus improved chilldown performance in experiments with upward inclination, as described in Chapter 5, is clearly attributable to the change in flow structure.

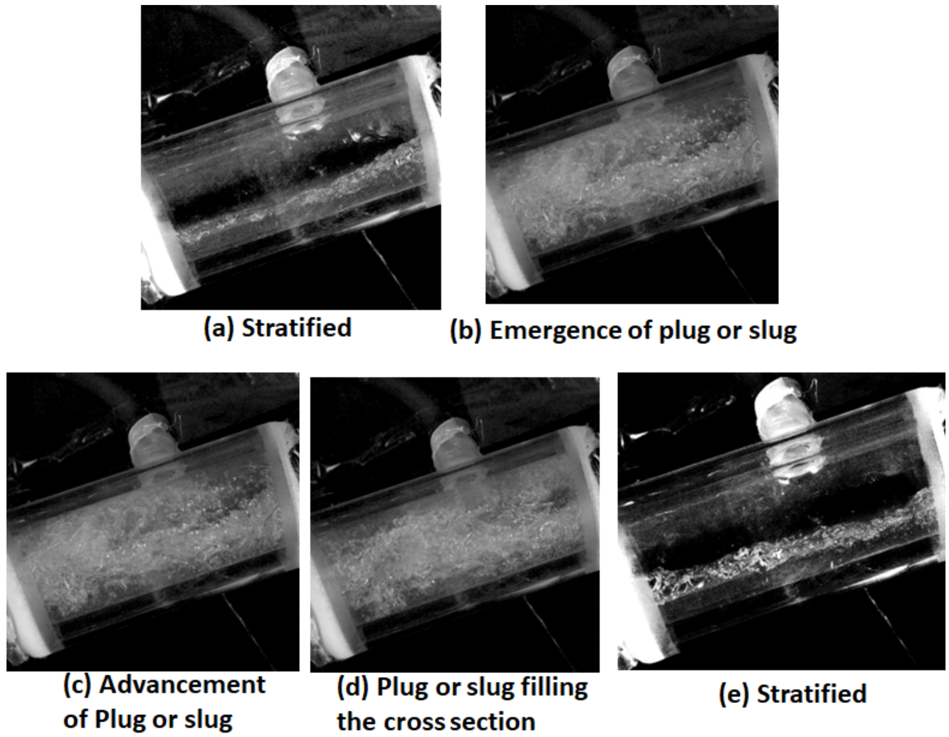

Figure 6.3: Flow structure observed in experiment with 20° upward inclination

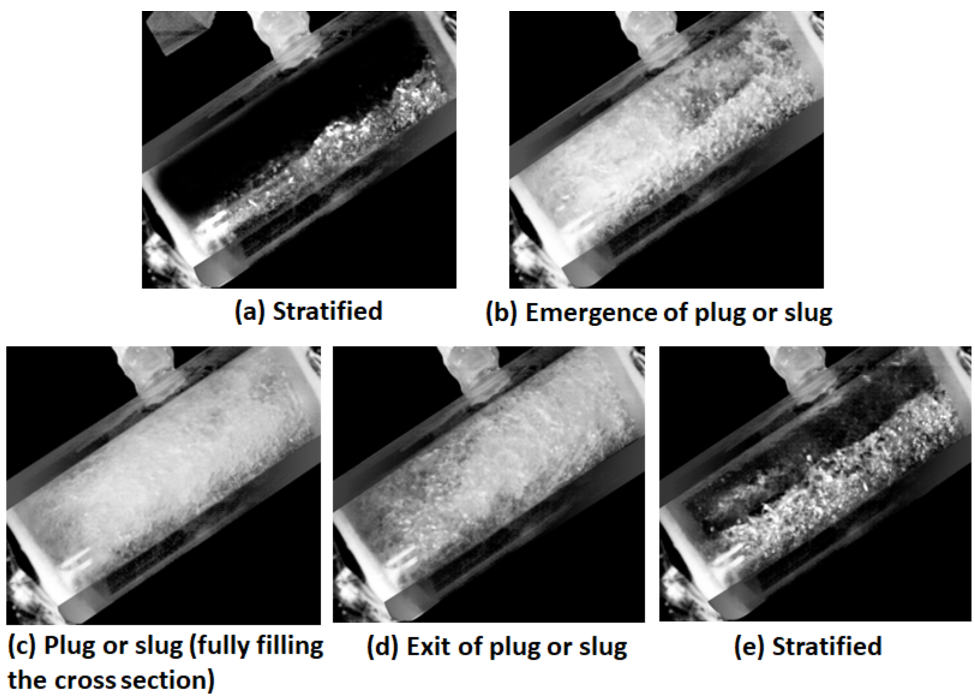

Figure 6.4: Flow structure observed in experiment with 45° upward inclination

Typical plot of top wall temperature profile observed at station 2 in the present study, during experiments with upward inclination is shown in Figure 6.5. Top wall temperature drop rate is fastest in experiment with 45° upward inclination and lesser with 20° upward inclination as compared to horizontal orientation.

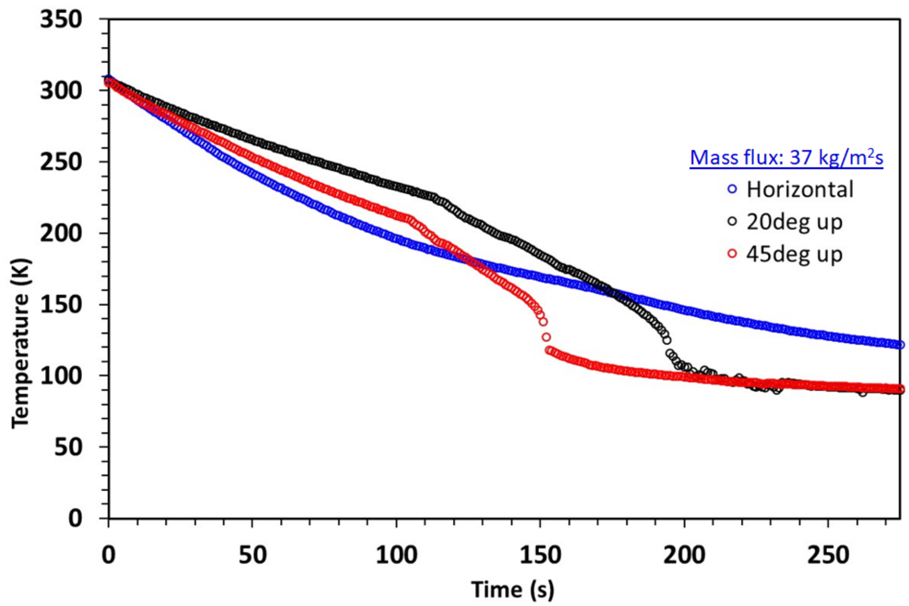

Figure 6.5: Top wall temperature profile at station 2 during experiments with upward orientation of test section as compared to horizontal

Certain interesting findings are seen in experiments with downward orientation of test section. The flow structure remains stratified with 20° downward inclination. Whereas in experiments performed with 30° and 45° downward orientation, it is seen to be vastly different from the observations with upward orientation and horizontal. Extent of liquid wetting at the bottom wall is considerably reduced as compared to horizontal and this is attributed to lesser quantity of liquid flowing along the bottom of the test section as compared to horizontal and 20° downward orientation. Liquid filaments and droplets are seen to be moving along the centre line of the test section and not participating in heat transfer at the wall. Photograph of flow structure observed in experiments with 30° and 45° downward orientation are shown in Figures 6.6 and 6.7.

Fall rate of bottom wall temperature at station 2 in experiments with 30° and 45° downward orientation is lower as compared to horizontal, as seen in Figure 6.8 and could be attributed to considerably reduced extent of liquid wetting at the bottom wall.

Large number of liquid filaments or droplets are seen to be flowing along the core. Some of these droplets are seen to be impinging on the top wall. This could explain marginally higher fall rate in the top wall temperature shown in Figure 6.9, observed during experiments with 30° and 45°

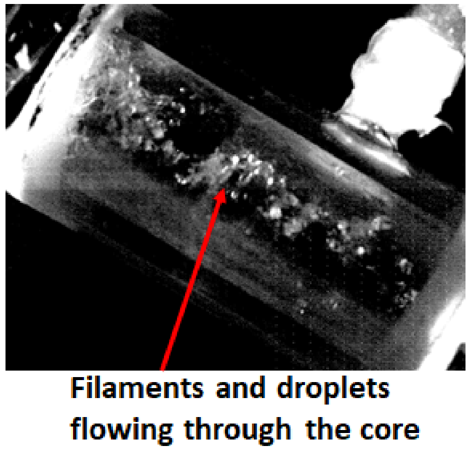

Figure 6.6: Flow structure observed in experiment with 30^o downward inclination of test section

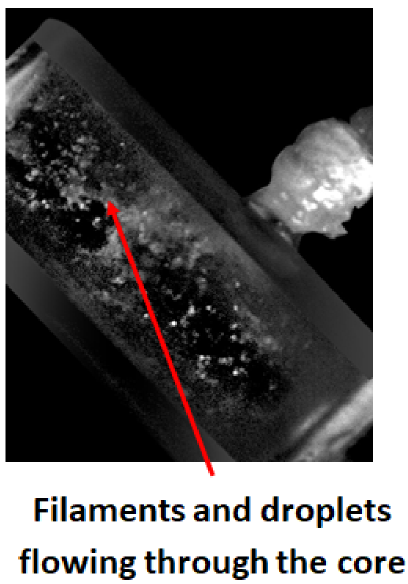

Figure 6.7: Flow structure observed in experiment with 45^o downward inclination of test section

downward orientation of test section as compared to horizontal and 20° downward orientation, as reported in Chapter 5.

The flow structure observed in experiments with 90° downward and upward orientations are different, as compared to other orientations. In experiments with 90° downward orientation, during the initial phase of chilldown, most of liquid is seen to be flowing as filaments and droplets along the core of the test section, not making any direct contact with the wall to participate in chilldown. Photograph of flow structure observed in experiments with 90° downward is shown in Figure 6.10.

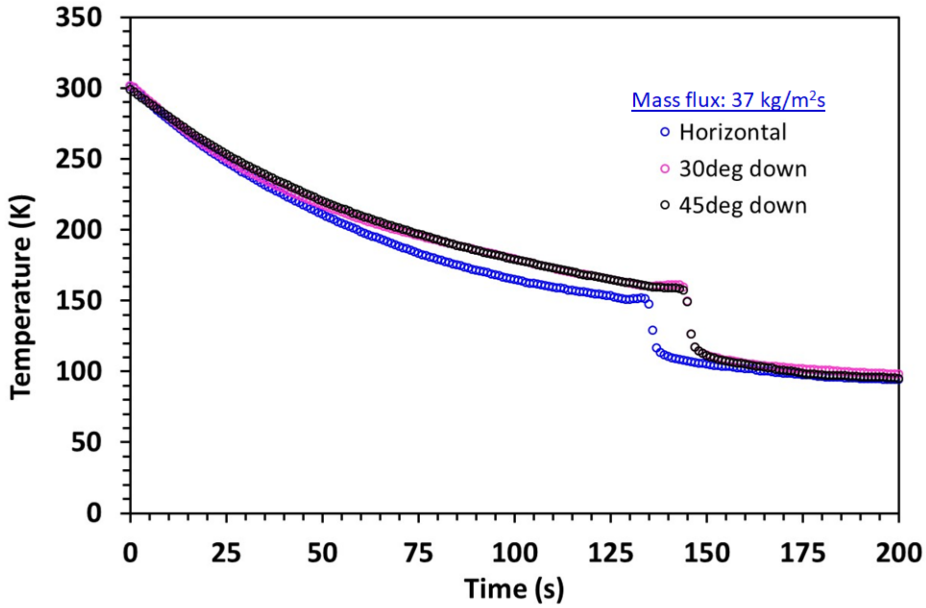

Figure 6.8: Bottom wall temperature profile at station 2 during experiments with downward orientation of test section as compared to horizontal

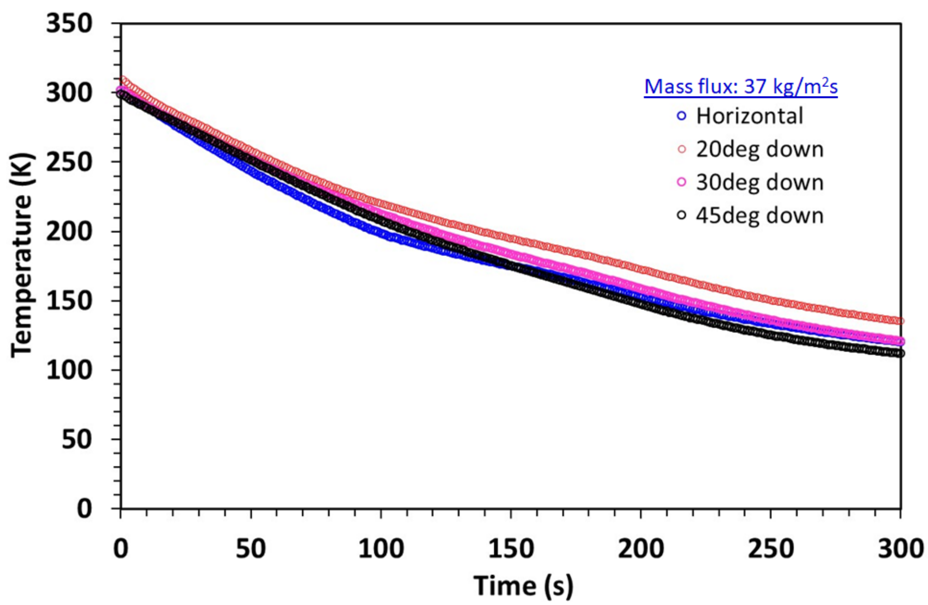

Figure 6.9: Top wall temperature profile at station 2 during experiments with downward orientation of test section as compared to horizontal

The flow structure observed during experiments with 90° upward orientation is shown in Figure 6.11. Though the flow structure is very similar to that in 90° downward direction during the initial phase of chilldown, it changes to a different one, fully filling up the test section, as chilldown

Figure 6.10: Flow structure as observed during experiments with 90° downward orientation of test section

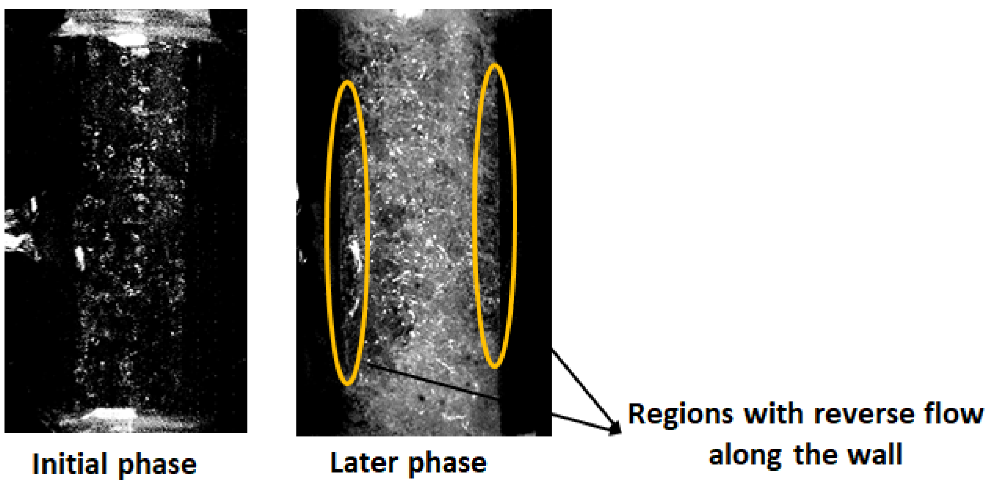

Figure 6.11: Flow structure as observed during experiments with 90° upward orientation of test section

proceeds. This change in flow structure ensures all around wetting of the wall with liquid and faster childown. At this instance, the flow is not fully symmetric and there are some regions of reverse flow seen, along the wall, while flow is in the positive upward direction in most of the other regions.

These experimental results also show that the childown performance is inferior with downward orientation of test section as compared to horizontal except for 90° downward orientation. Whereas with upward orientation, childown improves upto 45° upward inclination and becomes inferior with further increase in upward inclination.

Flow visualisation experiments performed as part of the present study have brought out certain interesting observations on the flow structure with different downward and upward orientations of the test section. Periodic plug or slug flow observed in experiments with upward orientation is the reason for faster chilldown performance with upward inclination. In experiments with downward orientation beyond 30°, lesser quantity of cryogen is flowing along the bottom wall. Liquid filaments or droplets are seen to be flowing along the core of the test section and not participating effectively in the chilldown process. This could be the reason for inferior chilldown in experiments with downward orientation.

Chapter 7

Numerical simulations to capture the chill-down process in test section with different upward and downward orientations

With a view to capture the temperature profile and have a better understanding of the physics associated with the chilldown process, numerical simulations are performed for a mass flux condition of 60 kg/m^{2}s with TS2 test section and compared with the experimental data. Details of the geometry considered, boundary conditions and methodology used, results and comparison with experimental data are brought out in the subsequent sections.

7.1 Computational domain

3D CFD simulations are carried out for horizontal, 20^o, and 45^o, upward and downward orientations of test section. Numerical simulations are performed for the test section TS2 for a mass flux of 60 kg/m^{2}s. As described earlier, TS2 test section is of 39 mm inner diameter, 1.5 mm wall thickness and 2 m length, made of stainless steel AISI321 material and insulated with poly-isocynurate foam of 28 mm thickness. As a typical case, 3D computational domain used for horizontal orientation of the test section is shown in Figure 7.1.

Computational domain includes the inlet section also, which is of inner diameter 10 mm and wall thickness 1 mm. This inlet section feeds the cryogen to the test section from the LN_2 storage dewar. Poly-isocynurate insulation of 28 mm thickness provided to minimise the ambient heat in-leak into the system is also modeled. Meshing is done using hexahedral elements and near wall effects are captured using finely spaced cells placed near the wall. Total number of cells employed is 7.5 lakhs with maximum skewness of 0.87. Computational domains for other test section orientations are also identical. Gravity effects for other test section orientations are considered by assigning suitable ’g’ values in the directions normal to and along the test section axis.

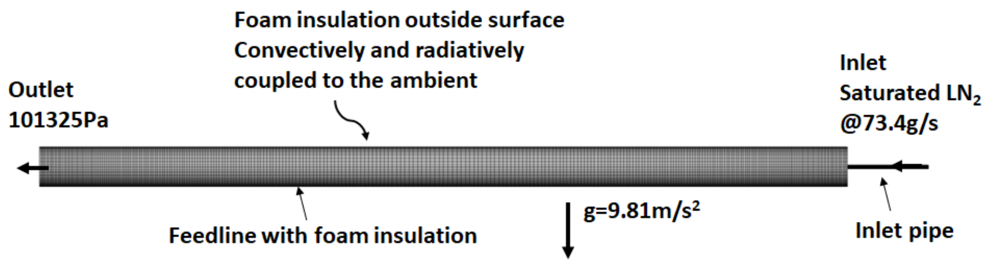

Figure 7.1: Computational domain used for numerical simulation of experiment with horizontal orientation of TS2 test section for mass flux condition of 60kg/m^{2}s

7.2 Boundary conditions and initial conditions

LN_2 flow rate of 73.4g/s is specified as an inlet boundary condition that corresponds to a mass flux condition of 60 kg/m^{2}s for TS2 test section. Boundary condition specified for the exit is pressure based and a value of 101325Pa is specified simulating the condition existing outside the test section during the experiments. Convective and radiative coupling of the outer wall of foam insulation to the ambient is also modelled. Computational domain is initialised with GN_2 medium and the inlet pipe with LN_2 at a temperature of 77K. To start the runs for numerical simulation, an initial pressure value of 101325Pa is assigned for the computational domain.

7.3 Solution methodology

Numerical simulations are performed using ANSYS Fluent. Semi-mechanistic boiling feature available in Mixture model is used to model the two phase flow heat transfer at the inner wall of test section. Heat transfer in film boiling regime is modelled using equation 7.1, as a weighted average of the heat transfer coefficients for vapour and liquid phases, based on the wetting fraction, which is the fraction of pipe wall wetted by the liquid.

$$h_{sp} = fh_l + (1 - f)h_v \tag{7.1}$$

$$q_{sp} = h_{sp}\Delta T \tag{7.2}$$

$$\Delta T = T_w - T_{cell} \tag{7.3}$$

Chen's correlation that considers an augmentation of the forced convective boiling term and suppression of the nucleate boiling term is used to estimate the effective heat flux at the inner wall, in transition and nucleate boiling regimes. Contribution from forced convection is estimated using the equations (7.1), (7.2) and (7.3), whereas the one from nucleate boiling is estimated using the equations (7.4) and (7.5).

$$h_{nb} = 0.00122\frac{{k_l}^{0.79}{c_{pl}}^{0.45}{\rho_l}^{0.49}}{\sigma^{0.5}{\mu_l}^{0.29}L^{0.24}{\rho_v}^{0.24}}[P_{sat,T_w} - P_{sat,T_sat}]^{0.75}[T_w - T_{sat}]^{0.24} \tag{7.4}$$

$$q_{nb} = h_{nb}[T_w - T_{sat}] \tag{7.5}$$

Net heat flux is estimated using the expressions (7.6) - (7.11).

$$\begin{aligned} F = 2.35\Big[\frac{1}{X_{tt}} + 0.213\Big]^{0.736} for X_{tt} > 10 \\ F = 1 for X_{tt} \leq 10 \end{aligned} \tag{7.6}$$

$$X_{tt} = \Big[\frac{1-x}{x}\Big]^{0.90}\Big[\frac{\rho_g}{\rho_l}\Big]^{0.50}\Big[\frac{\mu_l}{\mu_g}\Big]^{0.10} \tag{7.7}$$

$$S = S_{fc}S_{sub} \tag{7.8}$$

$$S_{sub} = \frac{T_w - T_{sat}}{T_w - T_{ref}} \tag{7.9}$$

$$\begin{aligned} S_{fc} = \Big[\frac{1}{1 + 0.12Re_{TP}^{1.14}}\Big] \qquad \text{for} \qquad Re_{TP} < 32.5 \\ S_{fc} = \Big[\frac{1}{1 + 0.12Re_{TP}^{0.78}}\Big] \qquad \text{for} \qquad 32.5 \leq Re_{TP} < 70 \\ S_{fc} = 1 \qquad \text{for} \qquad Re_{TP} \geq 70 \end{aligned} \tag{7.10}$$

$$q_w = Fq_{sp}M_{sp} + Sq_{nb}M_{nb} \tag{7.11}$$

$$\frac{\partial}{\partial t}(\rho_m) + \nabla\cdot(\rho_m \mathbf{v_m}) \;=\; 0 \tag{7.12}$$

$$\frac{\partial}{\partial t}(\rho_m \mathbf{v_m}) + \nabla\cdot(\rho_m \mathbf{v_m} \mathbf{v_m}) \;=\; -\nabla p + \nabla\cdot\left[\mu_m(\nabla \mathbf{v_m}) + \nabla \mathbf{v_m})^T)\right] + \rho_m \mathbf{g} \tag{7.13}$$

$$\frac{\partial}{\partial t}\sum_{k=1}^{2}(\alpha_k\rho_k E_k) + \nabla\cdot\sum_{k=1}^{2}\left[\alpha_k v_m(\rho_k E_k + p)\right] \;=\; \nabla\cdot\left[k_{eff}\nabla T\right] \tag{7.14}$$

$$\frac{\partial}{\partial t}(\alpha_v\rho_v) + \nabla\cdot(\alpha_v\rho_v v_v) \;=\; m_{l-v} - m_{v-l} \tag{7.15}$$

Two phase flow is modeled by solving the continuity, momentum, and energy equations (7.12), (7.13), and (7.14) for the mixture and the volume fraction equation for the liquid phase. Liquid to vapour mass transfer is governed by the vapour transport equation (7.15) and phase change is captured using the Lee model. A fixed value of 124K is imposed for the Leidenfrost temperature.

Second order upwind scheme is used for discretisation of convection terms and central differencing scheme is used for the diffusion terms. Time marching is achieved by a first order implicit scheme with a time step of 1x10^{-3}s. Iterations are continued till the residuals fall to the level of 10^{-4}.

7.4 Results and discussions

Stratified flow structure as observed in experiments could be captured in numerical simulations as well for horizontal and downward orientation of test section. As a typical case, flow structure observed with horizontal orientation of test section is shown in Figure 7.2.

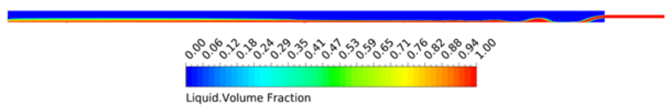

Figure 7.2: Flow structure observed in numerical simulation performed for horizontal orientation of TS2 test section

Whereas in simulations performed for 45° upward orientation, the test section is seen to be getting filled up gradually and flowing out, as shown in Figure 7.3, which is not matching with the experimental observation. In experiments, a pulsating plug or slug flow is observed.

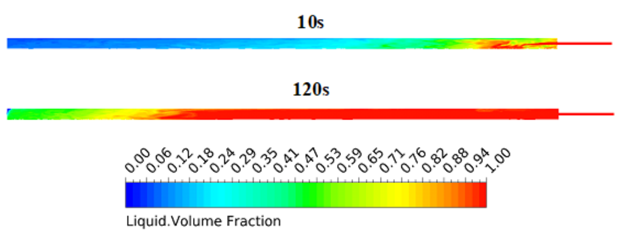

Figure 7.3: Flow structure observed in numerical simulation performed for 45° upward orientation of TS2 test section

Results of numerical simulations are compared with the experimental data to evaluate the bottom wall temperature fall rate. Trend of increasing and decreasing fall rate of bottom wall temperature with test section orientation is compared with experimental data. All comparisons are made for station 4, which is at a distance of 1610 mm from inlet of the test section. Changes in wall wetting pattern and void fraction at the bottom wall are also compared to draw a better understanding on the possible reason for variation in fall rate of bottom wall temperature with different test section orientations. Bottom wall temperature profile observed at station 4, for horizontal orientation of test section is compared with experimental data in Figure 7.4.

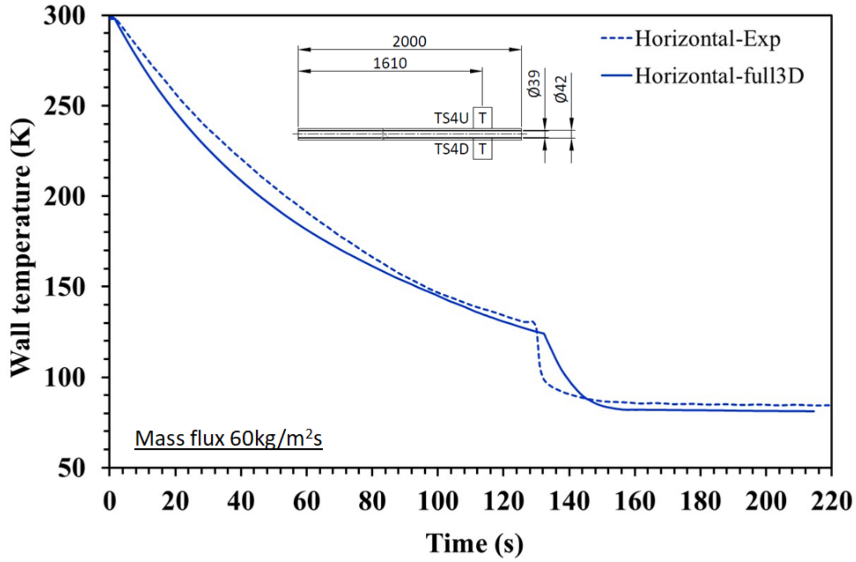

Figure 7.4: Comparison of bottom wall temperature profile at station 4 with CFD results for experiment with TS2 test section; Test section orientation-Horizontal, Mass flux-60kg/m^{2}s

As seen in Figure 7.4, a very good match is seen in the bottom wall temperature fall rate in film boiling regime, though the fall rate of wall temperature is lesser in transition and nucleate boiling regime as compared to experimental data. Deviation seen in transition and nucleate boiling regimes suggest that the correlations used in the numerical model to estimate the heat flux in these zones need to be fine tuned.

Comparison of bottom wall temperature profile observed at station 4 in simulations performed with 20° down and 45° upward orientations of test section are shown in Figures 7.5 and 7.6. In both the cases, the wall temperature profile shows a reasobly good match in the film boiling regime. Certain deviations are seen with respect to the instance at which transition and nucleate boiling starts and this needs to be looked at closely and the model needs refinement.

Trend of bottom wall temperature at station 4 in experiments with varying downward and upward orientations of TS2 test section is compared with the numerical results in Figures 7.7 and 7.8.

In the experiments performed, bottom wall temperature fall rate decreases with downward orientation of test section and improves with 20 and 45° upward orientation of test section. This trend of increasing or reducing bottom wall temperature fall rate with upward and downward orientations of test section, is captured well in the numerical simulations.

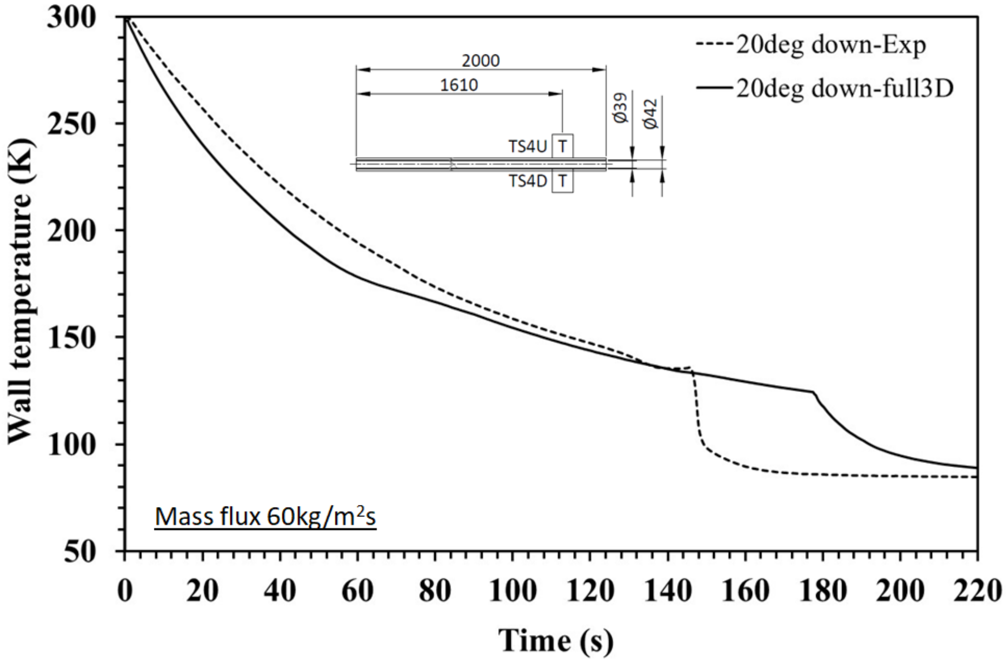

Figure 7.5: Comparison of bottom wall temperature profile at station 4 with CFD results for experiment with TS2 test section; Test section orientation-20° down, Mass flux-60kg/m^{2}s

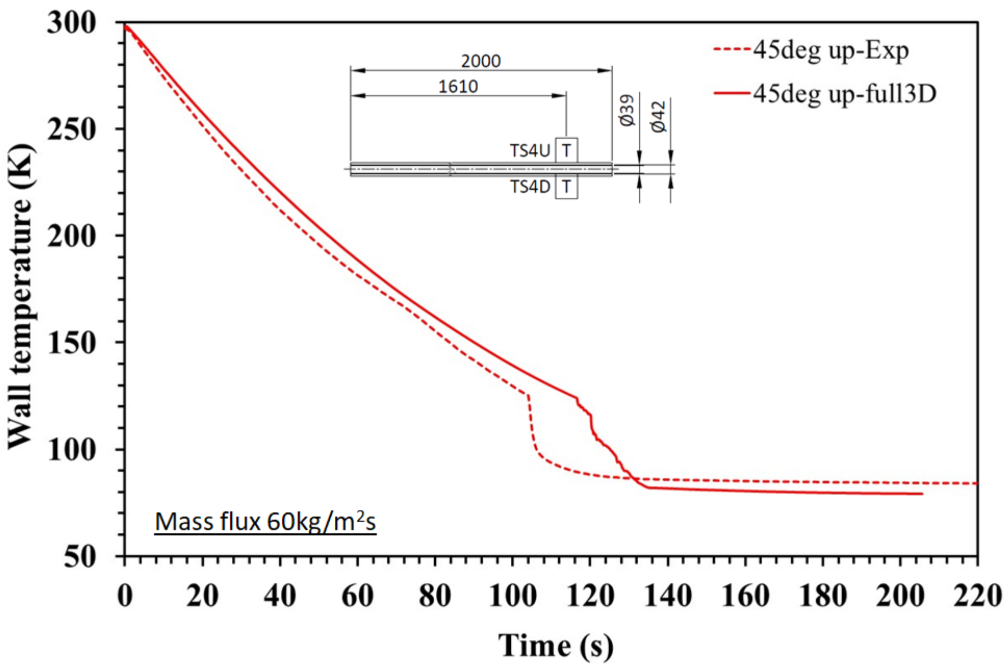

Figure 7.6: Comparison of bottom wall temperature profile at station 4 with CFD results for experiment with TS2 test section; Test section orientation-45° up, Mass flux-60kg/m^{2}s

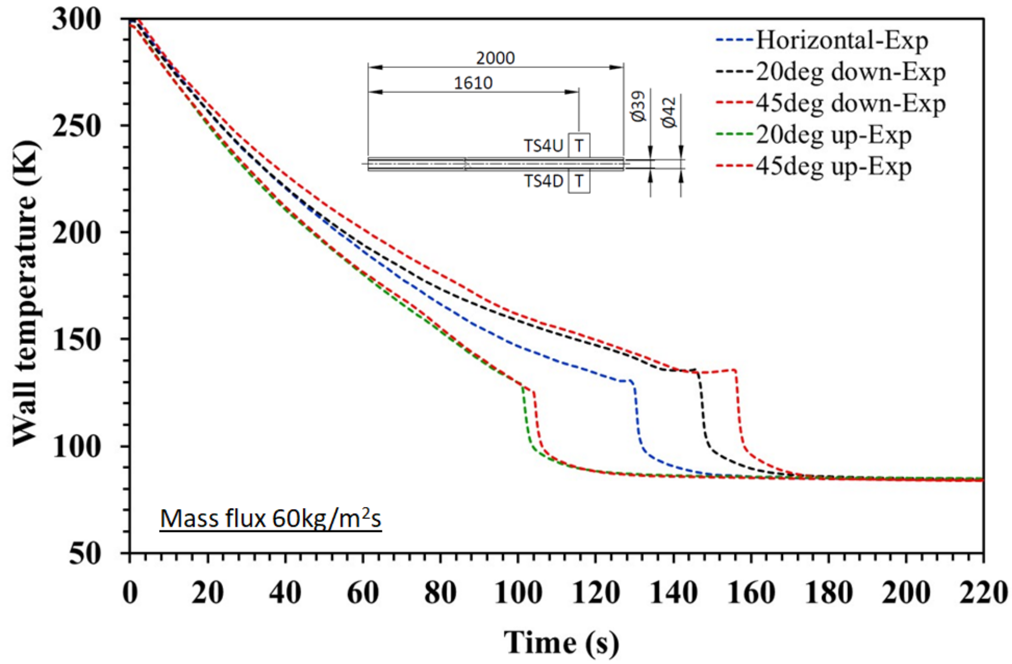

Figure 7.7: Trend of bottom wall temperature profile at station 4 as observed during experiments with TS2 test section

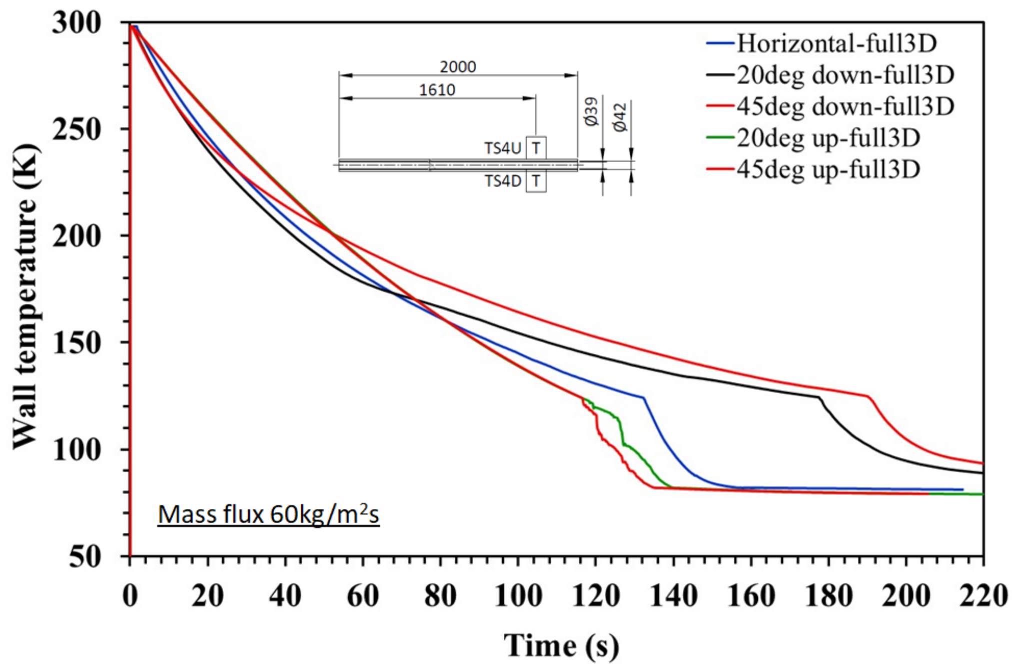

Figure 7.8: Trend of bottom wall temperature profile at station 4 as observed in numerical simulations with TS2 test section

Comparison of void fraction at station 4 at different instances of time, shown in Figure 7.9 indicates that the changing trend in bottom wall temperature with downward and upward inclinations of test section could be attributed to reduced and increased wetting of the bottom wall respectively. This observation is in line with results reported from flow visualisation studies.

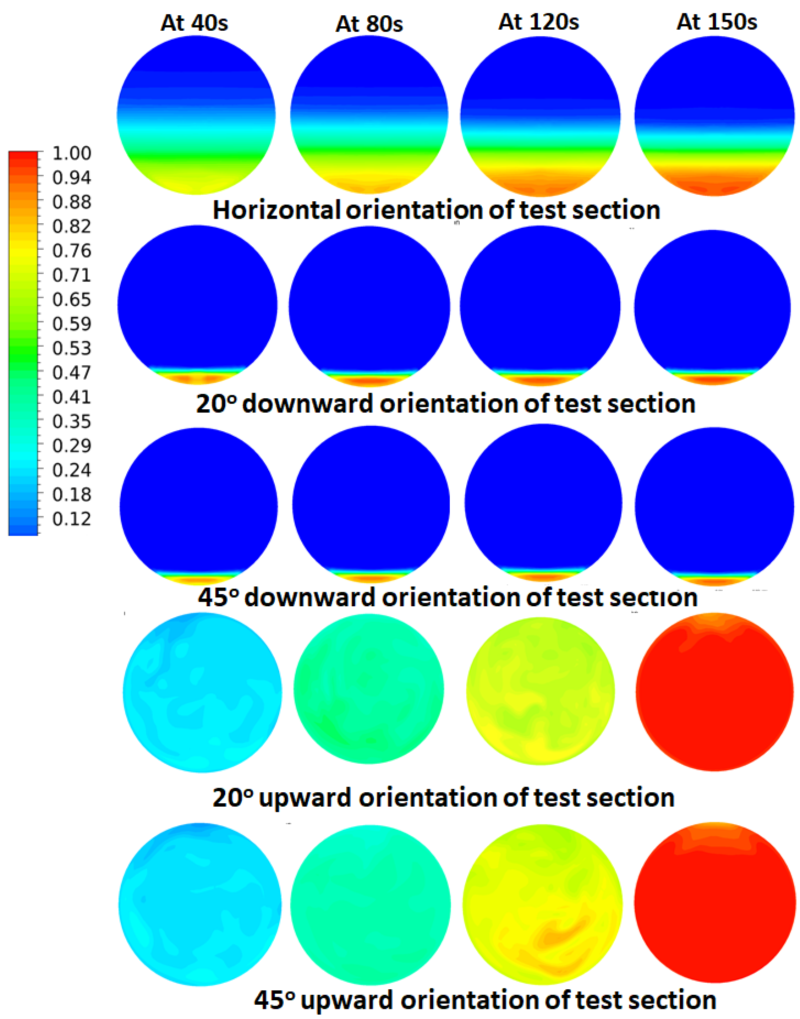

Figure 7.9: Variation of void fraction, as observed in numerical simulations at station 4, with different orientations of TS2 test section

Trend of average wetted perimeter at the bottom of the test section at station 4 (once the surface gets wetted), shown in Figure 7.10 also indicates that the extent of wall wetting at the bottom of the test section decreases with downward orientation of test section and increases with upward orientation.

The possible reason for lower and improved chilldown performance, during experiments with downward and upward orientation respectively, are studied in the numerical simulations performed with TS2 test section configuration. Reduced wall wetting, as seen in numerical results, could be

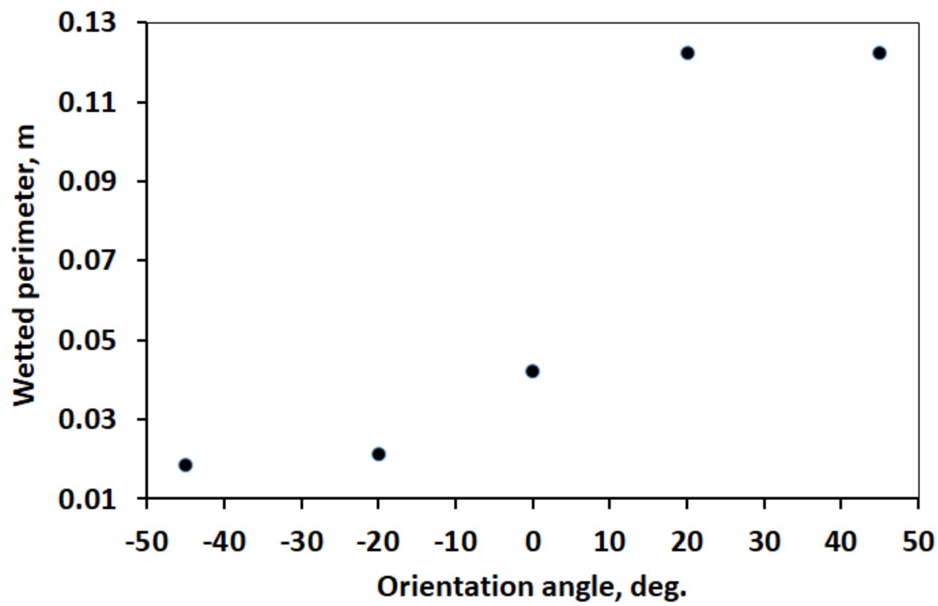

Figure 7.10: Variation of wetted perimeter, as observed in numerical simulations at station 4, with different orientations of TS2 test section

the probable reason for this observed phenomenon with downward orientation. Whereas increased wetting could be the reason for improved performance during experiments with upward orientation. Though the flow structure is captured for horizontal orientation, periodic slug or plug flow observed in upward flows and flow structure with liquid filaments and droplets moving along the core of test section in downward flows could not be captured well in numerical simulations. More simulations need to be performed to get a better match in terms of flow structure and bring in a complete understanding of these aspects.

Chapter 8

Experiments to study the effect of feedline thermal mass distribution on chilldown performance

Thermal mass distribution of feedline is also a sensitive parameter that can affect the chilldown of cryogenic feedlines. An attempt is made to study influence of this sensitive parameter by including an additional thermal mass near to the inlet and exit of the test section and comparing with a case of bare test section without this additional thermal mass introduced. Details of experimental set-up, instrumentation used, experiments carried out, results and assessment are brought out in the subsequent sections.

8.1 Experimental set-up

Details of the experimental set-up used and test section configurations employed for this study are already covered in Chapter 4. The influence of thermal mass is studied by performing experiments for two mass flux conditions of 103 kg/m^{2}s and 37 kg/m^{2}s, achieved by employing calibrated orifices of diameters 2.73 and 1.5 mm respectively at the inlet. As in other experiments, flow exiting the test section is freely let out into atmosphere, in these tests as well.

8.2 Instrumentation scheme

The set-up is equipped with three pressure sensors P1, P2, and P3, as in other experiments described under Chapter 4. It is also equipped with 4 numbers of T type thermocouples, two numbers each at two stations along the length of test section to measure its outside wall temperature and have an accuracy of $\pm$1.5K. Location of these four surface temperature measurements is shown in Figures

8.1, 8.2 and 8.3. During the tests, pressure and temperature values read by the sensors are acquired using a portable data acquisition system at a sampling rate of 1 Hz.

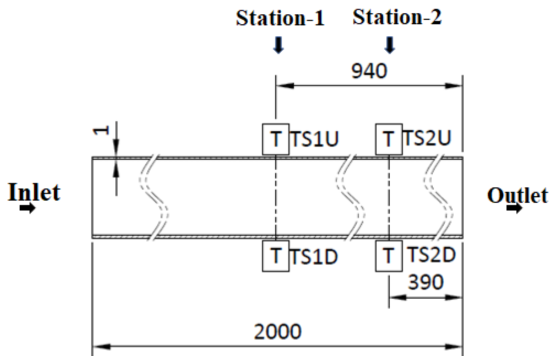

Figure 8.1: Instrumentation scheme employed for feedline configuration-1, used as reference for comparison

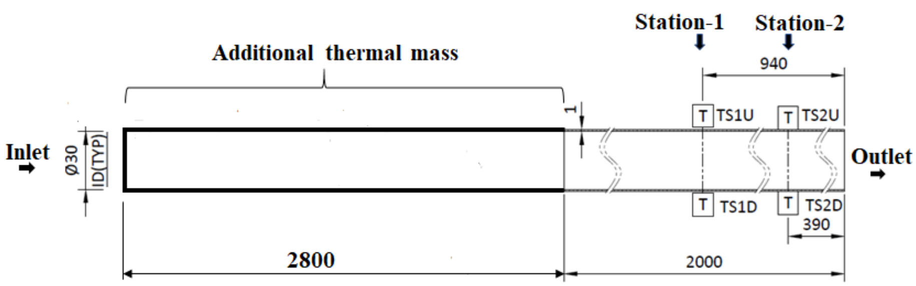

Figure 8.2: Instrumentation scheme employed for feedline configuration-2 with additional thermal mass placed near to the test section inlet

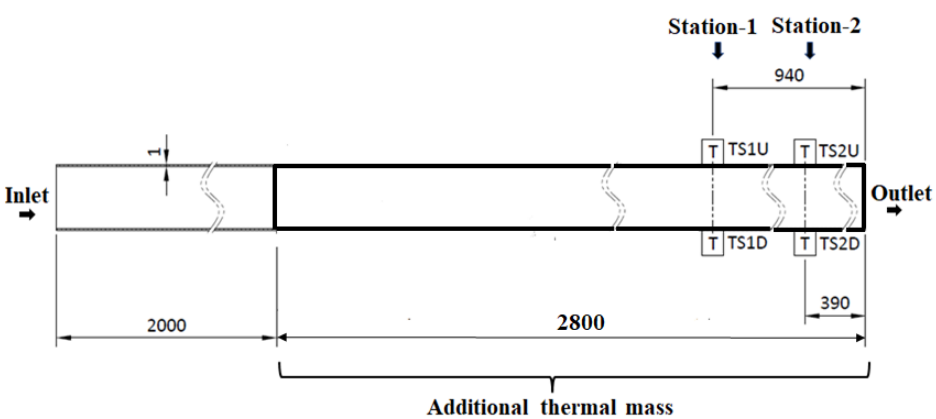

Figure 8.3: Instrumentation scheme employed for feedline configuration-3 with additional thermal mass placed near to the test section outlet

8.3 Test Matrix

Test procedure followed is already described in Chapter 4. As mentioned earlier, the influence of thermal mass distribution is studied by performing experiments for two different mass flux conditions of 103 kg/m^{2}s and 37 kg/m^{2}s. Six data sets are generated as part of the study. Experiments performed and the test conditions are listed in Table 8.1.

Table 8.1: Experiments performed to evaluate the influence of thermal mass distribution of test section

Sl. No.	Feedline configuration	mass flux	No. of tests
1	Configuration-1	103 kg/m^{2}s	3
2	Configuration-1	37 kg/m^{2}s	1
3	Configuration-2	103 kg/m^{2}s	2
4	Configuration-2	37 kg/m^{2}s	1
5	Configuration-3	103 kg/m^{2}s	2
6	Configuration-3	37 kg/m^{2}s	1

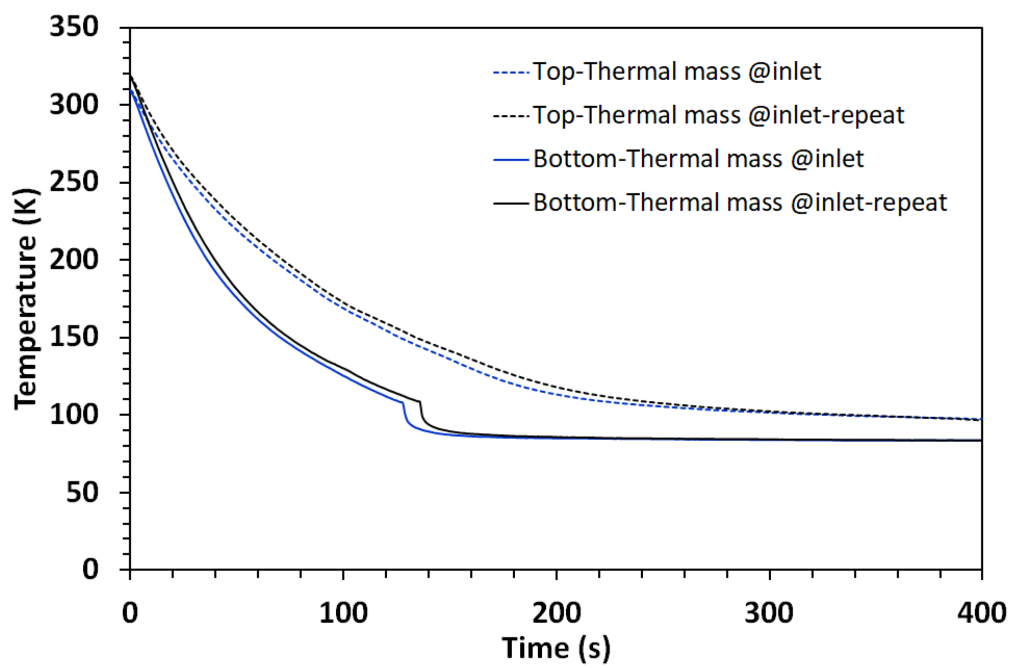

Figure 8.4: Comparison of wall temperature profile at station 2 as observed during repeat experiments with mass flux of 103 kg/m^{2}s with thermal mass placed near to test section inlet

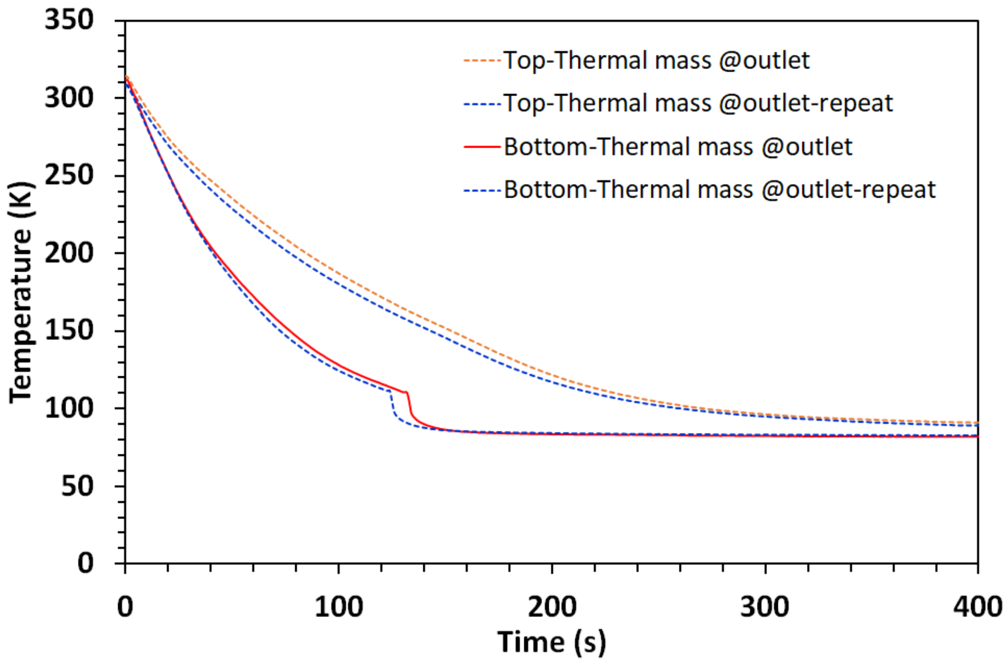

Figure 8.5: Comparison of wall temperature profile at station 2 as observed during repeat experiments with mass flux of 103 kg/m^{2}s with thermal mass placed near to test section outlet

Experiments are repeated for certain test conditions to establish consistency. Wall temperature profile observed in repeat experiments with thermal mass placed near to inlet and outlet are shown in Figures 8.4 and 8.5. As can be seen, the wall temperature profiles at top and bottom are very closely matching and the variation seen between experiments is less than 5K (excepting close to Leidenfrost point).

Experimental data is analysed to understand the influence of thermal mass distribution of feedline. Findings of the present study are brought out in the subsequent section.

8.4 Results and discussions

To understand the influence of thermal mass distribution of feedline on chilldown performance, wall temperature profile at stations 1 and 2 are compared for different test conditions. Wall temperature profile at stations 1 and 2 in experiments with mass flux of 103 kg/m^{2}s are brought out in Figures 8.6 and 8.7. Chilldown performance is seen to be best for the feedline section configuration-1 with minimum thermal mass. Chilldown performance is made inferior by the introduction of additional thermal mass into the test section. It is also seen that addition of thermal mass near the inlet to the test section gives better result, as compared to its introduction near to the exit.

The observations in experiments with lower mass flux of 37 kg/m^{2}s are similar and are shown

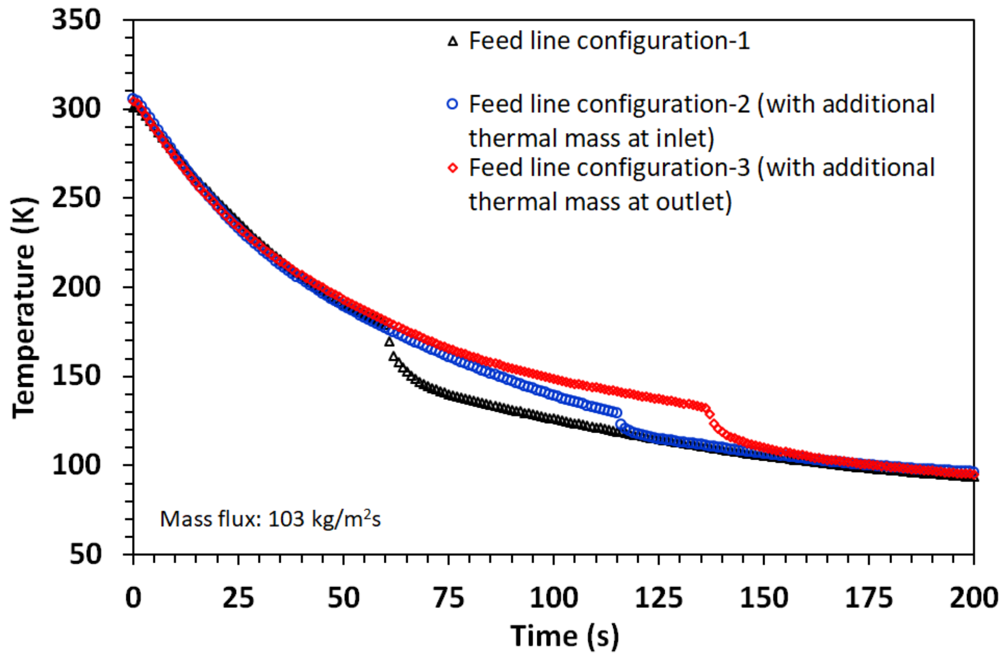

Figure 8.6: Comparison of wall temperature profile at station 1 in experiments with mass flux of 103 kg/m^{2}s

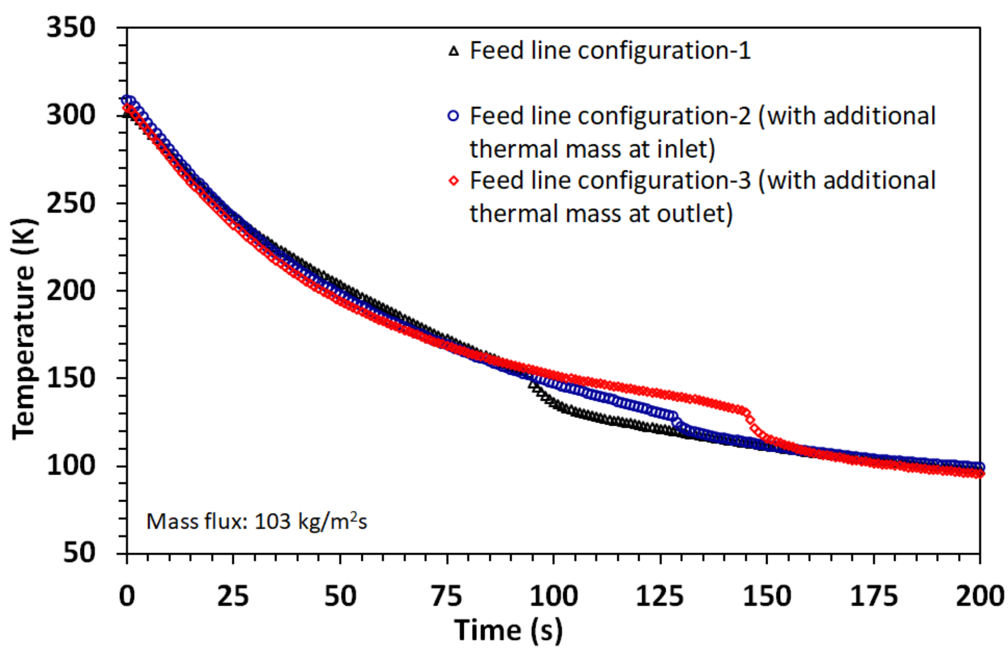

Figure 8.7: Comparison of wall temperature profile at station 2 in experiments with mass flux of 103 kg/m^{2}s

in Figures 8.8 and 8.9.

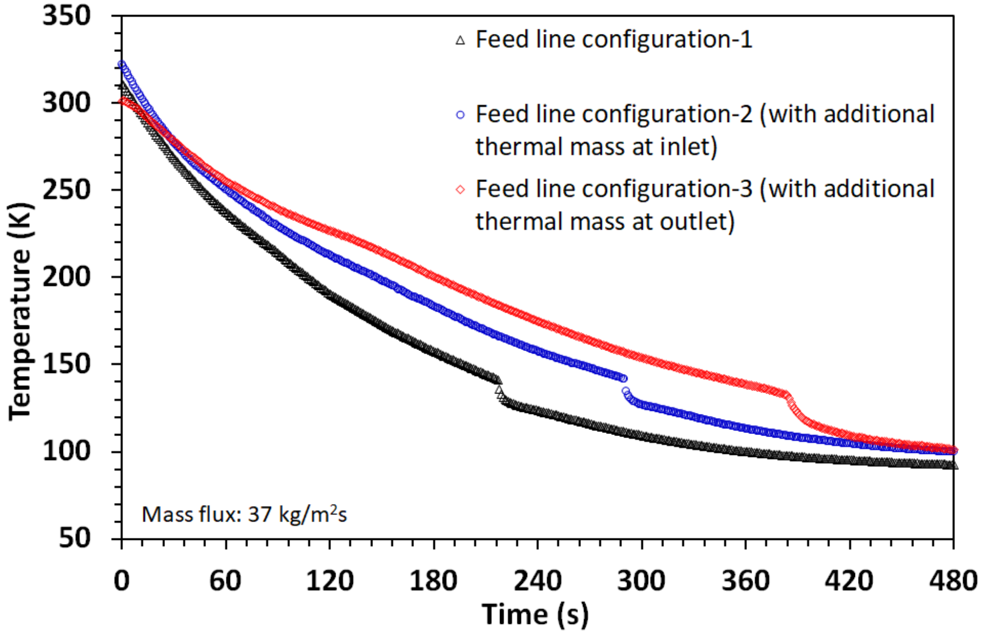

Figure 8.8: Comparison of wall temperature profile at station 1 in experiments with mass flux of 37 kg/m^{2}s

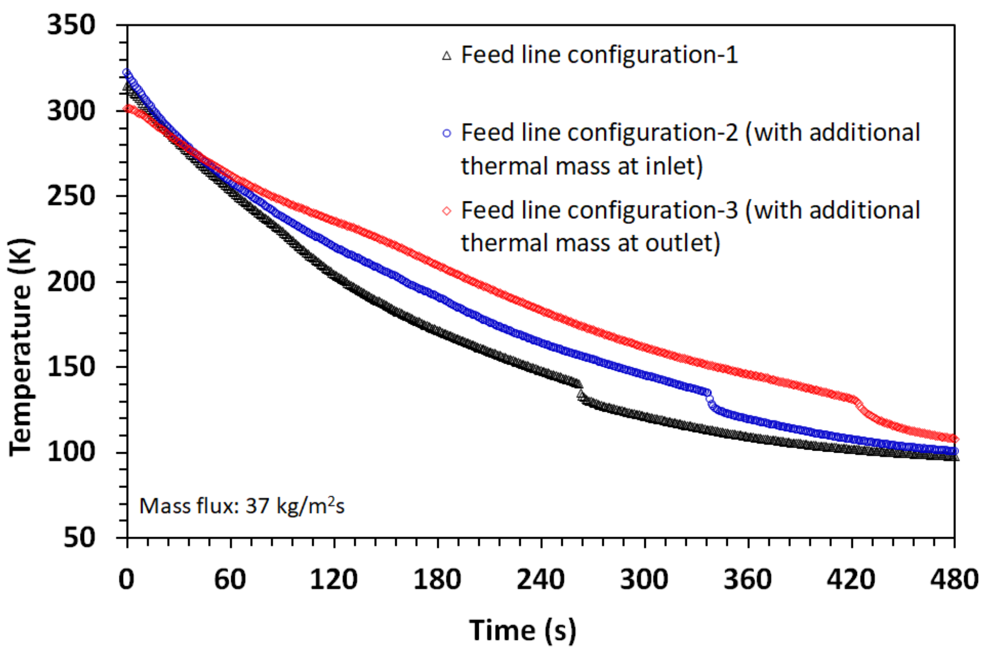

Figure 8.9: Comparison of wall temperature profile at station 2 in experiments with mass flux of 37 kg/m^{2}s

Best performance is achieved for configuration-1 without any additional thermal mass. Among configurations-2 and 3, configuration-2 with additional thermal mass placed near the inlet gives a better performance. As can be seen, impact on chilldown performance is more striking with lower mass flux of 37 kg/m^2s, as compared to mass flux condition of 103 kg/m^2s.

This is mainly due to the fact that during chilldown, the heat flux or the heat extraction rate decreases, as we move to downstream locations along the length of the feedline. This is caused by warming up of the cryogen as it moves downstream or lesser quantity of liquid cryogen participating in the chilldown at downstream locations compared to upstream locations. Thus in experiments with additional thermal mass placed near to the inlet, chilldown is expected to be better as compared to the one with additional thermal mass placed near the exit.

Thus it is evident from the present study that introduction of additional thermal mass near the exit influences the chill down performance more as compared to addition at inlet.

A typical cryogenic feed system in a rocket engine would consist of subsystems having higher thermal mass like pumps, valves etc. and this study has brought out an interesting assessment on the relative location that should be considered for cryogen entry for chilldown as compared to the location of subsystems having higher thermal mass. To minimize the chilldown time of cryogenic feed systems, it is required that cryogen should enter at a location close to and just upstream of subsystems having higher thermal mass. On the contrary, if these heavier thermal mass subsystems are placed at a point close to the location at which the cryogen exits after chilldown, it could lead to higher chilldown time and hence higher cryogen consumption.

Chapter 9

Experiments to study the effect of thermophysical properties, coatings, thermal mass and surface finish on chilldown performance

Thermophysical properties like thermal conductivity and thermal mass of feedline material have a profound influence on the chilldown performance of cryogenic feed lines. Apart from this surface parameters like presence of coatings and surface finish also affect the wetting and heat transfer characteristics, thereby strongly influencing the chilldown performance. Effect of each of these sensitive parameters on chilldown performance is assessed in the present study by employing evaluation sections of 250 mm length, in which these parameters are simulated. The evaluation section is placed in a feedline of 2 m length and the effect of location on the influence of these sensitive parameters is studied by placing the evaluation section at two different locations along the length of the feedline viz; 875 mm and 1500 mm from inlet. Details of experimental set-up, instrumentation used, experiments carried out, results and assessment made are brought out in the subsequent sections.

9.1 Instrumentation scheme

Details of the experimental set-up and evaluation sections used for the present study are already described in Chapter 4. Ten types of evaluation sections are used to meet the objectives of the present study. A schematic of instrumentation scheme employed for the experiments performed with the evaluation section placed at 875 mm from inlet is shown in Figure 9.1. The set-up is equipped with three pressure sensors P1, P2, and P3, as in other experiments described under Chapter 4, to measure the pressures at orifice inlet, orifice outlet and feedline inlet respectively. 2 numbers of 100Ω Platinum RTD, placed in the inlet and outlet sections are used to measure the fluid temperature.

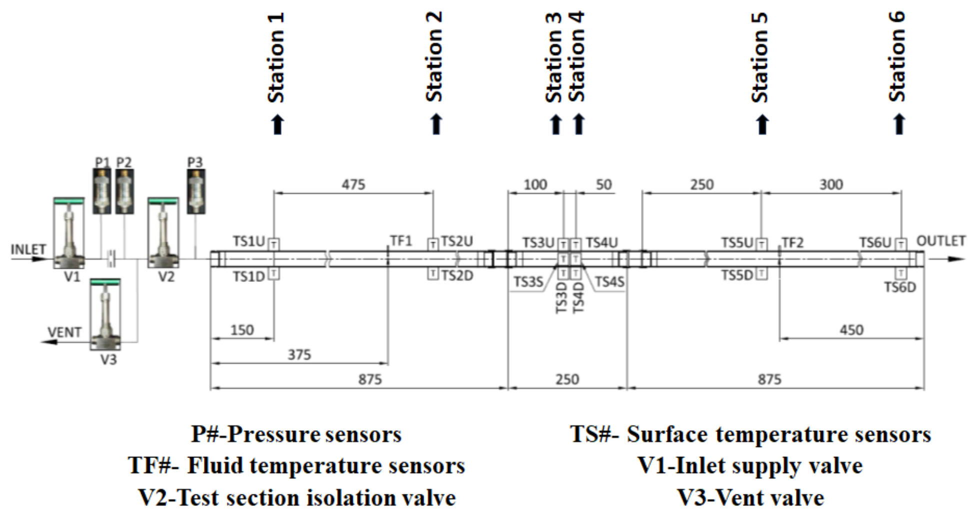

Figure 9.1: Schematic of instrumentation scheme employed during experiments performed to study the influence of thermophysical property, surface coatings, surface finish etc., with evaluation section placed at 875 mm from inlet

As mentioned earlier, RTDs used have an accuracy of ±0.55K at 73K (close to LN_2 temperature). Surface temperature sensors used are T-type thermocouples and measure the outer wall temperature at six stations along the length of the feedline. Fourteen numbers of surface temperature sensors are used, two numbers each are placed at four stations 1, 2, 5, and 6, one each at top and bottom, whereas at stations 3 and 4 in the evaluation section, three numbers each are provided, including a side wall temperature measurement. T-type thermocouples used have an accuracy of ±1.5K or better for the measured temperature range from ambient to 77K. Alphabets D, U, and S in the legend represent the measurements placed at bottom, top and side respectively. The values read by these pressure and temperature sensors are acquired using a Yokogawa data acquisition system at a sampling rate of 1Hz.

A schematic of instrumentation scheme employed for the second set of experiments performed with the evaluation section placed at 1500 mm from inlet is shown in Figure 9.2.

The instrumentation scheme adopted for these experiments is similar except for the following changes:

- Only one fluid temperature sensor, placed in the inlet section, is used for these experiments as against two numbers used for the first set of experiments.
- Stations 1, 2, 3, and 6 are provided with two numbers of T type thermocouples for surface temperature measurement, whereas stations 4 and 5 are equipped with three numbers each, including a side wall temperature measurement.

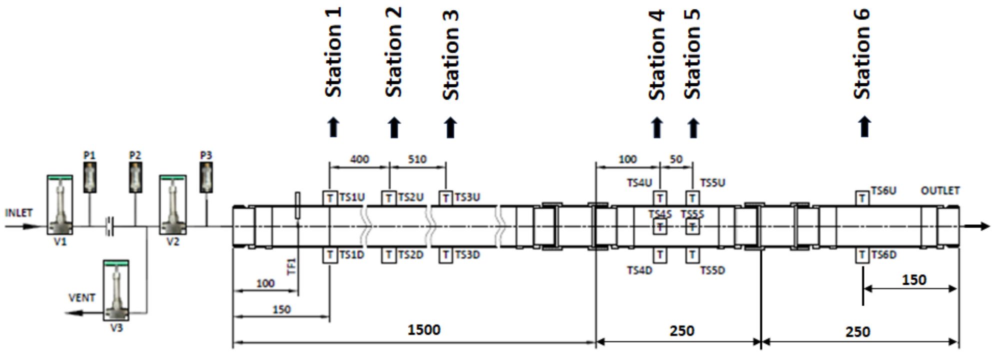

Figure 9.2: Schematic of instrumentation scheme employed during experiments performed to study the influence of thermophysical property, surface coatings, surface finish etc., with evaluation section placed at 1500 mm from inlet

9.2 Test Matrix

Test procedure followed is the same as the one described in Chapter 4. A total of ten sets of experiments, as listed in Table 9.1 are performed with the evaluation section placed at 875 mm from inlet to meet the objectives of the present study.

Table 9.1: Experiments performed to evaluate the influence of thermophysical property of evaluation section, surface coatings, surface finish etc.

Sl. No.	Evaluation section employed				Location of test section/No. of tests	
	Diameter (mm)	Thickness (mm)	Material	Type/thickness of coating (μm)	@875mm from inlet	@1500mm from inlet
1	30	1	AISI321	No coating	2	2
2	30	1	Cu alloy	No coating	2	2
3	30	1	AISI321	PFA coating, 30μm	2	2
4	30	1	AISI321	Cu coating, 100μm	2	2
5	30	1	AISI321	Cu coating, 200μm	2	2
6	30	5	AISI321	No coating	2	2
7	30	5	AISI321	PFA coating, 30μm	2	2
8	30	2.5	AISI321	Surface finish Ra0.3	2	-
9	30	2.5	AISI321	Surface finish Ra3	2	-
10	30	2.5	AISI321	Surface finish Ra8.4	2	-

Seven set of experiments are performed with the evaluation section placed at 1500 mm from inlet to evaluate the effect of location of the influence of sensitive parameters like thermal conductivity, coatings etc. Mass flux simulated during the experiments is 101 kg/m^{2}s. Every experiment is repeated at least once for confirmation and repeatability.

As mentioned earlier, in the first set of experiments, ten data sets are generated with different evaluation sections. Wall temperature profiles observed in repeat experiments are consistent and as a typical case, temperature profiles observed in repeat experiments with stainless steel bare section of 1 mm and 5 mm wall thickness, placed at 875 mm from inlet, are shown in Figures 9.3 and 9.4. As can be seen, the variation seen in top, bottom and side wall temperatures observed between experiments is very minor, establishing their consistency.

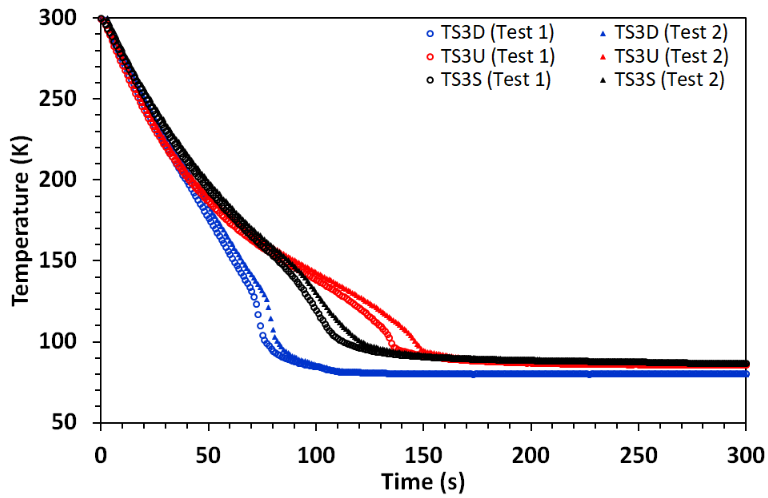

Figure 9.3: Wall temperature profile observed at station 3 during repeat experiments with bare 1 mm thick stainless steel evaluation section

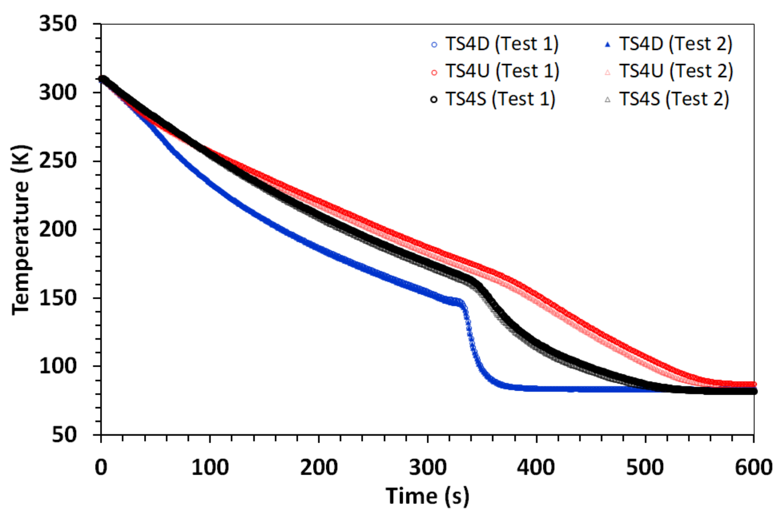

Figure 9.4: Wall temperature profile observed at station 3 during repeat experiments with bare 5 mm thick stainless steel evaluation section

9.3 Results and discussions

9.3.1 Influence of parameters like thermal conductivity, coatings, thermal mass and surface finish, with evaluation section placed at 875 mm from inlet

Experimental data generated with the evaluation section placed at 875 mm from inlet is analysed to understand the influence of thermal mass and thermophysical property on chilldown performance. Effect of coating and surface finish on wall wetting and chilldown performance are also assessed. Two types are coatings are evaluated for their performance viz; a nonmetallic PFA coating of 30μm thickness and metallic Cu coating of 100 & 200μm thicknesses. Average of the parameters like CPI and circumferential temperature gradient, derived from the two sets of experiments performed for each test condition, is used for the evaluation. Findings of the present study are brought out in the subsequent sections.

9.3.1.1 Influence of thermophysical property of evaluation section material on chilldown performance

The influence of thermophysical property of evaluation section material is studied by evaluating the chilldown performance with two materials having vastly different thermal conductivity viz; stainless steel AISI321 and Cu alloy.

Comparison of wall temperature profile and temperature gradient between top and bottom locations at stations 3 and 4 during experiments performed with evaluation sections of these two different materials are shown in Figures 9.5 and 9.6. As can be seen, the temperature fall rate and chilldown is much better with Cu alloy as compared to stainless steel. Temperature gradient between top and bottom locations is also lesser with Cu alloy evaluation section. It reduces from around 47 K with stainless steel to around 34 K with Cu alloy material. This improved performance with Cu alloy is attributed to its higher thermal conductivity as compared to stainless steel.

CPI (estimated using equation 5.1) is seen to be improving by around 62% in experiments with evaluation section made of Cu alloy as compared to stainless steel (taking stainless steel evaluation section as reference).

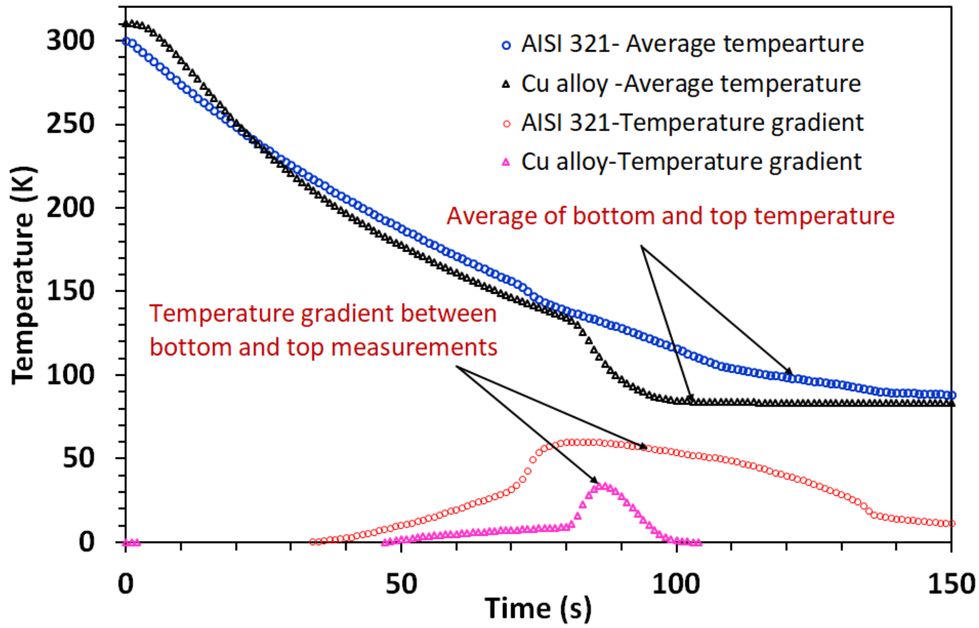

Figure 9.5: Comparison of wall temperature profile and circumferential temperature gradient at station 3 in experiments performed with evaluation sections made of stainless steel and Cu alloy

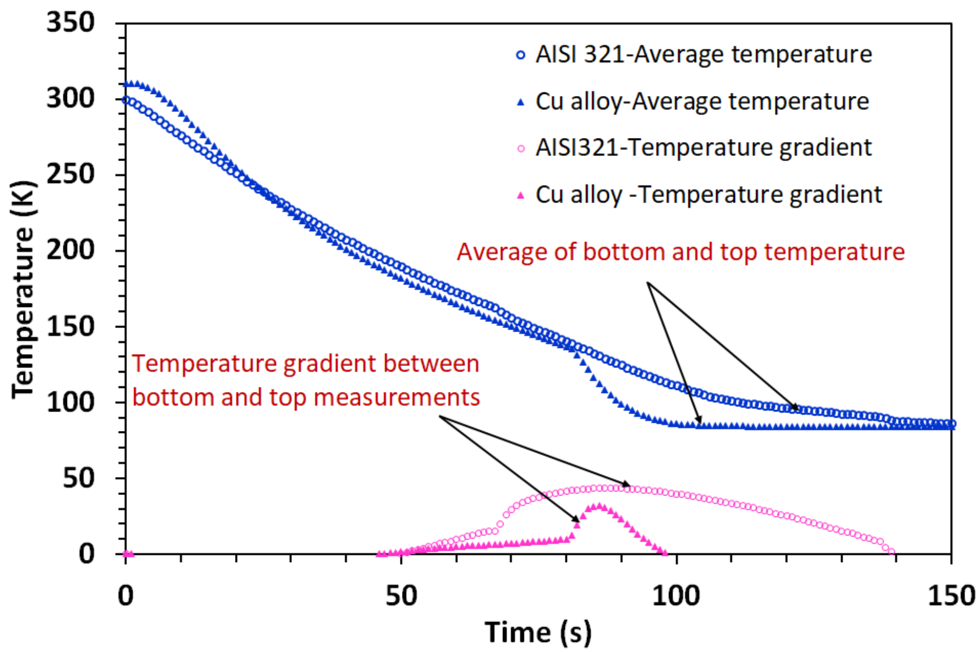

Figure 9.6: Comparison of wall temperature profile and circumferential temperature gradient at station 4 in experiments performed with evaluation sections made of stainless steel and Cu alloy

9.3.1.2 Influence of nonmetallic coating on chilldown performance

To evaluate the influence of nonmetallic coating on chilldown performance, experiments are performed with evaluation sections of 30 mm inner diameter and two different thicknesses viz; 1 mm and 5 mm wall thicknesses, both coated with PFA coating of 30μm thickness. Performance with coating is evaluated by comparing the results obtained without coating.

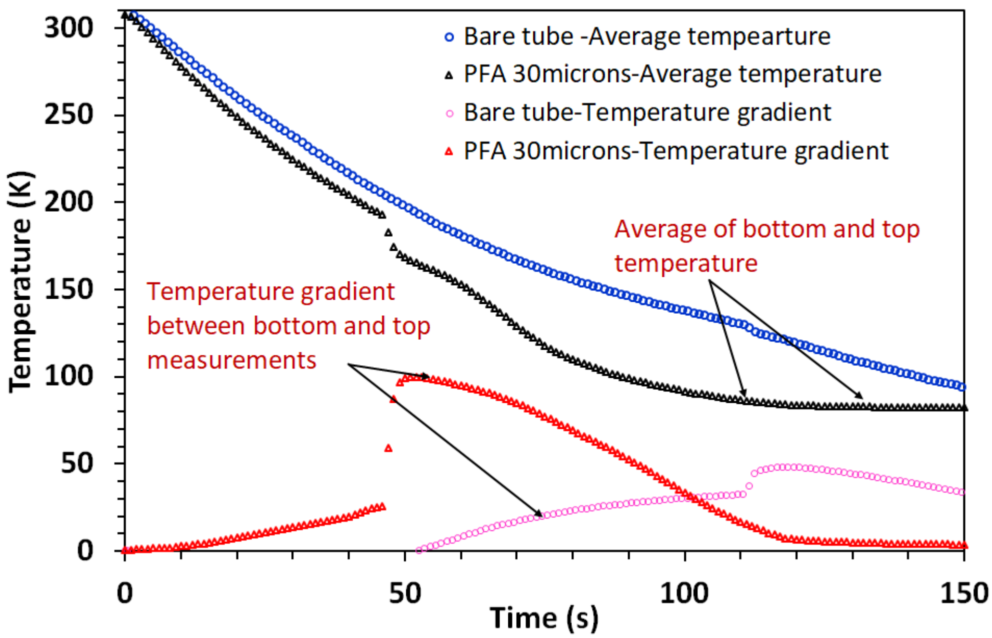

Figure 9.7: Comparison of wall temperature profile and circumferential temperature gradient at station 4 in experiments performed with evaluation sections of 1 mm wall thickness, with and without PFA coating

Average wall temperature profile and temperature gradient between top and bottom locations at station 4 during experiments with evaluation sections of 1 mm and 5 mm wall thicknesses are shown in Figures 9.7 and 9.8. Chilldown performance is significantly improved in the presence of PFA coating as compared to results obtained without coating. This is on account of two reasons viz; early wetting of the bottom wall and enhanced heat transfer taking place thereafter to achieve a higher average wall temperature fall rate.

Gain in CPI (estimated using equation 5.1) is around 46% with 5 mm thick evaluation section, compared to 53% with 1 mm thick evaluation section (taking the respective bare stainless steel evaluation section as reference). However, the presence of coating increases the temperature gradient between top and bottom locations. The gradient increases from 47 K with 1 mm bare section to 89 K with coated section. The corresponding values for 5 mm thick evaluation section are 76 K and 122 K respectively. This would result in higher thermal stresses in feed systems and needs to be addressed carefully to avoid bowing effects etc.

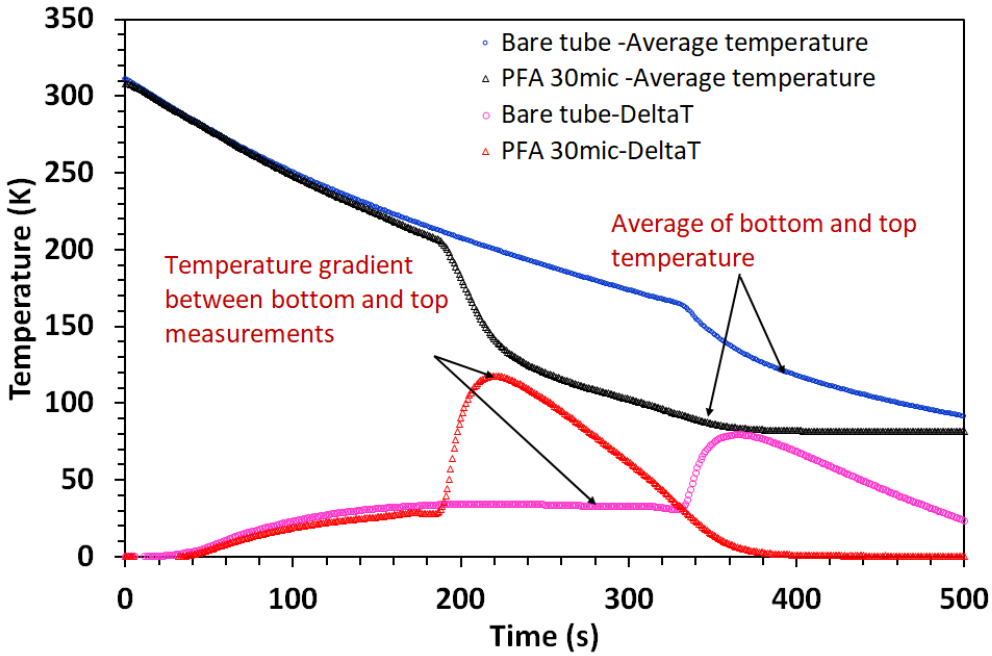

Figure 9.8: Comparison of wall temperature profile and circumferential temperature gradient at station 4 in experiments performed with evaluation sections of 5 mm wall thickness, with and without PFA coating

9.3.1.3 Influence of metallic coating on chilldown performance

As mentioned earlier, as part of this study to understand the influence of metallic coating, experiments are performed with evaluation sections of 30 mm inner diameter and 1 mm wall thickness coated with Cu coating of two different thicknesses viz; 100μm and 200μm. Performance is compared with bare section without coating. Average wall temperature profile and temperature gradient between top and bottom locations at stations 3 and 4 are compared in Figures 9.9 and 9.10.

As seen in Figures 9.9 and 9.10, though chilldown performance is not significantly affected by the presence of 100μm coating, there is a trend of marginal gain in CPI and improved circumferential temperature gradient with 200μm Cu coating. CPI is seen to be improving by around 17% and circumferential temperature gradient reduces from around 47K (with bare section) to 38K with 200μm Cu coating. This is expected in view of the high thermal conductivity of Cu coating, which would bring in a better heat conduction in circumferential direction as well, thereby improving the chilldown performance along with reduction in thermal gradient. Results are expected to be significantly improved with higher Cu coating thickness and needs experimental evaluation.

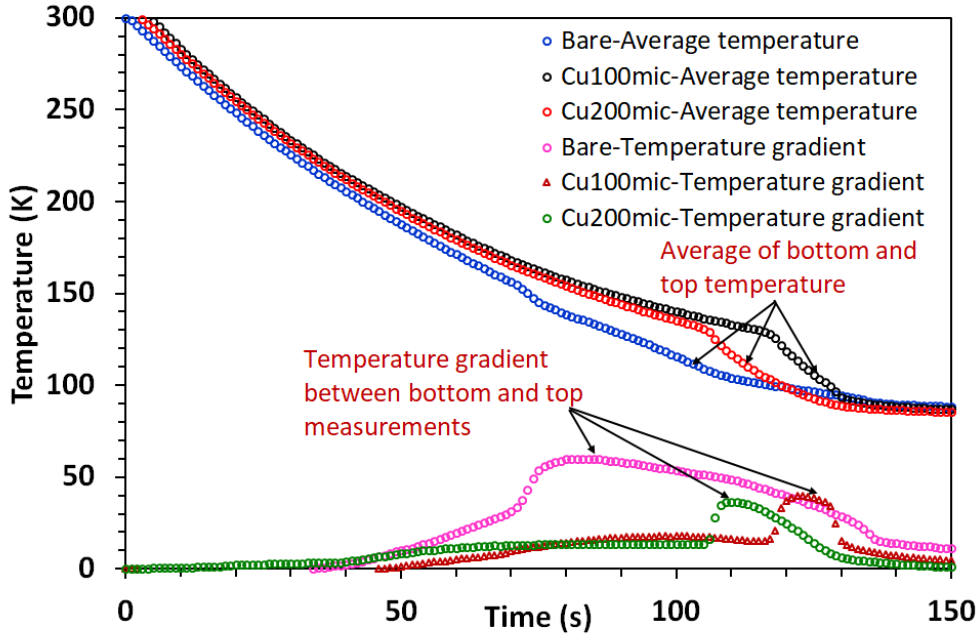

Figure 9.9: Comparison of wall temperature profile and circumferential temperature gradient at station 3 in experiments performed with evaluation sections made of stainless steel, with and without Cu coating

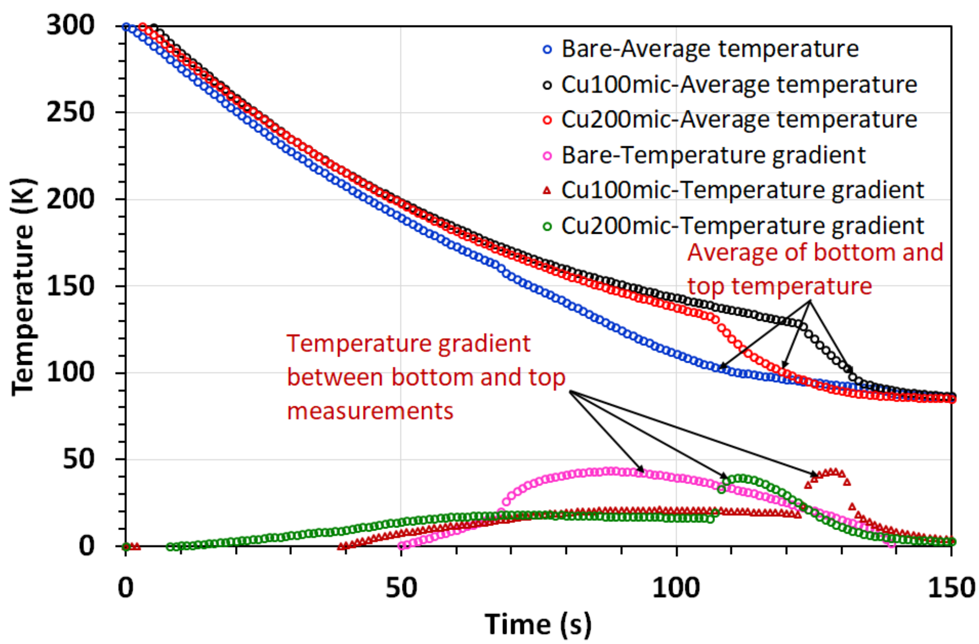

Figure 9.10: Comparison of wall temperature profile and circumferential temperature gradient at station 4 in experiments performed with evaluation sections made of stainless steel, with and without Cu coating

9.3.1.4 Influence of thermal mass of evaluation section on chilldown performance

Experiments are performed with two evaluation sections having the same 30 mm inner diameter and different thicknesses of 1 mm and 5 mm to assess the influence of thermal mass and evaluate the chilldown performance.

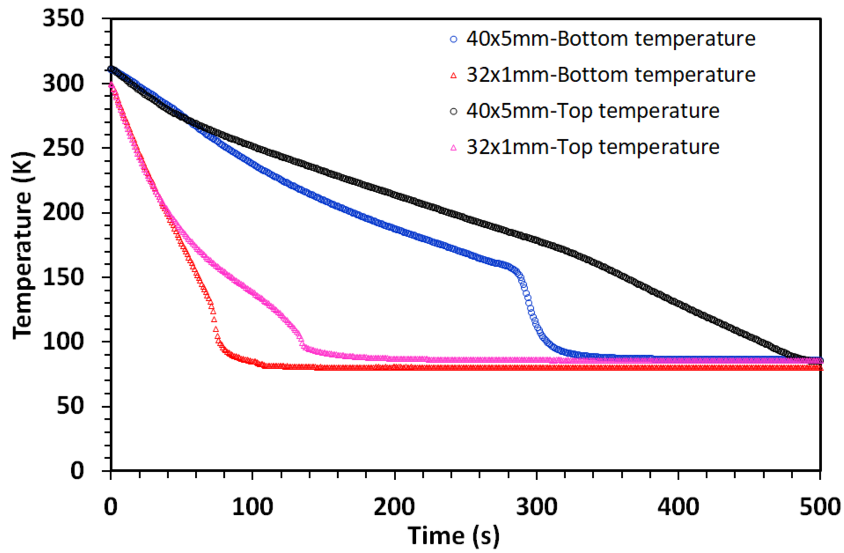

Figure 9.11: Comparison of wall temperature profile at station 3 in experiments with stainless steel evaluation sections of thicknesses 1 mm and 5 mm

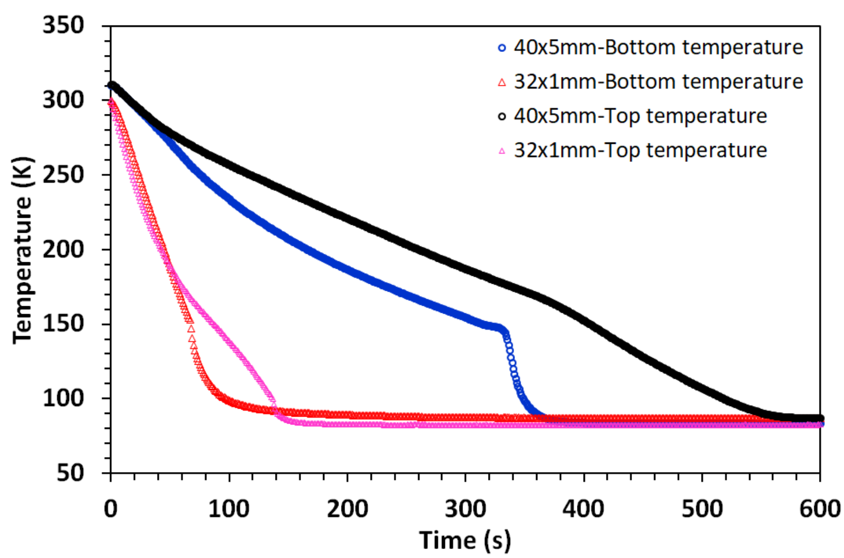

Figure 9.12: Comparison of wall temperature profile at station 4 in experiments with stainless steel evaluation sections of thicknesses 1 mm and 5 mm

A comparison of the wall temperature measurements made at stations 3 and 4 during experiments with evaluation sections of these two thicknesses is shown in Figure 9.11 and 9.12. In experiments with thicker section, chilldown time, as defined in Chapter 5, is seen to be increasing only by around 217% from around 154s to 488s, as compared to 1 mm thick evaluation section, though increase in thermal capacity is around 464%. Based on this, an increase in CPI (estimated using equation 5.1) of the order of 73% is seen in experiments with thicker section. This is mainly due to bottom wall wetting by LN_2 at a relatively higher outside wall temperature as seen in Figures 9.11 and 9.12 and higher extent of heat removal in nucleate boiling regime, in experiments with 5 mm thick section as compared to 1 mm thick evaluation section.

9.3.1.5 Influence of surface roughness on chilldown performance

Effect of surface roughness on chilldown performance is studied by performing experiments using evaluation sections having three different surface finish viz; Ra0.3, Ra3 and Ra8.4. Wall temperature profile observed at bottom location at station 3 during experiments with evaluation sections having different surface finish is compared in Figure 9.13.

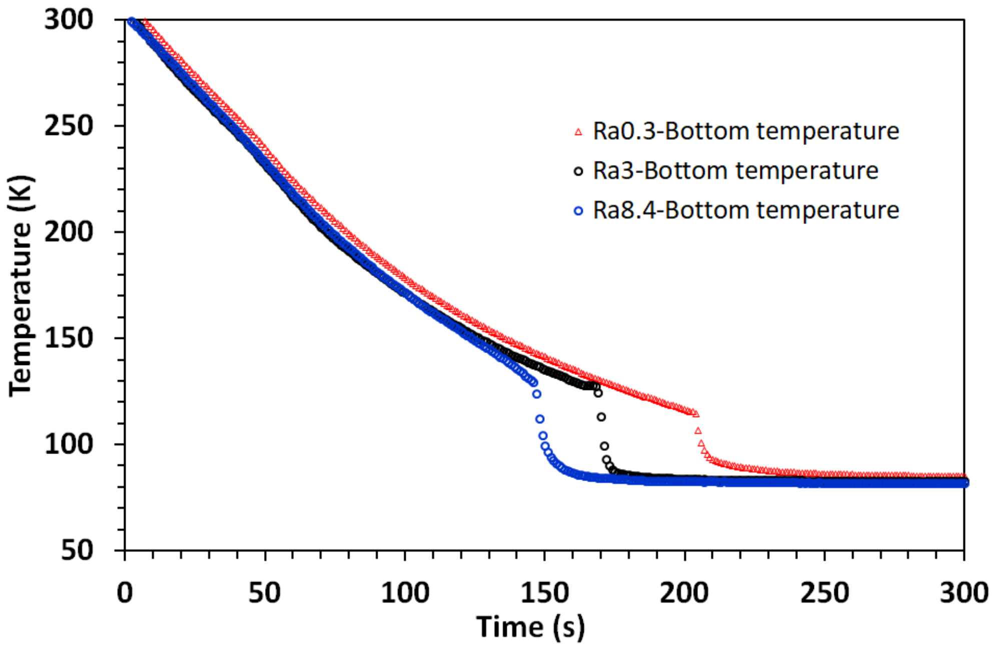

Figure 9.13: Comparison of wall temperature profile at bottom location at station 3 in experiments performed with evaluation sections having different surface roughness

Increased surface roughness helps in inducing wall wetting at a higher inner wall temperature and is clearly reflected in the bottom wall temperature profile. This is mainly due to the fact that in the presence of micro pores on the surface, nucleate boiling sets in early. This attribute can be used to improve the chilldown characteristics of cryogenic feedlines.

Wall temperature profile observed at bottom location at station 4 is compared in Figure 9.14

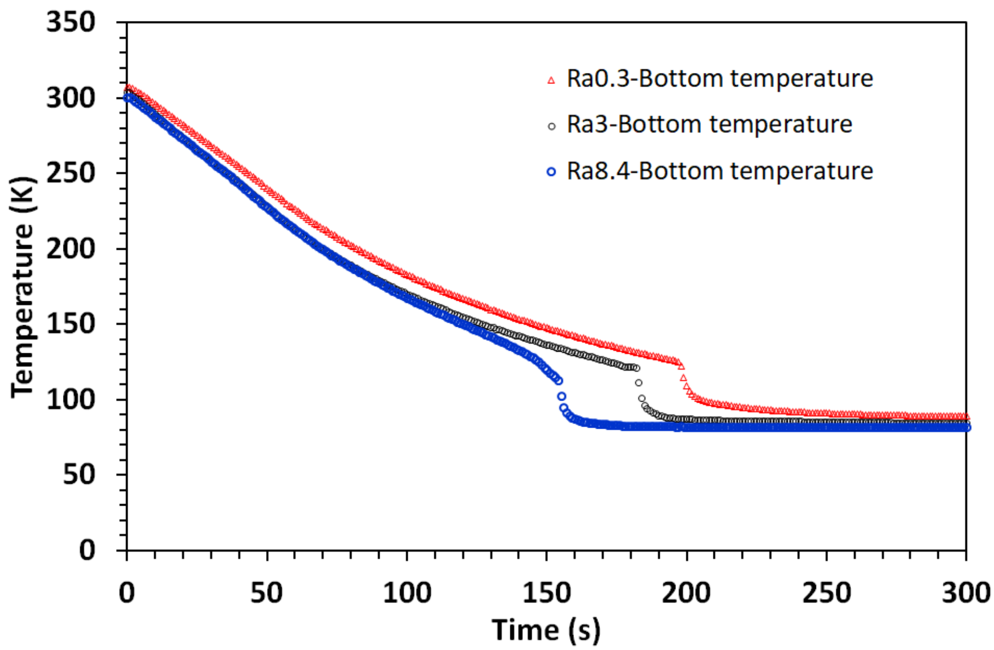

Figure 9.14: Comparison of wall temperature profile at bottom location at station 4 in experiments performed with evaluation sections having different surface roughness

9.3.2 Effect of location of evaluation section on the influence of sensitive parameters like thermal conductivity of wall material, coatings and thermal mass

To evaluate the influence of location on these sensitive parameters, experiments are repeated with the evaluation sections Sl. No. 1 to 7 of Table 9.1 placed at 1500 mm from the inlet of the feedline. Experimental data is analysed and compared with the results obtained with the evaluation sections placed at 875 mm from inlet. The results are summarised in Table 9.2.

Based on these experimental findings, the following conclusions are drawn on the effect of location on the influence of these sensitive parameters:

- The influence of higher thermal conductivity is more predominant at downstream locations as compared to locations upstream. Gain in CPI is much higher at around 133% with evaluation section placed at 1500 mm from inlet as compared to 62% for 875 mm location. Extent of reduction in circumferential temperature difference is also higher for downstream locations as compared to locations upstream. This increased gain is attributable to heat conduction in

Table 9.2: Results of experiments performed with evaluation section placed at 1500 mm from inlet

Parameter Studied	Effect @875 mm from inlet		Effect at 1500 mm from inlet	
	CPI gain (%)	Circumferential temperature gradient(K)	CPI gain (%)	Circumferential temperature gradient(K)
Effect of thermal conductivity	62	34 (47)	133	34 (85)
Effect of PFA coating on 1 mm thick evaluation section	53	89 (47)	57	125 (85)
Effect of PFA coating on 5 mm thick evaluation section	46	122 (76)	26	141 (82)
Effect of 100μm copper coating	-	40 (47)	70	61 (85)
Effect of 200μm copper coating	17	38 (47)	64	45 (85)
()Values observed with bare reference evaluation section				

the circumferential direction enabled by the higher conductivity of Cu alloy material and the extended duration of chilldown required, being a downstream location.

- With 1 mm thick PFA coated evaluation section, the performance gain is almost of similar order at locations upstream and downstream. But the temperature gradient in circumferential direction is much higher. Whereas with 5 mm thick section, performance gain with the evaluation section placed at downstream location is less as compared to the value achieved with its placement at upstream location. Temperature gradient in circumferential direction is also higher. Lesser CPI gain with 5 mm thick section placed at downstream location is mainly attributed to longer chilldown time demanded and lower circumferentially averaged wall heat flux, being a downstream location coupled with the larger thermal mass of evaluation section. Whereas this effect is not so significant for 1 mm thick evaluation section, as its thermal mass is lower.

- Performance is seen to be considerably improved with Cu coated evaluation sections, both of 100μm and 200μm thicknesses, when placed downstream. CPI is higher by around 64 to 70 % with Cu coating, as compared to values achieved for bare sections without coating. Temperature gradient in circumferential direction is significantly reduced by around 47% with

200μm Cu coating. This could be attributed to heat conduction in circumferential direction, resulting in lesser gradient in circumferential direction and thereby improved CPI.

Experiments performed as part of the present study have shown that with higher thermal conductivity test section material, the chilldown performance improves significantly, as demonstrated with Cu alloy material, as compared to AISI321 material. Presence of nonmetallic coating also reduces the chilldown time, but increases the temperature difference between top and bottom of the test section. Whereas the presence of Cu coating improves the chilldown performance and reduces the temperature gradient between top and bottom location. Experiments with varying surface finish have shown that higher surface roughness results in early wetting of the bottom wall. Apart from these, the influence of wall thickness of the test section material on Chilldown Performance Index is also studied. Sensitivity of each of these parameters with respect to location is also studied by placing the evaluation section at two locations along the feedline.

Chapter 10

Conclusions and outline for future work

In the present work, influence of factors like feedline orientation, thermophysical property of feedline material, coatings and thermal mass distribution on chilldown performance of cryogenic feedlines are studied experimentally. An experimental set-up is realised and experiments are performed, using two test sections TS1 and TS2, with varying test section orientations and mass flux conditions to study the influence of feedline orientation. Flow visualisation studies are performed using a vacuum jacketed view glass to capture the flow structure prevailing in the test section during experiments with horizontal, upward and downward orientations. Wall heat flux values are computed using inverse heat transfer technique and compared to understand the change in heat flux pattern with upward and downward orientations. Influence of coatings and thermophysical properties of feedline material are also evaluated and their influence on chilldown performance is captured through experiments performed with Cu alloy evaluation section, evaluation sections coated with nonmetallic Perflouroalkoxy Alkane (PFA) coating, and metallic Cu coating. Influence of surface finish on wall wetting is evaluated through experiments with evaluation sections having different surface finish. Effect of thermal mass distribution of feedline on chilldown performance is studied by introducing additional thermal mass near the inlet and exit of a standard test section. A total of ***176*** experiments are carried out to meet the various objectives of the present study. Apart from the above, in an attempt to capture the changes in wall temperature profile and flow field with test section orientation, numerical simulations are also performed simulating the test conditions with TS2 test section. Simulation are carried out for horizontal, 20° and 45° upward and downward orientations.

Experiments and theoretical studies carried out as part of the present study are depicted in Figure 10.1. Conclusions drawn based on these studies are brought out in the following sections.

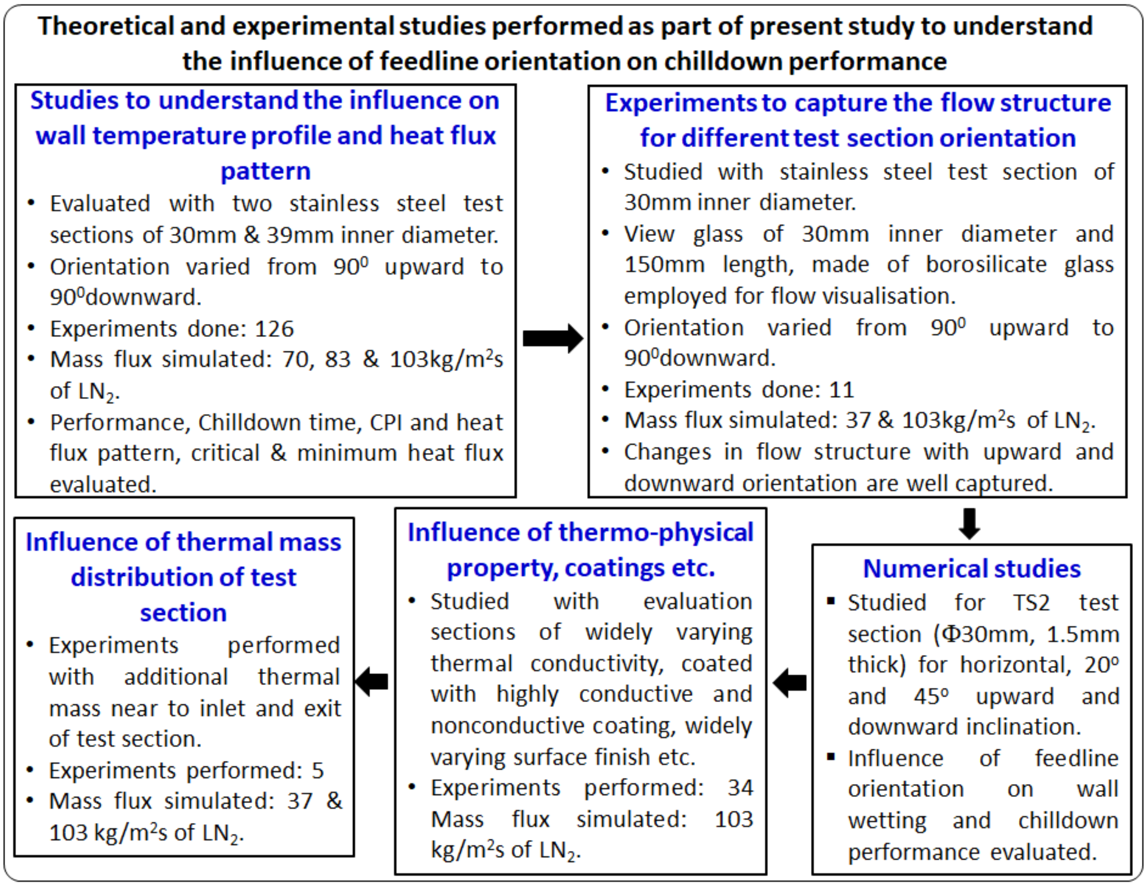

Figure 10.1: An overview of the experimental and theoretical aspects addressed through the present study

10.1 Major conclusions from the studies carried out

10.1.1 Influence of feedline orientation and mass flux on chilldown performance

Experiments are performed with the test section TS1 held at horizontal, 10°, 20°, 30°, 45°, 60°, and 90° inclinations, both in the upward and downward directions, whereas orientations up to 60° upward and downward directions are covered with TS2 test section. Using LN_2 as the simulant fluid, mass flux of 103 kg/m^{2}s and 83 kg/m^{2}s are simulated in TS1 test section and a mass flux of 60 kg/m^{2}s is simulated with TS2 test section. Wall temperature and heat flux profiles observed for different upward and downward orientations are compared. Chilldown performance is evaluated based on chilldown time and using a non dimensional parameter called Chilldown Performance Index (CPI). Findings from visualisation studies are also used to bring in a better understanding on the wall temperature profile related observations in experiments with varying angular orientations.

Major findings from these experiments are the following:

- Observation of lesser fall rate of bottom wall temperature in experiments with downward orientation is attributable to the flow structure, with reduced wetting at the bottom wall and good amount of liquid flowing as filaments and droplets along the core of the test section (as revealed during flow visualisation experiments).

- Earlier fall in top wall temperature and improved chilldown in experiments with upward orientation is due to presence of plug or slug flow, that induces top wall wetting by the liquid (as revealed during flow visualisation studies).

- In the range of mass flux studied, chilldown performance is inferior in experiments with downward inclination, as compared to horizontal and significantly improved with upward inclination. This is mainly due to reduced and improved fall rate in top wall temperature in experiments with downward and upward orientations respectively, which in turn is attributable to the flow structure, as revealed by visualisation studies.

- Chilldown time is found to be highly sensitive to mass flux, for horizontal, downward orientation and upward inclination up to 45°. Chilldown time is higher in experiments with lower mass flux. Beyond 45° upward inclination, influence of mass flux on chilldown performance is not so significant.

- Experiments with TS1 test section show that CPI is not significantly affected by mass flux. CPI is found to be maximum at around 45° to 60° upward orientation of test section and minimum in the range of 20-60° downward orientation.

- Among 90° upward and downward orientations tested, chilldown performance is better for upward orientation as compared to downward inclination. This could be attributed to the flow structure and all around wetting of the tube wall in experiments with upward inclination, as revealed in visualisation studies.

- Pattern of heat flux variation at top of the test section is similar in experiments with horizontal and downward orientation up to 60°. Whereas in experiments with upward orientation, top wall heat flux profile shows a significant jump, when the wall super heat reaches around 130-150 K and this is attributed to top wall wetting by liquid, as revealed by the slope change in top wall temperature profile.

- Average minimum heat flux values estimated using the published correlations are much higher compared to experimental values observed in the present study and could be attributed to these correlations being derived based on pool boiling studies.

- Average critical heat flux values observed in present experimental study are close to the values estimated by the correlation proposed by Darr et al. Deviation seen is around 33%.

- A particular pattern is seen in the variation of minimum heat flux and critical heat flux with respect to test section orientation. Pattern observed in variation of critical heat flux may be attributed to the heat capacity available in the test section on reaching the critical heat flux point.

10.1.2 Numerical studies

3D CFD simulations are carried out for horizontal, 20° and 45° upward and downward inclinations of TS2 test section to capture the wall temperature profile and flow field for different test section orientations. Simulations are performed for a mass flux condition of 60 kg/m^{2}s. Major finding from the study is as follows:

- Reduced fall rate in bottom wall temperature in experiments with downward inclination could be due to decrease in wetted perimeter and void fraction at the wall. Whereas increased fall rate in experiments with upward inclination is attributable to increase in wetted perimeter and void fraction at the wall.

10.1.3 Influence of feedline thermal mass distribution on chilldown performance

As part of the present study, experiments are performed by varying the thermal mass distribution of the test section. Thermal distribution is varied by placing an additional thermal mass near to the inlet and the exit of the test section. Studies are performed for two different mass flux conditions of 103 kg/m^{2}s and 37kg/m^{2}s. Conclusions drawn are as follows:

- Presence of additional thermal mass near to the exit affects the chilldown process and performance more significantly as compared to its introduction near the inlet. Chilldown is better with the additional thermal mass near to the inlet. This is due to the fact that during chilldown, heat flux at upstream locations is higher as compared to locations downstream, which in turn is due to warming up of the cryogen and lesser quantity of cryogen (in liquid form) participating in heat transfer at downstream location, as compared to locations upstream.

- Impact on chilldown performance is more with lower mass flux of cryogen.

10.1.4 Assessment of impact of thermophysical property of feedline material, surface coatings and surface finish on chilldown performance

Experiments are performed with evaluation section made of Cu alloy material having very high thermal conductivity and compared with the results with those of stainless steel material to understand the influence of thermophysical property on chilldown performance. Experiments with PFA coated and Cu coated evaluation sections have given considerable insight into the benefits of such coatings on chilldown performance and the associated thermal gradients across the cross section. Influence of surface finish on wall wetting is also studied by employing evaluation sections with surface finish Ra0.3, Ra3 and Ra8.4. Experiments are performed with the evaluation sections placed at 875 mm and 1500 mm from inlet, along the feedline of 2m length, to study the effect of location on influence of parameters like thermal conductivity, coatings, thermal mass etc. Major findings are:

10.1.4.1 Experiments with evaluation sections placed at 875 mm from inlet

- In view of its higher thermal conductivity, with Cu alloy, CPI improves significantly by around 62%, as compared to stainless steel material and circumferential temperature gradient reduces by 27% (from around 47K to 34K).

- With PFA coating, CPI is higher by around 46 to 53%, as compared to bare section and this is mainly due to early wetting of the tube wall with liquid, in the presence of coating. However, circumferential temperature gradient increases from around 47 K to 89 K with 1 mm thick evaluation section and from 76 K to 122 K with 5 mm thick section.

- Experiments with 1 mm and 5 mm thick evaluation sections show that CPI is higher by 73% with 5 mm thick section. This is mainly due to the fact that the bottom region of 5 mm thick evaluation section gets into nucleate boiling regime, while most of the top wall region is experiencing high wall superheat.

- Though there is no significant gain in CPI with 100μm Cu coating, CPI increases by around 17% with 200μm Cu coating. Circumferential temperature gradient is also reduced marginally to 38 K, as compared to 47 K with bare section. This can be attributed to the higher conductivity of Cu coating and the effect of conduction in circumferential direction.

- Higher surface roughness is able to induce earlier wetting of the bottom wall and thereby achieve improved chilldown performance.

10.1.4.2 Experiments with evaluation sections placed at 1500 mm from inlet

- Influence of thermal conductivity on chilldown performance is more significant at downstream locations as compared to locations upstream. Gain in CPI is much higher at around 133% as compared to 62% for 875 mm location. Extent of reduction in circumferential temperature gradient is also higher. This increased gain is attributable to the extended duration of chilldown required for a downstream location.

- With PFA coated evaluation section, the performance gain is almost of similar order or of lesser magnitude at locations downstream as compared to stations upstream. Circumferential temperature gradient is also higher. This could be attributed to longer chilldown time demanded and lower circumferentially averaged wall heat flux, being a downstream location.

- Performance with Cu coating is significantly improved at downstream location. CPI is higher by around 64 to 70 % with Cu coating, as compared to values achieved for bare sections without coating. Temperature gradient in circumferential direction is significantly reduced by around 47% with 200μm coating. This is attributable to heat conduction in circumferential direction, resulting in lesser temperature gradient and thereby improved CPI.

These studies have brought out certain findings on the influence of feedline orientation, mass flux, coatings and thermal mass distribution on chilldown performance. It is evident from the experimental data that upward orientation of test section gives a definite advantage in terms of chilldown performance and the maximum benefit is seen for 45° upward orientation. Experiments performed to study the influence of thermal mass distribution have shown that introduction of additional thermal mass at inlet gives a better performance as compared to its introduction near the exit. Studies have also shown that use of wall material with high thermal conductivity and presence of Cu coating helps in achieving a higher CPI and also reduced circumferential temperature gradient. These findings will be extremely useful to the designers in optimising the design of cryogenic feedlines to achieve better chilldown performance.

10.2 Outline proposed for future work

Following are the experimental and theoretical studies that can be taken up and pursued to improve further the understanding on chilldown of cryogenic systems:

- Experiments with varying test section orientations employing vacuum or super insulated test sections to understand the influence of external heat in-leak on chilldown performance.

- Experiments with varying test section orientations with test sections evacuated using ejectors to understand the influence of liquid sub-cooling on chilldown performance.

- Flow visualisation studies with the visualisation window placed in vacuum. This would help to achieve improved visibility and the studies can be extended to higher mass flux conditions.

- Numerical simulations can be pursued to capture the flow structure more precisely in upward flows. Fine tuning is also required to capture the top wall temperature profile more accurately, which is the deciding factor for chilldown completion.

- Use of the experimental data generated through the present study to derive improved correlations for prediction of wall temperature profile and chilldown time more accurately.

- Visualisation studies with collimated light source and Schlieren imaging to obtain better image quality and extraction of more detailed flow structure related information.

- Studies to investigate flow boiling physics in bends, elbows etc.

Bibliography

[1] JC Burke, WR Byrnes, AH Post, and FE Ruccia. Pressurized cooldown of cryogenic transfer lines. In *Advances in Cryogenic Engineering: Proceedings of the 1958 Cryogenic Engineering Conference*, pages 378–394. Springer, 1960.

[2] JWH Chi. Cooldown temperatures and cooldown time during mist flow. In *Advances in Cryogenic Engineering: Proceedings of the 1964 Cryogenic Engineering Conference (Sections AL)*, pages 330–340. Springer, 1965.

[3] JA Brennan, EG Brentari, RV Smith, and WG Steward. An experimental report on cooldown of cryogenic transfer lines. *NBS report*, 9264, 1965.

[4] MH Schwartz and JC Commander. Cooldown of large-diameter liquid hydrogen and liquid oxygen lines. *NASA-CR-54809*, 1966.

[5] F Edeskuty. Cooldown of cryogenic transfer systems. In *3rd Propulsion Joint Specialist Conference*, page 475, 1967.

[6] K Srinivasan, V Seshagiri Rao, and MV Krishna Murthy. Analytical and experimental investigation on cool-down of short cryogenic transfer lines. *Cryogenics*, 14(9):489–494, 1974.

[7] KA Durga Prasad, K Srinivasan, and MV Krishna Murthy. Cool-down of foam insulated cryogenic transfer lines. *Cryogenics*, 14(11):615–617, 1974.

[8] WG Steward, RV Smith, and JA Brennan. Cooldown transients in cryogenic transfer lines. In *Advances in Cryogenic Engineering: Proceedings of the 1969 Cryogenic Engineering Conference University of California at Los Angeles, June 16–18, 1969*, pages 354–363. Springer, 1995.

[9] MV Krishnamurthy, Rajneesh Chandra, S Jacob, S Kasthurirengan, and R Karunanithi. Experimental studies on cool-down and mass flow characteristics of a demountable liquid nitrogen transfer line. *Cryogenics*, 36(6):435–441, 1996.

[10] EK Kalinin, II Berlin, VV Kostyuk, and EM Nosova. Heat transfer in transition boiling of cryogenic liquids. *Advances in Cryogenic Engineering*, pages 273–277, 1975.

[11] D Steiner and EU Schlünder. Heat transfer and pressure drop for boiling nitrogen flowing in a horizontal tube: 1. saturated flow boiling. *Cryogenics*, 16(7):387–398, 1976.

[12] AA Kurilenko and SK Dymenko. Heat transfer in plug regime of film boiling of hydrogen in pipes. *Journal of engineering physics*, 40(4):341–345, 1981.

[13] Y Katto and H Ohno. An improved version of the generalized correlation of critical heat flux for the forced convective boiling in uniformly heated vertical tubes. *International journal of heat and mass transfer*, 27(9):1641–1648, 1984.

[14] MM Shah. Prediction of heat transfer during boiling of cryogenic fluids flowing in tubes. *Cryogenics*, 24(5):231–236, 1984.

[15] D Steiner. Heat transfer during flow boiling of cryogenic fluids in vertical and horizontal tubes. *Cryogenics*, 26(5):309–318, 1986.

[16] KE Gungor and RHS Winterton. A general correlation for flow boiling in tubes and annuli. *International Journal of Heat and Mass Transfer*, 29(3):351–358, 1986.

[17] SG Kandlikar. A general correlation for saturated two-phase flow boiling heat transfer inside horizontal and vertical tubes. 1990.

[18] Z Liu and RHS Winterton. A general correlation for saturated and subcooled flow boiling in tubes and annuli, based on a nucleate pool boiling equation. *International journal of heat and mass transfer*, 34(11):2759–2766, 1991.

[19] Neil T Van Dresar, James D Siegwarth, and Mohammad M Hasan. Convective heat transfer coefficients for near-horizontal two-phase flow of nitrogen and hydrogen at low mass and heat flux. *Cryogenics*, 41(11-12):805–811, 2001.

[20] J Hartwig, Samuel Darr, and Anthony Asencio. Assessment of existing two phase heat transfer coefficient and critical heat flux correlations for cryogenic flow boiling in pipe quenching experiments. *International Journal of Heat and Mass Transfer*, 93:441–463, 2016.

[21] SR Darr, JW Hartwig, J Dong, H Wang, AK Majumdar, AC LeClair, and JN Chung. Two-phase pipe quenching correlations for liquid nitrogen and liquid hydrogen. *Journal of Heat Transfer*, 141(4):042901, 2019.

[22] EK Kalinin and VP Firsov. Flow structure with film boiling in vertical tubes. *J. Eng. Phys.(Engl. Transl.);(United States)*, 53(6), 1988.

[23] R Das and S Pattanayak. Flow regime identification in cryogenic gas-liquid flow through vertical tubes. *Cryogenics*, 35(6):393–398, 1995.

[24] J Jackson, J Liao, JF Klausner, and R Mei. Transient heat transfer during cryogenic chilldown. In *Heat Transfer Summer Conference*, volume 47322, pages 253–260, 2005.

[25] K Yuan, Y Ji, and JN Chung. Cryogenic chilldown process under low flow rates. *International journal of heat and mass transfer*, 50(19-20):4011–4022, 2007.

[26] K Yuan, Y Ji, and JN Chung. Numerical modeling of cryogenic chilldown process in terrestrial gravity and microgravity. *International Journal of Heat and Fluid Flow*, 30(1):44–53, 2009.

[27] H Hu, JN Chung, and SH Amber. An experimental study on flow patterns and heat transfer characteristics during cryogenic chilldown in a vertical pipe. *Cryogenics*, 52(4-6):268–277, 2012.

[28] J Hartwig, H Hu, J Styborski, and JN Chung. Comparison of cryogenic flow boiling in liquid nitrogen and liquid hydrogen chilldown experiments. *International Journal of Heat and Mass Transfer*, 88:662–673, 2015.

[29] SR Darr, H Hu, R Shaeffer, JN Chung, JW Hartwig, and Alok K Majumdar. Numerical simulation of the liquid nitrogen chilldown of a vertical tube. In *53rd aiaa aerospace sciences meeting*, page 0468, 2015.

[30] L Jin, C Park, H Cho, C Lee, and S Jeong. Experimental investigation on chill-down process of cryogenic flow line. *Cryogenics*, 79:96–105, 2016.

[31] L Jin, H Cho, C Lee, and S Jeong. Experimental research and numerical simulation on cryogenic line chill-down process. *Cryogenics*, 89:42–52, 2018.

[32] L Jin, H Cho, and S Jeong. Experimental investigation on line chill-down process by liquid argon. *Cryogenics*, 97:31–39, 2019.

[33] L Jin, J Lee, and S Jeong. Investigation on heat transfer in line chill-down process with various cryogenic fluids. *International Journal of Heat and Mass Transfer*, 150:119204, 2020.

[34] J Mohammed, A Mohizin, and KE Reby Roy. Experimental investigations on transient cryogenic chilldown of a short horizontal copper transfer line. *Sādhanā*, 45:1–10, 2020.

[35] L Wang, Shi Shangguan, M Qu, J Wang, Y Li, and G Lei. Experimental study on cryogenic chilldown performance through a thick-wall tube. *Cryogenics*, 122:103436, 2022.

[36] K Yuan, Y Ji, JN Chung, and W Shyy. Cryogenic boiling and two-phase flow during pipe chilldown in earth and reduced gravity. *Journal of Low Temperature Physics*, 150:101–122, 2008.

[37] JN Chung and K Yuan. Recent progress on experimental research of cryogenic transport line chilldown process. *Frontiers in Heat and Mass Transfer (FHMT)*, 6(1), 2015.

[38] J Johnson and SR Shine. Transient cryogenic chill down process in horizontal and inclined pipes. *Cryogenics*, 71:7–17, 2015.

[39] SR Darr, H Hu, NG Glikin, JW Hartwig, AK Majumdar, AC Leclair, and JN Chung. An experimental study on terrestrial cryogenic transfer line chilldown i. effect of mass flux, equilibrium quality, and inlet subcooling. *International Journal of Heat and Mass Transfer*, 103: 1225–1242, 2016.

[40] AK Shukla, A Sridharan, and MD Atrey. Investigation of transient chill down phenomena in tubes using liquid nitrogen. In *IOP Conference Series: Materials Science and Engineering*, volume 278, page 012035. IOP Publishing, 2017.

[41] CW Cowley, WJ Timson, and JA Sawdye. A method for improving heat transfer to a boiling fluid. *Industrial & Engineering Chemistry Process Design and Development*, 1(2):81–84, 1962.

[42] L Manson. A periodic nonuniform heat-transfer mechanism in film boiling. 1967.

[43] F Moreaux, JC Chevrier, and G Beck. Destabilization of film boiling by means of a thermal resistance. *International Journal of Multiphase Flow*, 2(2):183–190, 1975.

[44] Y Kikuchi, T Hori, and I Michiyoshi. Minimum film boiling temperature for cooldown of insulated metals in saturated liquid. *International journal of heat and mass transfer*, 28(6): 1105–1114, 1985.

[45] GA Dreitser. Heat transfer enhancement in channels for film boiling of cryogenic liquids. *Applied thermal engineering*, 25(16):2512–2521, 2005.

[46] JN Chung, J Dong, H Wang, SR Darr, and JW Hartwig. Enhancement of convective quenching heat transfer by coated tubes and intermittent cryogenic pulse flows. *International Journal of Heat and Mass Transfer*, 141:256–264, 2019.

[47] W Xu, C Cheng, X Song, and P Zhang. Experimental investigation of cryogenic flow quenching of horizontal stainless steel tubes. *Cryogenics*, 117:103327, 2021.

[48] L Nguyen, M Kim, B Choi, K Do, and K Chung. Optimum coating thickness for the fastest chilldown of teflon-coated stainless steel flat plate in liquid nitrogen pool. *International Journal of Heat and Mass Transfer*, 194:123030, 2022.

[49] JW Hartwig, JN Chung, SR Darr, H Wang, B Huang, J Dong, Shreykumar Jain, Matthew Taliaferro, and Michael Doherty. The effect of gravity on cryogenic transfer line chilldown performance using pulse flow and low thermally conductive coatings. *International Journal of Heat and Mass Transfer*, 216:124549, 2023.

[50] JW Hartwig and J Vera. Numerical modeling of the transient chilldown of a cryogenic propellant transfer line. *Journal of Thermophysics and Heat Transfer*, 30(2):403–409, 2016.

[51] E Guerrero, F Muñoz, and Nicolás Ratkovich. Comparison between eulerian and vof models for two-phase flow assessment in vertical pipes. *CT&F-Ciencia, Tecnología y Futuro*, 7(1): 73–84, 2017.

[52] Y Umemura, T Himeno, K Kinefuchi, Y Saito, Barbara A Sakowski, Daniel M Hauser, Jason W Hartwig, Wesley L Johnson, and Andre LeClair. Numerical simulation on liquid hydrogen chill-down process of vertical pipeline. In *AIAA Propulsion and Energy 2019 Forum*, page 4439, 2019.

[53] JM Pesich, DM Hauser, JW Hartwig, M Kassemi, K Kinefuchi, Y Umemura, and T Himeno. Cfd modeling of cryogenic chilldown in a complex channel under normal and low gravity conditions. In *AIAA Propulsion and Energy 2020 Forum*, page 3818, 2020.

[54] KR Kunniyoor, R Govind, KS Venkateswaran, and P Ghosh. Liquid hydrogen pipeline chilldown: Mathematical modelling and investigation. *Cryogenics*, 118:103324, 2021.

[55] N Zuber. On the stability of boiling heat transfer. *Transactions of the American Society of Mechanical Engineers*, 80(3):711–714, 1958.

[56] PJ Berenson. Film-boiling heat transfer from a horizontal surface. 1961.

[57] N Zuber. *Hydrodynamic aspects of boiling heat transfer*. Number 4439. United States Atomic Energy Commission, Technical Information Service, 1959.

[58] JH Lienhard and VK Dhir. Hydrodynamic prediction of peak pool-boiling heat fluxes from finite bodies. 1973.

[59] I Mudawar and DE Maddox. Enhancement of critical heat flux from high power microelectronic heat sources in a flow channel. 1990.

List of Publications

Journal Publications

1. Venkatesh N., Deepak Kumar Agarwal, A. Salih, S. Sunil Kumar (2023), Chilldown of cryogenic feed lines - An insight into the influence of feed line orientation and mass flux. ***Cryogenics***, 130 (2023) 103644.

2. Venkatesh N., Deepak Kumar Agarwal, A. Salih, S. Sunil Kumar (2024), Effect of cryogenic feed line thermal mass distribution and orientation on chilldown performance. ***Cryogenics***, 138 (2024) 103781.

3. Venkatesh N., Deepak Kumar Agarwal, A. Salih, S. Sunil Kumar (2024), Role of wall material, coatings and configuration on cryogenic feedline chilldown performance. ***Communicated to International communications in Heat and Mass Transfer Journal***.

Peer-reviewed National and International Conferences

1. Venkatesh N., Anant Singhal, Deepak Kumar Agarwal, A. Salih, S. Sunil Kumar (2023), Studies to investigate the effect of feed line orientation on chilldown performance of cryogenic feed lines. ***National Conference on Systems Approach in Self Reliance in Advanced Technologies (SASAT-2023) organised by Indian Society of Systems for Science and Engineering, Defense Research and Development Organisation and Osmania University***, 2023.

2. Venkatesh N., Deepak Kumar Agarwal, A. Salih, S. Sunil Kumar (2023), IHMTC-2023-433 Experimental investigation on influence of thermophysical properties and coatings on cryogenic feed line chilldown performance. ***27th National and 5th ISHMT-ASTFE Heat and Mass Transfer Conference IHMTC-2023 organised jointly by Indian Society for Heat and Mass Transfer and American Society for Thermal and Fluids Engineers***, 2023.

3. Venkatesh N., Anant Singhal, A. Salih, S. Sunil Kumar (2024), CFD simulations on cryogenic feedline with different orientations. ***International Conference on advances in Aerospace and Energy systems, IAES-2024 Conference organised jointly by Indian Society for Heat and Mass Transfer and LPSC/ISRO, Valiamala, Thiruvananthapuram***, 2024.

4. Venkatesh N., Deepak Kumar Agarwal, A. Salih, S. Sunil Kumar (2024), Experimental investigation of flow structure and heat transfer in cryogenic vertical flows ***International Conference in Fluid, Thermal and Energy Systems (ICFTES-'24), organised by NIT, Calicut, University of Stellenbosch, South Africa, Indian Institute of Chemical Engineers and Indian Society for Heat and Mass Transfer***, 2024.